

---

# Performance of Continuously Reinforced Concrete Pavements, Volume VI—CRC Pavement Design, Construction, and Performance

---

PUBLICATION NO. FHWA-RD-97-151

FEBRUARY 1999



U.S. Department of Transportation  
**Federal Highway Administration**

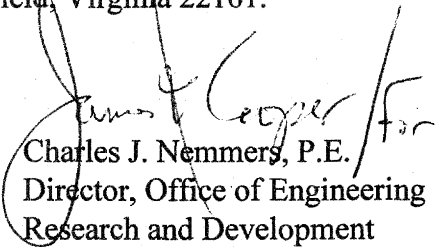
Research, Development & Technology  
Turner-Fairbank Highway Research Center  
6300 Georgetown Pike  
McLean, VA 22101-2296



## FOREWORD

This report is one volume of a seven-volume set presenting the results of a study to provide the state-of-the-art for the design, construction, maintenance and rehabilitation of Continuously Reinforced Concrete Pavement (CRCP). Through a thorough literature review of current and past research work in CRCP and extensive field and laboratory testing of 23 in-service CRC pavements, the effectiveness of various design and construction features were assessed; performance of CRCP was evaluated; and procedures for improving CRC pavement technology were recommended. The 23 test pavements were located in six states that participated in this national pooled fund study. In addition the data available for 83 CRCPs included in the General Pavement Study (GPS) number 5 of the Long Term Pavement Performance (LTPP) Program was presented and analyzed. A number of CRCP maintenance and rehabilitation techniques that have been used over the years including joint and crack sealing, cathodic protection of reinforcing bars, full-depth patching, resurfacing, etc., were also evaluated. This report will be of interest to engineers and researchers concerned with the state-of-the-art design, construction, maintenance and rehabilitation of CRCP including predictive models. The study was made possible with the financial support of Arizona, Arkansas, Connecticut, Delaware, Illinois, Iowa, Louisiana, Oklahoma, Oregon, Pennsylvania, South Dakota, Texas and Wisconsin.

Sufficient copies of this report are being distributed to provide two copies to each FHWA regional office and three copies to each FHWA division office and each state highway agency. Direct distribution is being made to the division offices. Additional copies for the public are available from the National Technical Information Service (NTIS), United States Department of Commerce, 5285 Port Royal Road, Springfield, Virginia 22161.

  
Charles J. Nemmers, P.E.  
Director, Office of Engineering  
Research and Development

## NOTICE

This document is disseminated under the sponsorship of the Department of Transportation in the interest of information exchange. The United States Government assumes no liability for its' contents or use thereof. This report does not constitute a standard, specification, or regulation.

The United States Government does not endorse products or manufacturers. Trade and manufacturers' names appear in this report only if they are considered essential to the object of the document.

<b>1. Report No.</b> FHWA-RD-97-151	<b>2. Government Accession No.</b>	<b>3. Recipient's Catalog No.</b>	
<b>4. Title and Subtitle</b> PERFORMANCE OF CRC PAVEMENTS Volume VI - CRC Pavement Design, Construction, and Performance		<b>5. Report Date</b> February 1999	
		<b>6. Performing Organization Code</b>	
<b>7. Author(s)</b> Dan G. Zollinger, Neeraj Buch, Dapeng Xin, and Jorge Soares		<b>8. Performing Organization Report No.</b>	
<b>9. Performing Organization Name and Address</b> PCS/Law Engineering A Division of Law Engineering, Inc. 12104 Indian Creek Court, Suite A Beltsville, Maryland 20705		<b>10. Work Unit No. (TRAIS)</b> 3C1A	
		<b>11. Contract or Grant No.</b> DTFH61-90-C-00073	
<b>12. Sponsoring Agency Name and Address</b> Federal Highway Administration Office of Research and Development 6300 Georgetown Pike McLean, Virginia 22101-2296		<b>13. Type of Report and Period Covered</b> Final Report August 1990 - December 1994	
		<b>14. Sponsoring Agency Code</b>	
<b>15. Supplementary Notes</b> Contracting Officer's Technical Representative (COTR): Jim Sherwood (current); Roger Larson (previous), HNR-30 Subcontractors: Transportation Technologies USA, Inc. (S.D. Tayabji, Principal Investigator) Texas Transportation Institute (D.G. Zollinger, Co-Principal Investigator) Special thanks are given to the following highway agencies for their assistance in the conduct of this study: Arizona, Arkansas, Connecticut, Delaware, Illinois, Iowa, Louisiana, Oklahoma, Oregon, Pennsylvania, South Dakota, and Texas.			
<b>16. Abstract</b> This report is one of a series of reports prepared as part of a recent study sponsored by the Federal Highway Administration (FHWA) aimed at updating the state-of-the-art of the design, construction, maintenance, and rehabilitation of CRC pavements. The scope of work of the FHWA study included the following: <ol style="list-style-type: none"> <li>1. Conduct a literature review and prepare an annotated bibliography on CRC pavements and CRC overlays.</li> <li>2. Conduct a field investigation and laboratory testing related to 23 existing in-service pavement sections. This was done to evaluate the effect of various design features on CRC pavement performance, to identify any design or construction related problems, and to recommend procedures to improve CRC pavement technology.</li> <li>3. Evaluate the effectiveness of various maintenance and rehabilitation strategies for CRC pavements.</li> <li>4. Prepare a Summary Report on the current state of the practice for CRC pavements.</li> </ol> Each of the above four items is addressed in a separate report. The following reports have been prepared under this study: Performance of CRC Pavements Volume I - Summary of Practice and Annotated Bibliography Volume II - Field Investigation of CRC Pavements Volume III - Analysis and Evaluation of Field Test Data Volume IV - Resurfacings for CRC Pavements Volume V - Maintenance and Rehabilitation of CRC Pavements Volume VI - CRC Pavement Design, Construction, and Performance Volume VII - Summary This report is Volume VI in the series.			
<b>17. Key Words</b> Concrete, concrete pavement, continuously reinforced pavement, nondestructive testing, pavement evaluation, pavement performance, pavement testing, reinforcement.		<b>18. Distribution Statement</b> No restrictions. This document is available through the National Technical Information Service, Springfield, Virginia 22161.	
<b>19. Security Classification (of this report)</b> Unclassified	<b>20. Security Classification (of this page)</b> Unclassified	<b>21. No. of Pages</b> 111	<b>22. Price</b>

# SI\* (MODERN METRIC) CONVERSION FACTORS

## APPROXIMATE CONVERSIONS FROM SI UNITS

APPROXIMATE CONVERSIONS TO SI UNITS		APPROXIMATE CONVERSIONS FROM SI UNITS						
Symbol	When You Know	Multiply By	To Find	Symbol	When You Know	Multiply By	To Find	Symbol
<b>LENGTH</b>				<b>LENGTH</b>				
in	inches	25.4	millimeters	mm	mm		inches	in
ft	feet	0.305	meters	m	m		feet	ft
yd	yards	0.914	meters	m	m		yards	yd
mi	miles	1.61	kilometers	km	km		miles	mi
<b>AREA</b>				<b>AREA</b>				
in <sup>2</sup>	square inches	645.2	square millimeters	mm <sup>2</sup>	mm <sup>2</sup>		square inches	in <sup>2</sup>
ft <sup>2</sup>	square feet	0.093	square meters	m <sup>2</sup>	m <sup>2</sup>		square feet	ft <sup>2</sup>
yd <sup>2</sup>	square yards	0.836	square meters	m <sup>2</sup>	m <sup>2</sup>		square yards	yd <sup>2</sup>
ac	acres	0.405	hectares	ha	ha		acres	ac
mi <sup>2</sup>	square miles	2.59	square kilometers	km <sup>2</sup>	km <sup>2</sup>		square miles	mi <sup>2</sup>
<b>VOLUME</b>				<b>VOLUME</b>				
fl oz	fluid ounces	29.57	milliliters	mL	mL		fluid ounces	fl oz
gal	gallons	3.785	liters	L	L		gallons	gal
ft <sup>3</sup>	cubic feet	0.028	cubic meters	m <sup>3</sup>	m <sup>3</sup>		cubic feet	ft <sup>3</sup>
yd <sup>3</sup>	cubic yards	0.765	cubic meters	m <sup>3</sup>	m <sup>3</sup>		cubic yards	yd <sup>3</sup>
NOTE: Volumes greater than 1000 l shall be shown in m <sup>3</sup> .								
<b>MASS</b>				<b>MASS</b>				
oz	ounces	28.35	grams	g	g		ounces	oz
lb	pounds	0.454	kilograms	kg	kg		pounds	lb
T	short tons (2000 lb)	0.907	megagrams (or "metric ton")	Mg (or "t")	Mg (or "t")		short tons (2000 lb)	T
<b>TEMPERATURE (exact)</b>				<b>TEMPERATURE (exact)</b>				
°F	Fahrenheit temperature	5(F-32)/9 or (F-32)/1.8	Celsius temperature	°C	°C		Fahrenheit temperature	°F
<b>ILLUMINATION</b>				<b>ILLUMINATION</b>				
fc	foot-candles	10.76	lux	lx	lx		foot-candles	fc
fl	foot-Lamberts	3.426	candela/m <sup>2</sup>	cd/m <sup>2</sup>	cd/m <sup>2</sup>		foot-Lamberts	fl
<b>FORCE and PRESSURE or STRESS</b>				<b>FORCE and PRESSURE or STRESS</b>				
lbf	poundforce	4.45	newtons	N	N		poundforce	lbf
lbf/in <sup>2</sup>	poundforce per square inch	6.89	kilopascals	kPa	kPa		poundforce per square inch	lbf/in <sup>2</sup>

(Revised September 1993)

\* SI is the symbol for the International System of Units. Appropriate rounding should be made to comply with Section 4 of ASTM E380.

## TABLE OF CONTENTS

<u>Section</u>	<u>Page</u>
CHAPTER 1 - INTRODUCTION .....	1
CHAPTER 2 - CRC PAVEMENT PERFORMANCE AND DESIGN FACTORS .....	3
Important Factors Affecting Cracking in CRC Pavements .....	3
Evolution of Cracking in CRC Pavements .....	6
Concrete Characteristics .....	8
Reinforcing Steel Characteristics .....	10
Depth of Cover of Longitudinal Steel .....	13
Climatic Factors .....	14
Importance of the Cracking Interval .....	17
CHAPTER 3 - IMPROVED CRC PAVEMENT THICKNESS DESIGN CONCEPTS .....	21
Present CRC Design Methodology .....	21
Basic Failure Modes in Terms of a Design Framework .....	22
Thickness Design Procedure .....	27
Summary .....	50
CHAPTER 4 - CONSTRUCTION METHODS TO IMPROVE CRC PAVEMENT	
CRACK PATTERNS .....	53
Experimental Pavement Sections to Improve Crack Patterns .....	54
Suggested Guidelines for CRC Pavement Construction and Crack Control .....	66
Conclusions .....	68
CHAPTER 5 - ADVANCEMENTS IN THE EVALUATION OF	
CRC PAVEMENT PERFORMANCE .....	69
Crack Pattern Evaluation .....	70
Characterization of Pavement Support Conditions .....	75
Load Transfer Efficiency .....	76
Application to Overlay Design .....	92
CHAPTER 6 - SUMMARY, CONCLUSION, AND NEEDED RESEARCH .....	97
Suggestions for Further Research .....	98
REFERENCES .....	101

## LIST OF FIGURES

<u>Figure</u>		<u>Page</u>
1	CRC pavement elements and distributions of various stresses .....	5
2	Stress distribution between cracks of CRC member subject to shrinkage .....	6
3	Stress distribution between cracks of CRC member subject to temperature drop .....	7
4	Influence of the linear coefficient of thermal expansion of aggregate on the coefficient of thermal expansion of concrete .....	8
5	Change in average crack interval over time for 178 mm and 203 mm (7 and 8 in) CRC pavement .....	11
6	Effect of bar size on crack spacing .....	12
7	Relationship between steel bond area and crack spacing .....	12
8	Frequency histograms showing crack interval distributions .....	13
9	Failure modes related to punchout distress in CRC pavement .....	18
10	PCA joint load transfer tests .....	23
11	PCA test slab results relative to dimensionless shear and joint stiffness .....	24
12	Shear load stress for various load conditions of a 229 mm (9 in) CRC slab .....	25
13	Shear capacity relationships based on PCA tests and laboratory test data .....	26
14	Effect of crack spacing on maximum tensile stress (0 percent LTE) .....	29
15	Effect of load transfer efficiency across transverse cracks on maximum transverse stress in CRC pavement .....	30
16	Wheel load stresses in a loaded CRC pavement system .....	31
17	Comparison of $\sigma_a$ and $\sigma_b$ with crack spacing for a 254 mm (10 in) pavement thickness .....	32
18	Transverse bending stress: CRC pavement with bituminous shoulder .....	33
19	Shear stress as a function of load transfer efficiency provided by a concrete shoulder .....	35
20	Adjustment of dimensionless shear stress for cracking spacing .....	36
21	Maximum crack width limits based on shear capacity requirements .....	37
22	Curling stress coefficients .....	40
23	Suggested design stress locations as a function of a typical pavement/shoulder configuration .....	44
24	Transverse bending equivalent damage ratios (0.46 m (18 in) from pavement edge) .....	45
25	Metallic crack inducer located on the top of longitudinal rebar .....	56
26	Typical relative humidity variation with time at 25 mm from the surface of the pavement .....	57
27	Relative humidity in the section cured by polyethylene sheet .....	58
28	Temperature variations in the sections with different curing methods .....	59
29	Effect of curing method on relative humidity in concrete pavement .....	60

## LIST OF FIGURES (Continued)

<u>Figure</u>		<u>Page</u>
30	Early-aged saw cutting technology .....	61
31	Cracking development at saw cut locations .....	62
32	Percentage of cracks that occurred at rebar in Cypress section .....	64
33	Percentage of cracks that occurred at rebar in LaPorte section .....	64
34	Uncontrolled cracking test sections placed in morning hours .....	65
35	Uncontrolled cracking test sections placed in afternoon hours .....	65
36	Shapes of cracks and possible cracks on random cracks .....	72
37	Ideal CRC pavement cluster cracking probability .....	74
38	Load transfer efficiency .....	76
39	Shape of deflection basin under a slab of high stiffness and weak subgrade support .....	77
40	Shape of the deflected basin under a slab of low stiffness and subgrade support .....	78
41	The deflection basin "area" concept .....	79
42	Variation of deflection basin area with $l$ .....	80
43a	NDT load transfer efficiency, morning results (prior to 1000 h), I-72WB .....	83
43b	NDT load transfer efficiency, afternoon results (after 1300 h), I-72WB .....	84
44a	CRC pavement with transverse crack (morning case) .....	85
44b	CRC pavement without transverse crack (morning case) .....	85
45a	CRC pavement with transverse cracks (afternoon case) .....	86
45b	CRC pavement without transverse cracks (afternoon case) .....	86
46a	Radius of relative stiffness, morning results (prior to 1000 h), I-72WB .....	87
46b	Radius of relative stiffness, afternoon results (after 1300 h), I-72WB .....	88
47a	Comparison of LTE and $l_k$ for I-55WB .....	89
47b	Comparison of LTE and $l_k$ for I-77WB, South Carolina .....	90
48	Section overlay and existing jointed pavement .....	92
49	Improvement of layer modulus with load transfer efficiency .....	94
50	Overlay design: composite stiffness versus design criteria .....	95

- Steel/concrete bond
- Steel amount and depth
- Crack width
- Shoulder type
- Concrete strength

Time (Performance Related)

- Aging concrete properties
- Environmental Conditions
  1. Temperature variations
  2. Precipitation
- Reduced bond characteristics
- Rebar Corrosion
  1. Deicing chemicals or salt water exposure
- Traffic and environmental loads
- Subbase erosion and loss of support
  1. Moisture warping in the transverse direction

If the transverse cracks are spaced at adequate and uniform intervals, the potential for widened cracks and punch out development, which is the primary distress type in CRC pavement, is reduced. Based on the above factors, one would expect that CRC pavements that develop crack patterns with adequate intervals would typically show the best performance. Most of the failures in CRC pavements occur because of either widened transverse cracks or closely spaced transverse cracks. However, there are instances where good performance has been achieved in CRC pavements with average crack intervals of less than 0.6 m (2 ft) but excellent support conditions have also accompanied these pavements. Several researchers have suggested that the crack pattern should consist of cracks displaying crack widths small enough to minimize the entrance of surface water and maintain adequate load transfer through aggregate interlock.<sup>(2, 24)</sup> Many naturally occurring CRC pavement crack patterns can frequently display average crack spacings that fall within the preferred range of 1.7 to 2.4 m (3.5 to 8 ft), but the typical variability associated with them can result in a number of cracks spaced less than 1.7 m (3.5 ft).<sup>(1, 2, 40 - 43)</sup>

In CRC pavements, the concrete is typically subjected to non-uniform/non-linear (from top to bottom) volumetric changes that results in stress development due to temperature, moisture, and shrinkage effects. The resulting stresses caused by these effects are relieved by the formation of transverse cracks. Crack development may be thought of in two phases: initial crack development and secondary crack development. Initial cracking in CRC pavements may be due to environmentally induced temperature and moisture gradients related to the slab  $\ell$ -value and its curling and warping behavior. Initial cracking typically occurs rapidly and will be equal to or less than  $4.4 \ell$  where  $\ell$  is the radius of relative stiffness of the pavement surface layer. Secondary cracking results in a stable crack pattern and is a function of the factors discussed

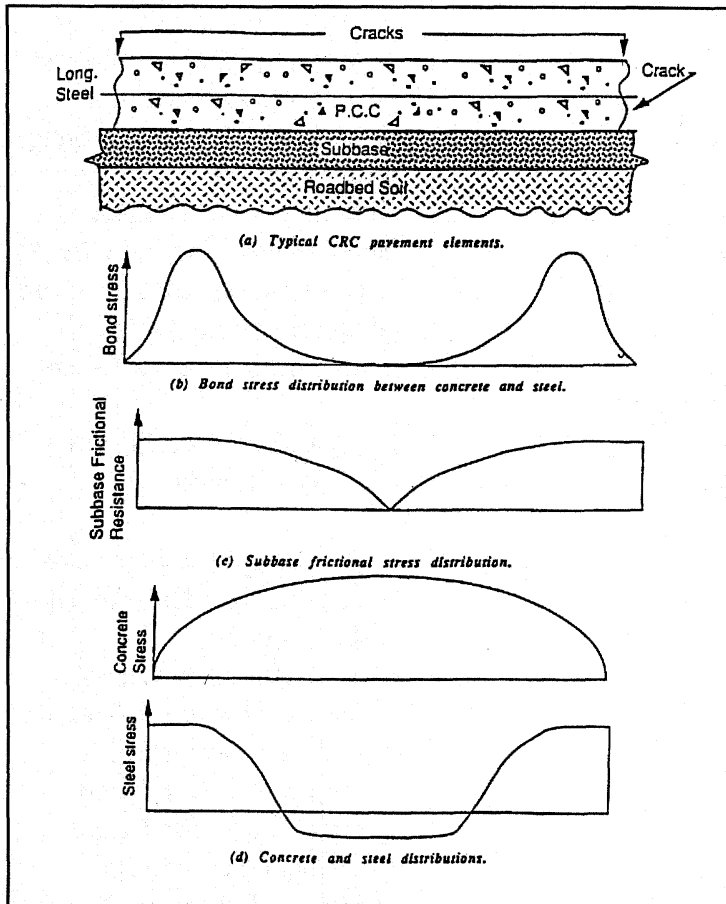


Figure 1. CRC pavement elements and distributions of various stresses.<sup>(1)</sup>

above. Figure 1(a) shows a typical CRC pavement section between two adjacent transverse cracks.<sup>(1)</sup> When the pavement experiences a change in temperature or a change in drying shrinkage, the concrete movement in the longitudinal direction is restrained by the longitudinal steel and subbase friction.

The reinforcing steel, embedded in the concrete, behaves stress and strain-wise in a different manner from the concrete. This behavior results in interfacial shear stress (referred to as bond stress) at the interface between the steel bar surface and the concrete. The magnitude of the bond stress depends on the concrete strength and mechanical shape of the bearing face of the ribs on the longitudinal bar. These factors have been the subject of recent improvements in the design of reinforcing steel rib patterns.<sup>(33)</sup> Because of the anchor and lug characteristics of the reinforcing promoting strong bond between the

concrete and the embedded steel, a bond stress will develop. Figure 1 (b) shows a typical bond stress distribution between concrete and steel<sup>(1)</sup> over a segment of cracked CRC pavement.

The direction of frictional resistance provided by the subbase is opposite to that of concrete displacement. Subbase friction depends upon the subbase material type and when the concrete contracts, the subbase friction, and the steel resist the concrete displacement, thereby increasing the level of concrete tensile stress which contributes to the resultant crack spacing. Figure 1 (c) shows a typical distribution of frictional resistance.<sup>(1)</sup> The resistance to the concrete contraction through bond stress and subbase friction cause the concrete tensile stress to build up and the concrete displacement to be reduced. Figure 1 (d) illustrates the concrete and steel stress distribution along the CRC pavement slab.<sup>(1)</sup> If the resultant concrete stress exceeds the concrete tensile strength, a crack will develop. Past performance data has indicated that dense graded asphaltic concrete (AC) interlayer provide the most desirable subbase frictional characteristics. Although not shown in Figure 1, it is good design practice to incorporate an AC interlayer between the CRC layer and the subbase - particularly where stabilized bases are used.

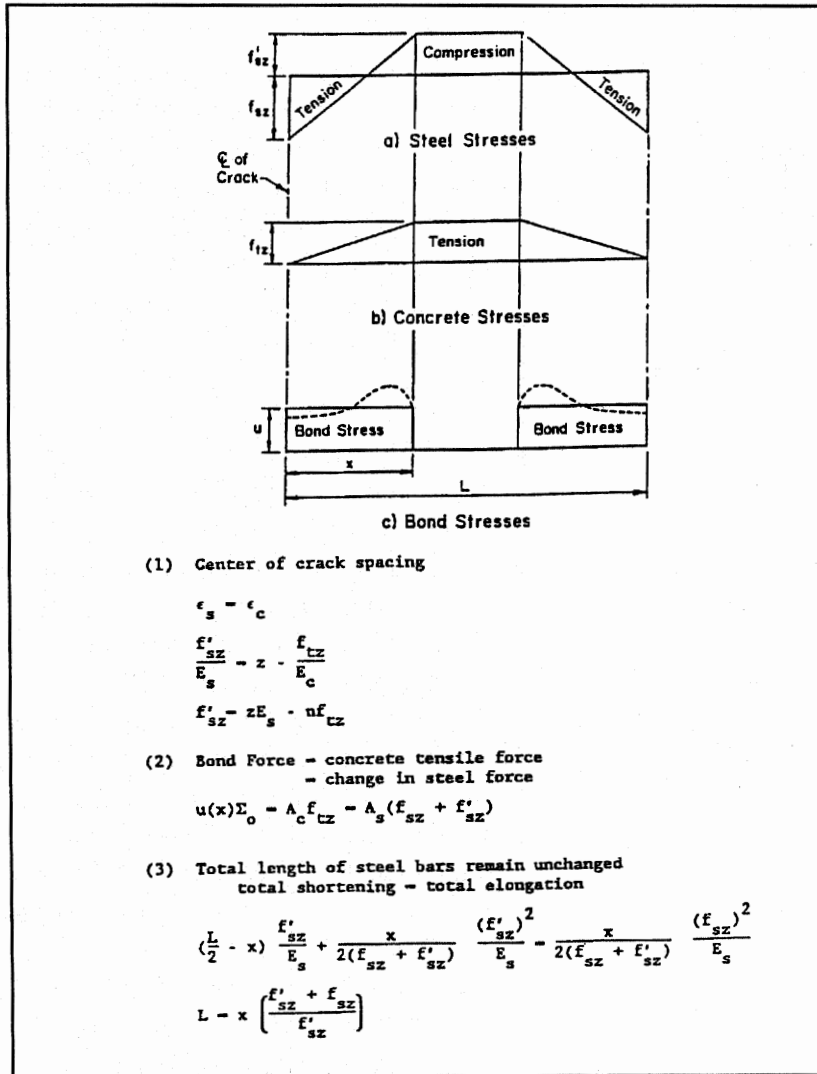


Figure 2. Stress distribution between cracks of CRC member subject to shrinkage.<sup>(5)</sup>

reinforcement (i.e., internal restraint) which inhibits free movement of the concrete matrix after the formation of primary cracks. Stresses that develop at this stage are referred to as restraint stresses. According to data recently obtained in Texas,<sup>(4)</sup> primary cracks constitute the rapidly evolving crack pattern at intervals approximately 4.4ℓ (radius of relative stiffness) or less, which form the beginning secondary crack intervals and the development of a stable cracking pattern.

A significant contribution was made by Vetter,<sup>(5)</sup> who developed relationships for crack spacing in reinforced concrete illustrated in stress diagrams for drying shrinkage and temperature drop shown in figures 2 and 3 (L is the crack spacing and u is the bond stress). After the formation of the first crack due to restrained shrinkage, a new state of equilibrium and strain compatibility develops. The restrained shrinkage is accommodated by the crack, by the bond slip, and by the uncracked concrete. The following equations for average crack spacing are

Characteristic of good performing CRC pavements are non-erodible support conditions while maintaining minimal bonding conditions. Open-graded, permeable bases, in combination with AC interlayers have also provided adequate service towards maintaining minimal erosion.

### Evolution of Cracking in CRC Pavements

Several factors have been identified that affect how cracks form in CRC pavements. As previously noted, initial cracking in CRC pavements may be due to environmentally induced temperature and moisture gradients related to slab curling and warping. Field observations of initial or primary cracks suggest that these cracks form within the first 3 to 7 days after placement of the concrete. Secondary cracks form due to the continuity of

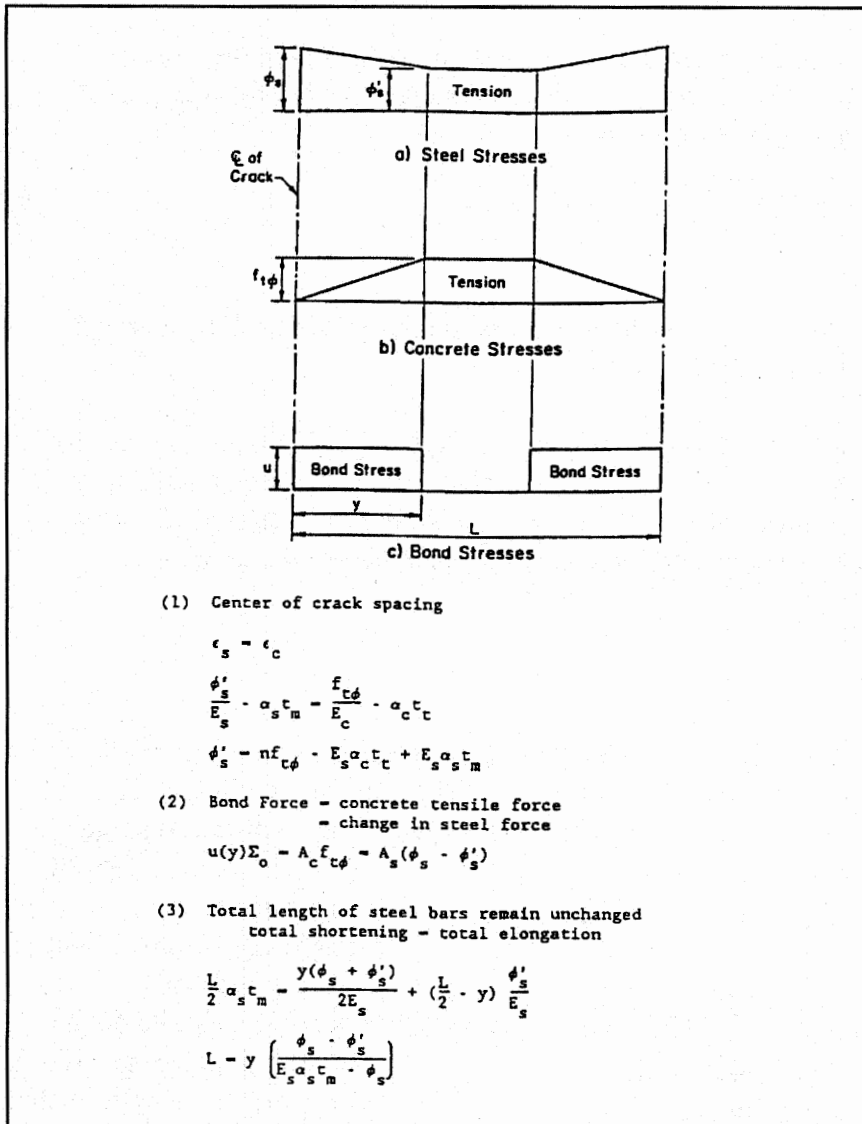


Figure 3. Stress distribution between cracks of CRC member subject to temperature drop.<sup>(5)</sup>

derived from Vetter's basic assumptions.<sup>(5)</sup> Vetter assumed that secondary cracks form within an initial crack interval. A formula for the average crack spacing due to shrinkage restraint is shown below:

$$L = \frac{f_{tz}^2}{\{Q \cdot u \cdot n \cdot p^2 (z \cdot E_c - f_{tz})\}} \quad (1)$$

where

- $L$  = crack spacing (L)
- $f_{tz}$  = concrete tension stress due to shrinkage strain at the center of crack ( $F/L^2$ )
- $Q$  = ratio of bond area to concrete volume
- $u$  = average bond stress ( $F/L^2$ )
- $p$  = percent reinforcement
- $n$  = modular ratio ( $E_s/E_c$ )
- $E_c$  = elastic modulus of concrete ( $F/L^2$ )
- $z$  = drying shrinkage

A formula for the average crack spacing formula is also derived for a drop in temperature in a similar manner:

$$L = \frac{f_{t\phi}^2}{\{Q \cdot u \cdot n \cdot p^2 (\alpha_s t_m E_c - f_{t\phi})\}} \quad (2)$$

where

- $f_{t\phi}$  = Concrete tension stress due to temperature drop at the center of the crack spacing ( $F/L^2$ )
- $\alpha_s$  = Coefficient of thermal expansion of steel

$t_m$  = Temperature drop on the surface of the pavement (°F)

A formula for the average crack spacing when both shrinkage and temperature drop occur simultaneously is later derived<sup>(5)</sup> by considering the combined stress diagram for steel and the concrete, which is expressed in a simplified form as:

$$L = f_t^2 / \{Q \cdot u \cdot p^2 (E_s \alpha_s t_m + z \cdot E_s - n \cdot f_t)\} \quad (3)$$

where

$f_t$  = Total tension stress in concrete (which for CRC pavement analysis is assumed equal to the tensile strength of concrete)

All the other terms are as defined in equations 1 and 2. Equation 3 indicates a close crack spacing may be obtained by a high bond stress. The same effect can also be obtained through increasing the percentage of reinforcement or using smaller diameter bars. Major factors that affect the crack pattern in terms of material, climatic, and pavement design factors are subsequently discussed.

### Concrete Characteristics

The primary constituents of concrete, mortar and coarse aggregate, have coefficients of thermal expansion (CTE) relative to the makeup and nature of the materials with the CTE for concrete being a combination of the two constituents. Since a major portion of the concrete

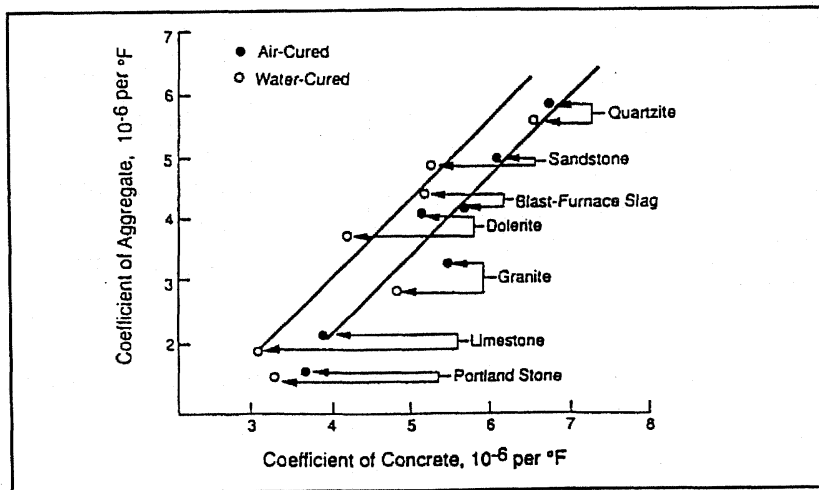


Figure 4. Influence of the linear coefficient of thermal expansion of aggregate on the coefficient of thermal expansion of concrete.<sup>(1)</sup>

volume is coarse aggregate, the primary factor influencing the coefficient of thermal expansion of concrete appears to be the coarse aggregate type. Of all the factors that may influence the development of the crack pattern, coarse aggregate type may be the most significant (a river gravel may have a coefficient of thermal expansion of approximately 60 percent higher than that for a crushed limestone). Figure 4<sup>(1)</sup> indicates how the CTE of the coarse aggregate affects the CTE of the concrete. Thermal coefficient of

expansion of concrete can influence the volumetric change due to temperature change. Thermal strains in concrete usually result from dissipation of the heat of hydration or cyclic changes in the ambient temperature. Figure 4 indicates, for practical purposes, that a linear relationship exists between the CTE of the aggregate and the CTE of the concrete. Table 1<sup>(1)</sup> gives the thermal coefficient values of different coarse aggregate types that were measured during a project conducted at the University of Texas at Austin. According to table 2, as the siliceous gravel content decreases, the thermal coefficient value decreases. It has been shown that the effect of silica content in the aggregate on the thermal coefficient of expansion of the concrete is very significant. The greater the silica content of the aggregate the greater the CTE of the aggregate<sup>(1)</sup>.

Loss of moisture is another characteristic of concrete that is related to the environmental conditions at the time of construction. Loss of moisture can affect concrete in terms of strength gain and in terms of induced strain relative to drying shrinkage.<sup>(4)</sup> Drying shrinkage depends to a great extent upon the water cement ratio used to place the concrete pavement. Other factors are related to the degree of hydration, moisture diffusivity, and the method of curing (discussed later) used during the concrete hardening process. These factors, which are indirectly related to the strength of concrete, are also important to the degree of permeability and durability achieved by the concrete. In design, although the amount of drying shrinkage that concrete will ultimately achieve is difficult to predict, the degree of drying shrinkage has been correlated to the concrete strength.<sup>(34)</sup> Australian practice for CRC pavement construction calls for a minimum compressive strength requirement for  $37 \pm 5$  mPa.<sup>(50)</sup> However, a further research is needed to better understand in design the balance that should be maintained between the amount of steel reinforcement and the requirements for concrete shrinkage relative to performance. Shrinkage should not be excessively reduced since a certain amount is necessary to adequately develop the crack pattern.

Table 1. Thermal coefficient values.<sup>(1)</sup>

Aggregate Type	Thermal Coefficient ( $\mu\epsilon/^\circ\text{F}$ )
SRG (Siliceous River Gravel)	8.18
SRG-LS	6.15
Dolomite	5.90
Granite	5.74
LS-SRG	5.44
LS/LS-SRG*	4.84

\*Blend of 50% LS (limestone) and 50% LS-SRG; Note:  $\Delta 1^\circ\text{F} = \Delta 0.6^\circ\text{C}$

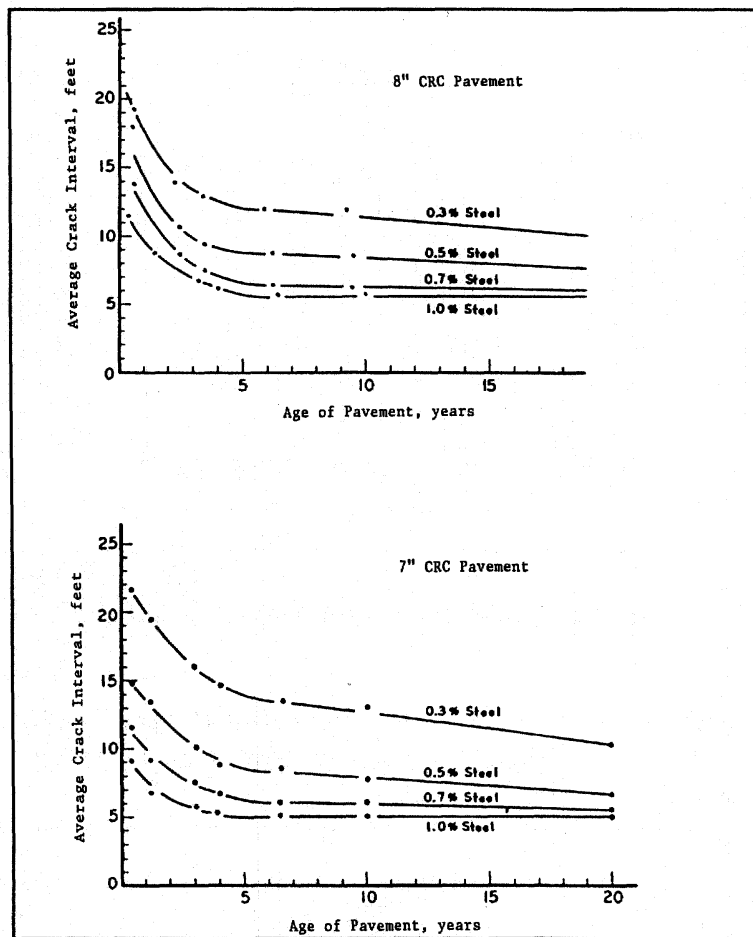
## Reinforcing Steel Characteristics

Steel is used in CRC pavement to develop the crack pattern because of high yield and tensile strengths characteristics. Since steel exhibits these characteristics, it is used in CRC pavements to maintain crack widths below certain limits. There are several pavement design variables related to steel bars which have significant effect on the cracking behavior of CRC pavements. They include such factors as percentage of longitudinal steel, longitudinal bar diameter, steel rib pattern characteristics, depth of cover, and the number of layers of longitudinal

Table 2. Coefficient of thermal expansion of aggregates and concrete.<sup>(1)</sup>

		Thermal Coefficient of Expansion per °F (x 10 <sup>-6</sup> / °F)			
		Rock		Concrete	
Rock Group	Normal Silica Content (wt. %)	Range	Average	Range	Average
Chert	94	4.1-7.2	6.6	6.3-6.8	7.3
Quartzite	94	3.9-7.3	5.7	6.5-8.1	6.7
Quartz	94	-	-	5.0-7.3	-
Sandstone	84	2.4-6.7	5.2	5.1-7.4	6.3
Marble	Negligible	1.2-8.9	4.6	2.4-4.1	5.9
Siliceous Limestone	45	2.0-5.4	4.6	4.5-6.1	5.9
Granite	66	1.0-6.6	3.8	4.5-5.7	5.3
Dolerite	50	2.5-4.7	3.8	-	5.3
Basalt	51	2.2-5.4	3.6	4.4-5.8	5.2
Limestone	Negligible	1.0-6.5	3.1	2.4-5.7	4.8
Glacial Gravel	5-95	-	-	5.0-7.6	-
Light-weight Aggregate	-	-	-	2.8-6.1	4.4

Note:  $\Delta 1^\circ\text{F} = \Delta 0.6^\circ\text{C}$



1 in = 25.4 mm, 1 ft = 0.305 m  
 Figure 5. Change in average crack interval over time for 178 mm and 203 mm (7 and 8 in) CRC pavement.<sup>(7)</sup>

steel. Pavement engineers in some countries are placing extra steel to stiffen free edges of jointed concrete pavements.<sup>(35-38)</sup> This practice may have some application to CRC pavement systems to minimize punch-out development particularly where widen lanes are not an options.

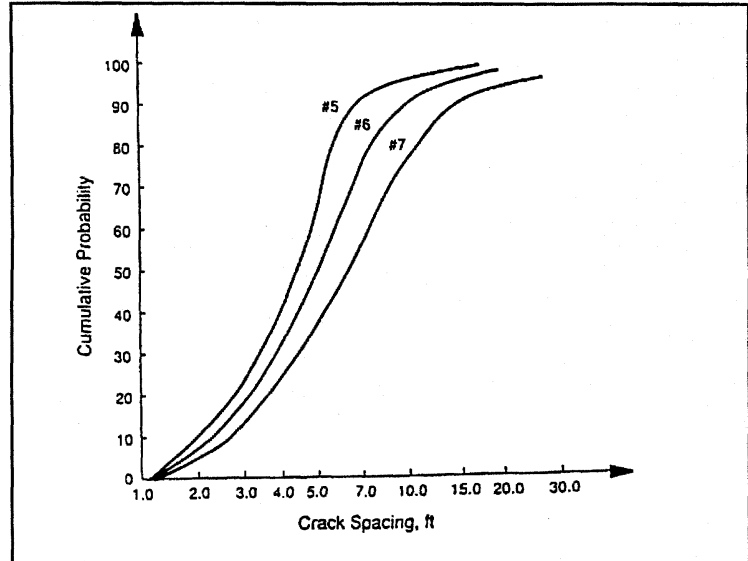
#### Percent of Longitudinal Steel

The reinforcement in CRC pavement causes a restraining effect to contraction strain, which increases as the amount of percentage of steel increases. Figure 5 shows the increased crack spacing associated with increased steel percentages for Vandalia, Illinois CRC test sections.<sup>(2)</sup> It is important to point out that the Q factor ( $4p/d_b$ ) is also changing significantly in these sections and is a key factor in affecting the crack pattern. In terms of crack spacing experience in the U.S. has indicated good performance with steel percentages of 0.55 to 0.70.

However, European experience has indicated good performance with percentages ranging from 0.65 to 0.85 percent. Relative to practical limits, it has been reported that the average crack interval does not significantly decrease with steel amounts above 1 percent while average cracking intervals may greatly increase with steel amounts below 0.4 percent. As pointed out previously, the Q factor must not be over looked in the role of the percent steel content on the crack pattern. As the percentage of longitudinal steel increases the crack widths decrease, the aggregate interlock increases, the load transfer increases, and stiffness at the transverse cracks improves<sup>(1)</sup>. Both field observations and design theories confirm that crack width in CRC pavements decreases with an increase in percentage of longitudinal reinforcement.<sup>(6)</sup> Season of placement and construction weather may also significantly effect the crack pattern. Key elements in the development of the crack pattern are steel design (p and Q) and weather conditions at the time of construction.

## Bar Size and Bond Characteristics

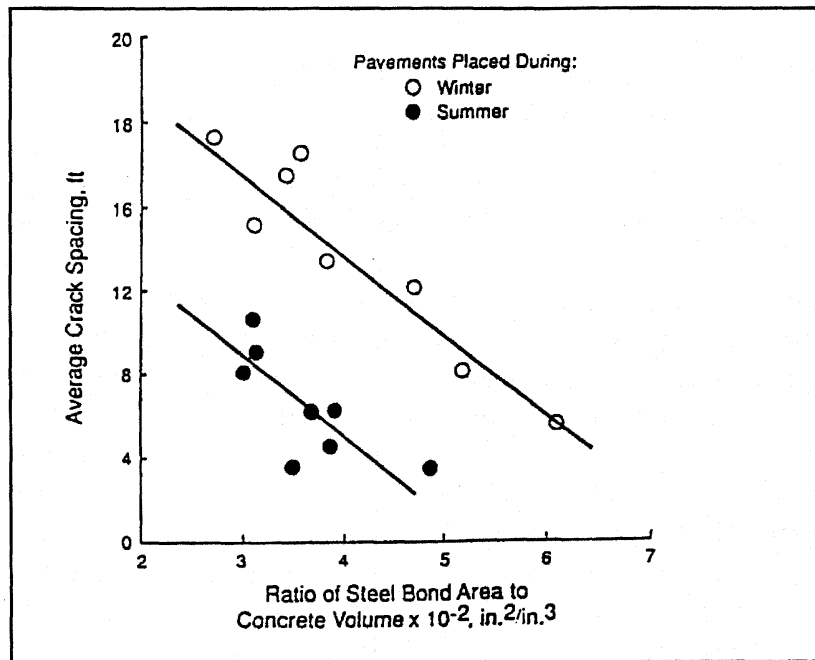
Bar size (as reflected in the Q factor) has an influence on crack development in that the restraint of the longitudinal steel depends on the bond area provided by the reinforcing bar. The development of concrete stress in CRC pavements results from the transfer of stress from steel to the concrete at the vicinity of the transverse crack. The stress transfer from the longitudinal steel to the concrete depends on the reinforcing steel surface area and the surface deformation shape of the longitudinal steel. For the same percent of longitudinal steel, the smaller size bar results in a larger steel surface area, which increases stress transfer from the steel to the concrete and results in a shorter crack spacing. The deformation pattern of the steel may also have an effect as would epoxy coating to a much lesser extent.<sup>(51)</sup>



1 ft = 0.305 m

Figure 6. Effect of bar size on crack spacing.<sup>(1)</sup>

Figure 6<sup>(9)</sup> shows the effect of bar size on the crack spacing. McCullough et al.<sup>(9)</sup> noted that the crack spacing was inversely proportional to the Q factor as shown in figure 7. Analysis and experience have indicated that the reinforcement Q factor will affect the crack spacing in CRC pavement and that the parameter Q is related to the time of year of construction. As a result, minimum Q values of 0.03 for summer construction and 0.04 for fall or winter conditions are recommended. Although no guidelines are available, it is



1 ft = 0.305 m, 1 in = 25.4 mm

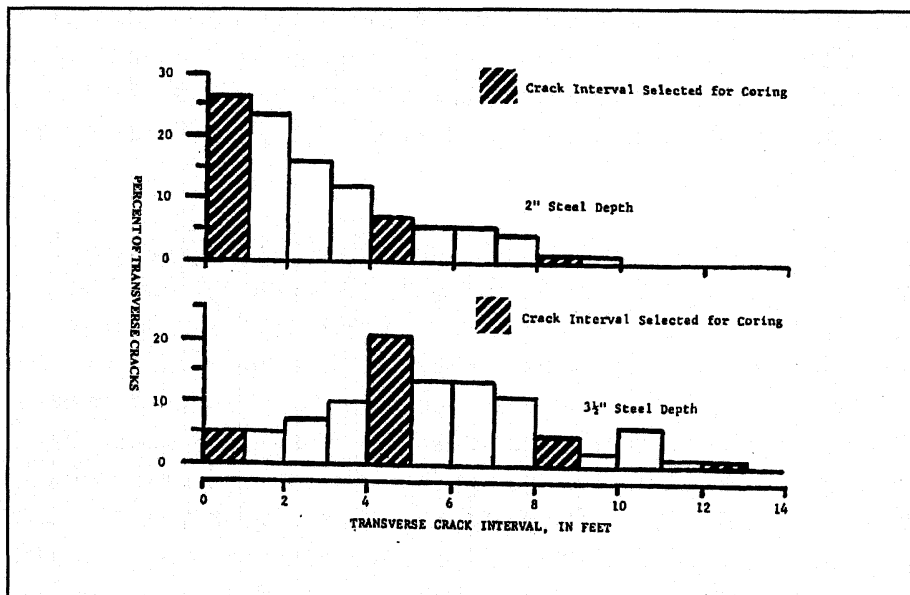
Figure 7. Relationship between steel bond area and crack spacing.<sup>(48)</sup>

suggested that these factors be increased 10 percent for epoxy coated reinforcement. It is pointed out, however, that one study indicated epoxy coated reinforcement has little effect on CRC pavement crack patterns.<sup>(51)</sup> Based on the equation for Q, it is evident how the value of Q can be held constant for various combinations of percent steel and the diameter of the reinforcing steel. The relationship of these rebar parameters suggests their sensitivity to crack pattern development. Studies have documented this sensitivity, which can also be related to transverse crack widths. However, coarse aggregate and effects due to construction weather, as noted above, may significantly influence this sensitivity.

### Depth of Cover of Longitudinal Steel

The vertical location of longitudinal steel has an effect on the crack pattern. The volumetric strains are greatest at the pavement surface and decrease with depth. If the steel is placed near the surface of the slab, the restraint to the induced movements increases, which

results in an increase in the number of transverse cracks. Figure 8<sup>(8)</sup> shows the significance of the effect of the vertical steel location on the crack pattern for Illinois CRC 178 and 203 mm (7 and 8 in) pavements with deformed bars and wire fabric reinforcement. Other studies<sup>(3)</sup> indicate that the reinforcement placed above mid-depth in the pavement will tend to cause an irregular cracking pattern although the



1 ft = 0.305 m, 1 in = 25.4 mm

Figure 8. Frequency histograms showing crack interval distributions.<sup>(8)</sup>

average crack spacings are closer. A survey<sup>(1)</sup> of CRC pavements in South Dakota shows an average crack spacing of 0.53 m (1.7 ft) with the steel 64 mm (2.5 in) below the surface, and an average spacing of 0.88 m (2.9 ft) with the steel 93 mm (3.68 in) below the surface. An aspect related to the depth of steel is the use of two layers of longitudinal steel. The position of the top layer of steel has been shown to be significant in past studies, and the use of two-layer placements has been adopted in Texas DOT construction standards<sup>(1)</sup> for pavements thicker than 330 mm (13 in) in order to maintain optimum steel bond area to concrete volume ratios. As pointed out previously, thicker pavements may experience a greater degree of volumetric

restraint due to a reduced depth of cover caused by use of two layers of reinforcing steel. Two layers of reinforcing steel also requires two layers of transverse steel, which tends to cause a weakened plane of transverse cracking. A high incidence of transverse cracking coincidental with the position of the transverse steel was noted on projects in Texas<sup>(39)</sup> that used two layers of reinforcing steel where the transverse bars in each layer were vertically aligned. Transverse steel in Belgium is placed in a skewed orientation (rather than orthogonal) with respect to the longitudinal steel as recommended by PIARC.<sup>(49)</sup>

### **Climatic Factors**

Ambient temperature conditions will affect the crack pattern in CRC pavements primarily to the extent it influences the thermal gradient and uniform temperature changes within the slab. Naturally, geographic location affects the climate to which concrete pavement may be exposed. Temperature ranges (highest annual temperature minus lowest annual temperature) can be as large as 65.5°C (150°F), depending on the location. Historical temperature records may be used to establish these temperature levels, however, normal temperature ranges may not be as severe as indicated by such records. Whatever the basis for the minimum temperature, the expected minimum yearly temperatures have been used in design because they have correlated well in terms of prediction of crack width of the transverse crack based on the average crack spacing and the amount of linear slab movement.<sup>(1)</sup>

The cracking process in CRC pavement consists of cracking both at an early age and at later ages as previously noted. It is important to point out that some cracks that initiate at an early-age may not become evident at the surface for several years. Cracking of this nature in CRC pavements is propagated in part by daily, nonuniform temperature change within the pavement due to changes in ambient temperature conditions. Shrinkage and contraction stresses that cause cracking to develop at an early-age are the result of restrained movement caused by temperature and moisture changes. Even though concrete and steel can have a relatively similar coefficient of thermal contraction (0.000005 in/in/°F) depending on the aggregate type, stresses develop in part because the reinforcing steel has a higher modulus of elasticity than the concrete. Consequently, the stress intensity within the concrete becomes too high and the crack propagates. A similar effect may result from early-aged concrete shrinkage. The stress intensity in both instances is enhanced due to the resistance between the subbase and the slab. As a result, high temperature drops and moisture loss are as associated with drying shrinkage conducive to rapid crack development. This can occur under summer weather and windy conditions where concrete pavement is placed in the morning hours leading to maximum setting temperatures and stresses that can cause cracking as early as the next day or later (2 to 3 days) depending on the type of aggregate used.<sup>(45)</sup> Delayed early-aged cracking can also result under some circumstances due to a buildup of drying shrinkage in combination with temperature effects.

Vetter<sup>(5)</sup> has developed the following equation that indicates the percentage of steel required to hold shrinkage and temperature cracks intact to prevent yielding of the steel:

$$p = \left[ \frac{S_c'}{S_s + zE_s - nS_c'} \right] 100 \quad (4)$$

where

- $S_c'$  = ultimate tensile strength of the concrete
- $S_s$  = elastic limit of steel

According to Vetter, the distance between the cracks is described by the following equation:

$$L = \frac{(S_c')^2}{np^2 \frac{\Sigma_o}{A_s} u(zE_c - S_c')} \quad (5)$$

where

- $L$  = length between cracks
- $\Sigma_o$  = perimeter of reinforcing bar in inches
- $A_s$  = required steel per foot of width

In order to achieve adequate cracking patterns, a certain amount of temperature change and drying shrinkage needs to occur to ensure a certain level of cracking. If induced stress levels are too low (due to excessive curing), then crack patterns may be too far apart or contain too many clusters of closely spaced cracks to provide adequate performance or the opposite can be the case if the induced stress levels are too high. In terms of the factors that affect the development of the crack pattern, there are a number of combinations that must be balanced to achieve the required pavement performance. Additional research will lead to design products for CRC pavements to indicate material combinations and construction methods to achieve appropriate shrinkage and temperature sensitivity levels to enhance optimal performance of the pavement.

### Time and Season of Placement

Concrete strength gain rates due to environmental conditions during fall and winter time periods are the lowest since the prevailing temperatures are typically the lowest. Therefore, concrete placed in this time of year may have less time to develop sufficient concrete strength before maximum cracking stress occurs than concrete placed in the spring or summer. Concrete pavement placed in the fall is considered to have a shorter crack spacing than that placed in the spring due to the relatively lower concrete strengths caused by typically lower ambient temperatures. However, this effect may be somewhat offset because the reference temperature (upon which the concrete stresses are based) is also lower in comparison to construction periods

at hotter times of the year. CRC pavements, particularly those placed with river gravel coarse aggregates, constructed under cool weather conditions develop longer crack spacing and smaller crack widths than those placed in the summer months under warm weather conditions. Because of the greater drying shrinkage under hot weather conditions, CRC pavement performance may be significantly affected due to the effect seasonal conditions have on the resulting crack widths.<sup>(39)</sup>

Whether the concrete was placed in the morning or the afternoon can affect CRC pavement cracking behavior, as previously pointed out. Concrete placed in the morning typically sets at higher temperature and consequently develops greater stress-related cracking than concrete placed in the afternoon. The effect is that concrete placed in the morning has shorter crack spacings than concrete placed in the afternoon.<sup>(1, 45)</sup> These effects on the crack pattern are independent of those that result from excessive subbase bond.

### Curing Conditions

The curing temperature at the time of concrete slab placement also affects cracking in CRC pavements. The pavements constructed at higher curing temperatures have shorter cracking spacings than the pavements constructed at lower temperatures.<sup>(45)</sup>

A factor that affects the development of cracking in CRC pavement is the curing methods used during the paving process. A significant amount of cracking occurs early in the pavement life. The cause of this cracking may be related to how concrete is cured.

It is generally accepted that the more the water loss from the concrete mixture during the hardening process, the greater will be the shrinkage and the lower the degree of hydration. Therefore, concrete shrinkage stress will have a greater potential to exceed the concrete strength inducing early-aged cracks in the CRC pavements. Curing of CRC pavements is a crucial step in minimizing early cracking potential of CRC pavements. The most common method for curing concrete pavements is membrane curing. The curing methods are as follows:

- (1) Membrane curing compound
- (2) Polyethylene film curing, and
- (3) Cotton mat curing.

The research conducted by Tang et al.<sup>(39)</sup> revealed that both cotton mats and polyethylene film reduced daily temperature variation and reduced moisture loss from the pavement surface. Accordingly, the number of surface cracks in pavements that develop initially with cotton mat or polyethylene curing is much lower than that cured with membrane compound.

It should also be pointed out that drying shrinkage in the field may not match the drying shrinkage found from laboratory specimens since the drying condition may be very different. Under hot weather paving conditions, early shrinkage and creep may be absorbed by the early-

aged cracks that then tend to be wider than the cracks that develop at a later age. Therefore, different amounts of drying shrinkage should be taken into account depending not only on the age of the concrete but also on the method and conditions of curing.

### **Importance of the Cracking Interval**

Now that the important factors relative to the evolution of the crack pattern in CRC pavements have been delineated, it is important to understand the significance of the crack pattern in terms of the performance of CRC pavement with respect to the potential for distress development, which can occur in one of two forms. One form is associated with wide transverse cracks that often occur with wide crack spacings or clustered crack patterns. Wide cracks are frequently associated with steel corrosion (in the vicinity of the crack) that consequently increases the potential for steel rupture. The end result, once the longitudinal steel fails, is faulting on widened transverse cracks. The second form of distress is the loss of load transfer on adjacent transverse cracks leading to the development of a punchout—the greatest concern of designers of CRC pavements. The punchout process is associated with load transfer mechanisms inherent to the behavior of CRC pavement. Certainly a widened crack results in a significant decrease in load transfer but punchout distress is always associated with aggregate interlock wearout and the loss of load transfer on two adjacent, closely spaced cracks. The focus of identified failure modes of the punchout process is consequently closely aligned with the load transfer, crack width, and the effective slab bending stiffness of adjacent transverse cracks characteristic to CRC pavement as discussed below. Detailed field and laboratory study<sup>(2)</sup> has clearly indicated that punchouts are initiated as a result of lost or reduced pavement support rather than as a result of ruptured steel reinforcement, as commonly heretofore assumed. Relative to punchout formation, rupturing of the steel reinforcement does not (if it does at all) occur until well into the final stages of the punchout process and, consequently, is only an artifact of the loss of support, load transfer, and pavement stiffness. As previously noted, steel rupturing is a factor primarily in cases of widened transverse cracks where advanced corrosion has severely reduced the cross-sectional area of the reinforcement. The ruptured steel in this instance results in cases of widened transverse cracks that leads to faulting of the transverse crack where punchouts frequently occur in the absence of widened transverse cracks.

### **Basic Failure Modes Leading to Punchout Distress**

Punchout development in CRC pavement systems is closely tied to the degree of support provided in the pavement structure. Although punchouts are recognized as the primary form of distress in the performance of CRC pavements, CRC pavements in the 200 to 230 mm thickness range have performed very well (with no punchouts) sustaining several million ESALs. Even though performance of this level of traffic can be achieved with good design practice and adequate crack widths, it is still important to consider the mechanisms associated with this form of distress.

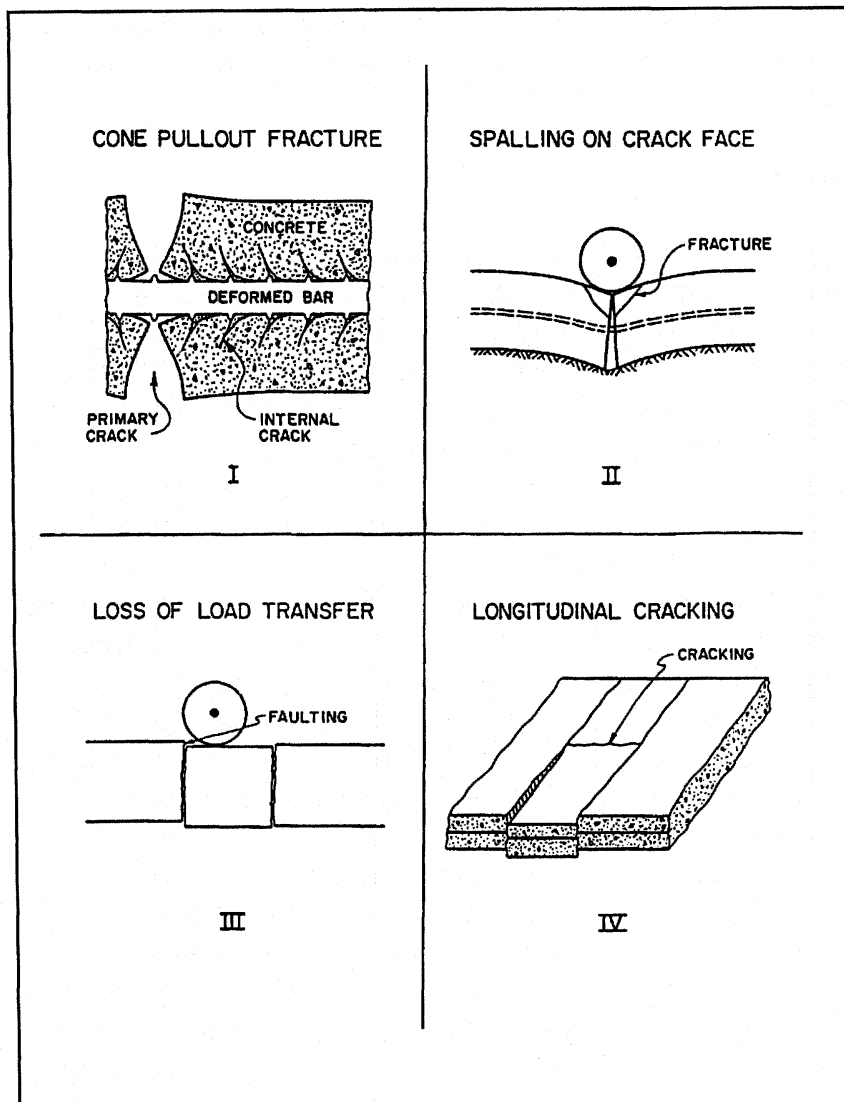


Figure 9. Failure modes related to punchout distress in CRC pavement.<sup>(2)</sup>

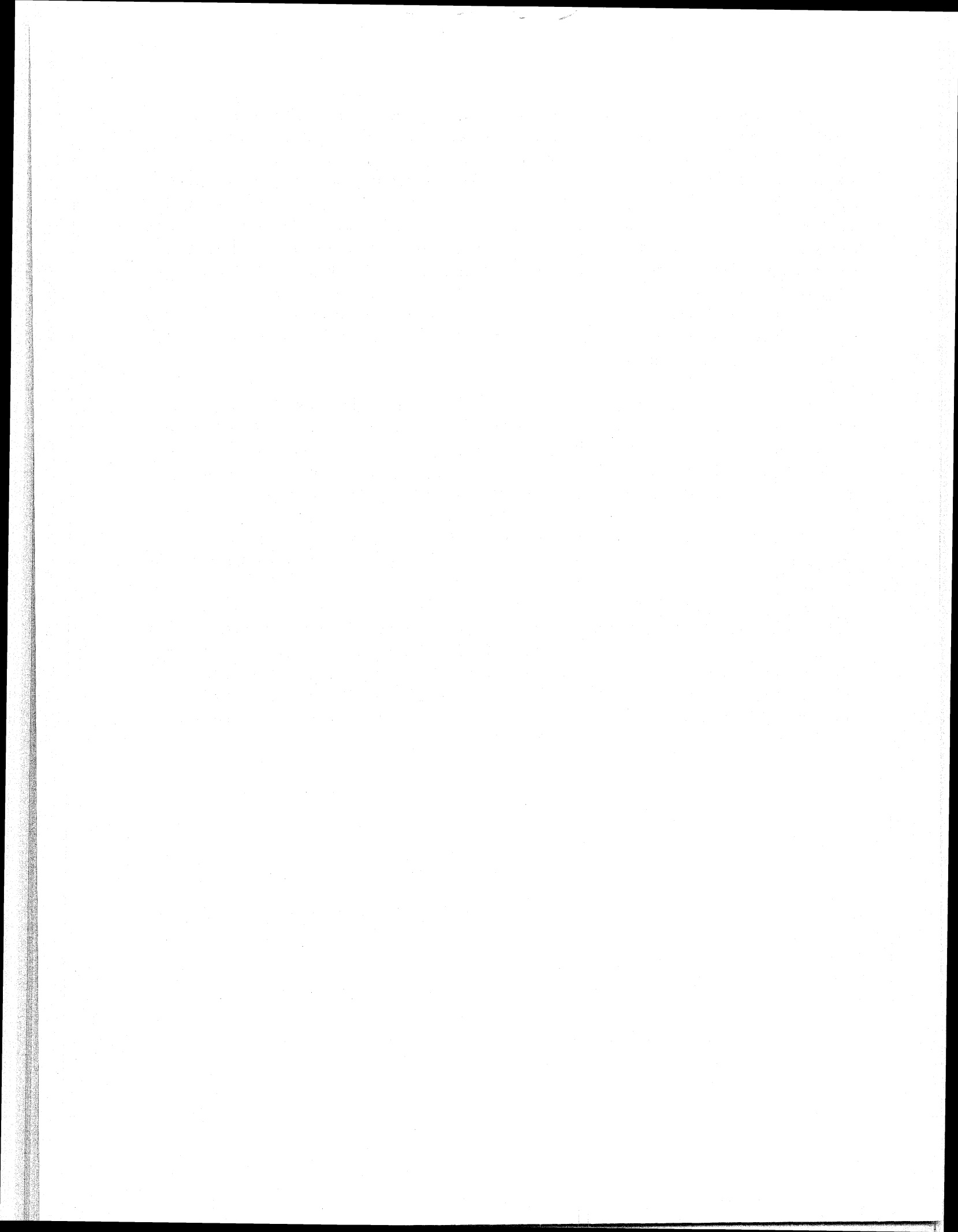
Four failure modes relating to punchout distress have been identified (and verified in this study) based on field observations<sup>(2)</sup> that comprise the fundamental failure mechanism of CRC pavements developing punchout distress. The development of these failure modes is based a priori on uniform support conditions. The failure modes are illustrated in figure 9 in typical developmental sequence. The first three modes of failure are associated with factors contributing to the loss of load transfer across the transverse crack. Mode I focuses on concrete fracturing associated with the reinforcing steel at the crack face. Cracking with this form is due to reinforcing bar pullout from the surrounding concrete. Fracturing of this nature has been noted in concrete pullout tests<sup>(10, 11)</sup> and develops in the concrete at a

steel stress range of 96.5 to 124.1 kPa (14 to 18 ksi). Field measurements of steel strains at the crack face indicate that this range of stress is frequently exceeded in the colder months of the year. Cyclic bond stresses in the concrete induced from environmental factors can result in a crack growth process, noted in the field study, around the reinforcing bar, effectively destroying the load transfer capability of the bar as a void develops. In addition, a loss of bond stiffness<sup>(12)</sup> and pavement bending stiffness occurs. Bearing failure or rebar looseness can also lead to a void around the reinforcement and can have a detrimental effect upon the pavement performance similar to what the pullout fracture does. Pullout failure may be difficult to avoid since the threshold stress is frequently exceeded. In any case, the load transfer contribution of the reinforcing steel (relatively small bearing areas and small diameters) should be ignored in design.<sup>(2)</sup> This emphasizes the importance of crack width on pavement stiffness and performance.

Mode II failure, spalling of the transverse crack, affects the pavement stiffness at the transverse crack. Due to the development of voids around the reinforcing steel described above, the pavement stiffness is significantly reduced. As pointed out below with regard to mode III failure, a reduction in pavement stiffness at the cracks may also develop due a gradual loss of aggregate interlock and load transfer efficiency.<sup>(12)</sup> The pavement stiffness cycles between high and low, mostly as a function of the temperature and the concomitant opening and closing of the transverse cracks. The reduced stiffness behavior, which occurs on a daily basis, can be assumed to predominate during the winter season. Reduced pavement stiffness is not only a function of the crack width<sup>(13)</sup> but also of the position of the reinforcing steel<sup>(14)</sup> among other factors discussed later in chapter 3. The narrower the transverse cracks, the stiffer the overall pavement system, which in turn lowers spalling-related stresses. This mode of failure is a visual sign of progressive punchout development.<sup>(2)</sup>

Failure mode III, shown in figure 9, is a loss of load transfer along transverse cracks due to wear out of the aggregate interlock. Since the reinforcing steel provides little load transfer, the load transfer of the crack is solely a function of the crack width. Given a constant crack width, the load transfer will decrease under repetitive loading. Loss of support due to erosion plays a major role in accelerated wear out of the aggregate interlock along a transverse crack.

The final mode of failure, mode IV, is related to bending stresses in the transverse direction. These stresses typically are not significant in CRC pavement so long as there is a high load transfer across the cracks (prior to spalling), a high quality of support, or the crack spacing is greater than 1.2 m (4 ft).<sup>(2, 46)</sup> The process relative to CRC pavement design can be optimized with respect to crack spacing and crack width. Obviously, the need for erosion resistant subbase system is required to insure quality performance for CRC pavements. This normally requires that stabilized subbases consist of approximately 8 percent cement. As previously pointed out, AC interlayers provide the optimal combination of bond and friction to develop desirable crack patterns in CRC pavement. Excessive bonding of the slab to cement stabilized subbases often results in poor crack patterns and wide crack widths.



## CHAPTER 3 - IMPROVED CRC PAVEMENT THICKNESS DESIGN CONCEPTS

Early thickness designs for CRC pavements were based on the premise that CRC thicknesses did not need to be as great as jointed concrete pavement thicknesses due to a certain equivalence in structural capacity. Past and present thickness design procedures consider several factors associated with the prediction of the average crack spacing due to contraction restraint. Crack prediction methods included in these procedures are based on environmental stresses and material thermal properties of the concrete and steel. The design crack spacing is limited to certain criteria to minimize the potential of punchout distress, thus indirectly arriving at a design thickness. Based on the performance factors indicated in chapter 2, it is apparent that CRC pavement thickness design should also consider load transfer characteristics of the transverse crack and the mechanisms associated with it. In terms of the punchout mechanism previously elaborated in chapter 2, the prevention of steel rupture as a design objective is well encompassed within the provision of load transfer across the transverse cracks.

### Present CRC Design Methodology

Existing CRC pavement design procedures are based on either a thickness ratio between CRC pavement and jointed concrete pavement design thickness and/or indirectly related to limiting design criteria for selected structural response parameters (i.e., crack width, steel stress, and cracking spacing). The latter criteria focuses on the prediction of crack spacing, crack width, and steel stress as a function of thermal material properties and environmentally induced contraction stress and strain. The design crack width and steel stress are dependent upon the design crack spacing, which is primarily a function of the size and percentage of steel reinforcement. Although very important to the performance of CRC pavement, present CRC design methodology ignores crack width requirements (relative to support conditions) as far as they pertain to the degree of load transfer afforded by a transverse crack in CRC pavement systems.

Previous field studies have identified definite trends between average crack spacing and percent reinforcement. The average decrease in crack spacing due to an increase in reinforcement may result in a decrease in the rate of punchout distress. In spite of this, the effects caused by changes in the reinforcement are apparently not as predominant as other factors that also influence the distribution of crack spacing. These other factors are largely dependent on weather conditions at the time of paving and their pertinence to drying shrinkage and moisture loss characteristics of the concrete used for paving. Greater attention should perhaps be afforded the mix design and the methods of curing (elaborated in chapter 4). The effects of wheel load stress may also tend to propagate cracking in CRC pavements which most likely was initiated during the early life of the pavement. Apparently, few load applications are required to cause this additional cracking to show on the pavement surface since, historically speaking, the cracking pattern in the adjacent paving lanes subjected to different traffic levels is similar. The probability of cracking due to Westergaard interior and edge load conditions may be very remote because of the low level of stress due to the nature of the crack pattern. If the focus of the design

is based on the pavement stresses associated with short crack intervals, then wheel load stresses in the longitudinal direction are not and should not be a major concern; transverse stresses are more important and are a function of the degree of load transfer provided by the transverse cracks. Inclusion of a punchout mechanism in thickness design should center on transverse stresses, which if great enough (due to poor load transfer conditions), will cause longitudinal cracking in CRC pavements.

As previously indicated, existing design procedures noted in the American Association of State Highway Transportation Officials (AASHTO), and the Continuous Reinforcing Steel Institute (CRSI), etc. do not directly consider specific limiting crack width criteria in terms of ranges of load transfer for optimal pavement/punchout performance. Therefore, a design tool that is needed and would prove to be very useful is one providing a relationship between load transfer, crack width, and the percent reinforcement for a given crack spacing. Control of crack width is the key to good performance of CRC pavement as facilitated through uniformly configured and optimally spaced cracks.

Correlations between CRC pavement thickness and jointed pavement thickness are taken from present serviceability index ratings for jointed concrete pavement. The thickness design of jointed pavements was derived from the performance equations developed from the AASHTO Road Test predicting the future serviceability as a function of 80 kN (18 kip) single-wheel load applications. These methods usually resulted in thicknesses less than that for jointed concrete pavement. The performance equations are based on traffic level, concrete strength, modulus of support, load transfer, terminal serviceability, and design reliability. It should be pointed out that the applicability of these equations to CRC pavement design has never been verified.

Several early failures have been attributed to excessive deflections under heavy loads suggesting that greater thickness will improve performance. Moving towards greater design thicknesses for CRC pavements is likely to be beneficial for performance, but it appears that the recommended increase in thickness is arbitrarily determined in the most recent version of the AASHTO Design Guide. Since punchouts are the primary type of distress in CRC pavements, the need to achieve a greater understanding of punchout distress, pavement support, and load transfer mechanisms and how they relate to design thickness and pavement performance is obvious to establish a basis for improved CRC pavement design practice.

### **Basic Failure Modes in Terms of a Design Framework**

Early thickness designs for CRC pavements were based on the premise that CRC pavement thicknesses did not have to be as great as jointed concrete pavements as offset by assigned equivalencies in structural capacity. This reduction in pavement thickness was pursued from a first cost basis to allow CRC pavements to be more competitive with jointed concrete pavement systems. These design procedures considered the important design factors to be those related to the development of the crack pattern due to contraction restraint. However, these methods do not directly address the effect of shear and load transfer across the transverse crack. Since it is clear

that the punchout process, as associated with load transfer mechanisms on transverse cracks on transverse cracks in CRC pavements should be the focus of CRC pavement design, the analysis of the failure modes is closely related to the level of wear out of load transfer, and the width of the crack along with the effective slab bending stiffness across the transverse crack. As far as a design framework, it will be important to represent the effect of the loss of load transfer across the transverse crack due to failure modes I, II, and III in terms of aggregate wearout and pavement support across the transverse cracks in CRC pavement systems.

Shear and Load Transfer Mechanism Across a Crack

As suggested in the description of failure modes I, II, and III, a reduction in pavement stiffness may result either from rebar pullout; from bearing failure around the steel; from

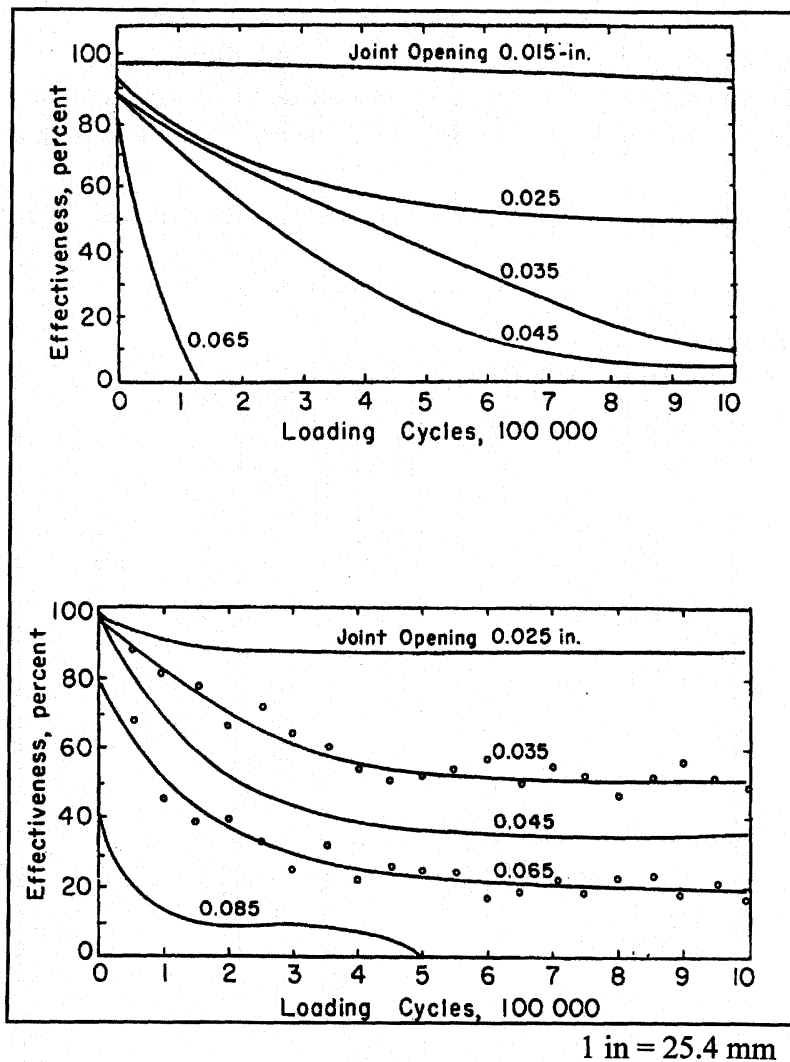


Figure 10. PCA joint load transfer tests.<sup>(16)</sup>

spalling; or from aggregate wearout. All have been observed in field studies. With respect to the loss of load transfer due to aggregate wearout, Colley and Humphrey<sup>(16)</sup> of the Portland Cement Association (PCA) investigated the effect of the aggregate interlock on load transfer characteristics in concrete pavements (figure 10). This study was conducted using an instrumented test slab containing a transverse joint subjected to a repetitive 40 kN (9 kip) load. The joint in the test slab was an induced crack from a metal strip 25.4 mm (1 in) in height placed at the pavement bottom and the top. During the repetitive loading, measurements of joint opening and slab deflections on the loaded and unloaded slab were made at regular intervals. The loading sequence across the joint was similar to a continuous application of truck loads traveling approximately 48 km/h (30 mi/h). Test results in

the form of joint effectiveness (EJ—which is different from load transfer efficiency), joint opening, and loading cycles for a 17.8 and 22.9 mm (7 and 9 in) slab thickness using a 15 cm (6 in) gravel subbase were obtained. The load transfer efficiency (LTE) is the unloaded deflection divided by the loaded deflection, in percent.

The results indicate the joint effectiveness tends to level off after about 700,000 to 800,000 load applications (figure 10). The level of joint effectiveness at various levels of applications may provide a useful basis relating joint or crack width to joint effectiveness for design purposes. Figure 10 provides an indication of the relationship between joint effectiveness and the joint opening for the 17.8 and 22.9 mm (7 and 9 in) thicknesses.

The PCA test data provide the basis in which to develop a universal relationship between the shear capacity ( $\tau$ ) generated through aggregate interlock on the transverse crack interface relative to the deflection load transfer efficiency (LTE) of the joint in the test slab. This relationship is key with respect to characterizing the correlation for a CRC pavement configuration and support condition to the degree of shear capacity at a transverse crack interface and the load transfer across a transverse crack. In terms of design, it is convenient to characterize

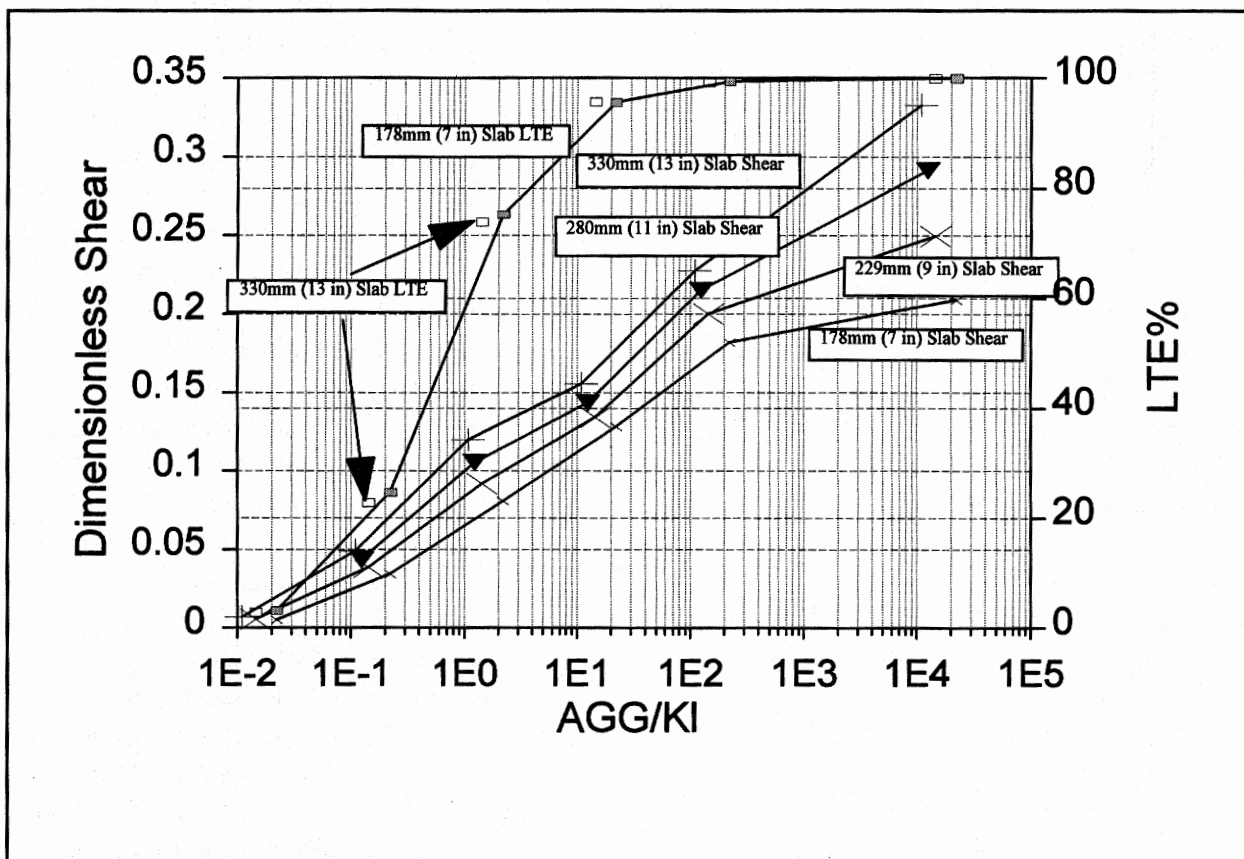
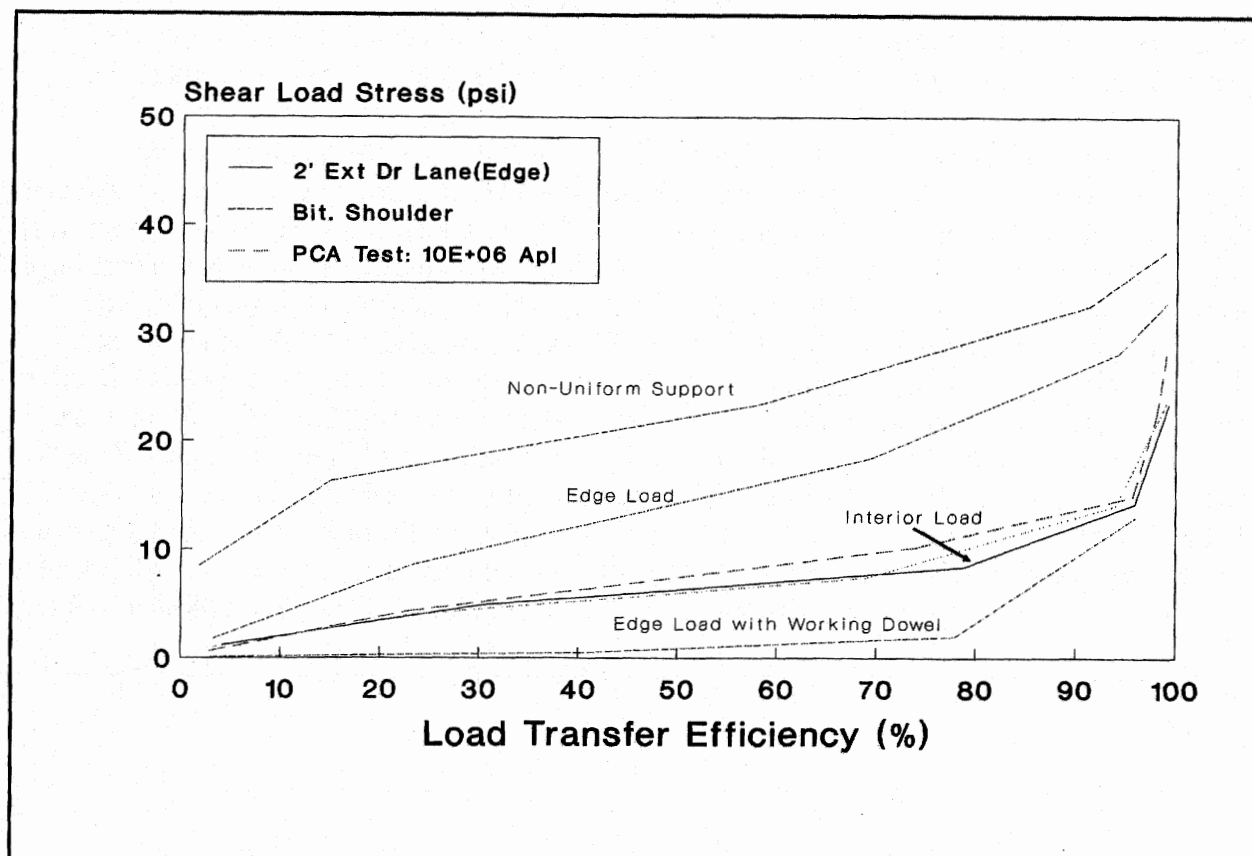


Figure 11. PCA test slab results relative to dimensionless shear and joint stiffness.



1 psi = 6.89 kPa, 2 ft = 0.6 m

Figure 12. Shear load stress for various load conditions of a 229 mm (9 in) CRC slab.<sup>(2)</sup>

shear capacity in terms of a dimensionless shear parameter ( $\tau h^2/P = s$ , where  $h$  is the pavement thickness and  $P$  is the wheel load).<sup>(15)</sup> This dimensionless parameter can be correlated to a dimensionless joint or crack stiffness parameter ( $AGG/k\ell$ , where  $AGG$  is the aggregate interlock factor,  $k$  is the  $k$  value of the foundation support, and  $\ell$  is the radius of relative stiffness). The deflection LTE is related to the dimensionless parameter  $AGG/k\ell$ , which is in turn related to the dimensionless shear as illustrated in figure 11.

From analysis, shear stresses can be found for different CRC slab loading configurations as shown in figure 12 and compared to the PCA test slab conditions. Comparison of a CRC pavement under an edge loading condition (with a bituminous shoulder) with a CRC pavement under an interior loading condition with a 0.6 m (2 ft) extended driving lane is made in figure 12 to the load configuration used for the PCA test slab. Greater shear stresses (and a greater rate of loss of load transfer) occur in CRC pavements with bituminous shoulders. The edge loading of a bituminous shoulder with nonuniform support represents the most severe loading conditions in terms of shear stresses on the crack interface. The loading condition for a 0.6 m (2 ft) extended driving lane is not as severe as the loading conditions for the PCA test slab. Little difference in

shear stress is noted between the interior load position (inner wheel path) and the edge load position with the extended driving lane. Similar results were found for a tied concrete shoulder.

The magnitude of the shear loading can be accounted through the relationship of dimensionless shear stress ( $\tau h^2/P$ ) to joint stiffness ( $AGG/kl$ ) as a function of pavement thickness ( $h$ ) and shoulder configuration.<sup>(17)</sup> The importance of this relationship, illustrated in figure 11, is key to determining how load transfer is lost as shear capacity is reduced due to crack widening or load repetition. The loss of load transfer in a CRC pavement system results in an increase in cracking stress. Since crack width significantly affects load transfer and slab shear capacity, shear capacity-crack width relationships were extracted from the PCA test data and illustrated in figure 13. Slab shear capacity is illustrated prior to and after load application for 178 mm and 229 mm (7 and 9 in) thicknesses. A shear capacity curve based on a laboratory study<sup>(15)</sup> is also included in figure 13. The PCA test data indicate that there are certain threshold crack widths before loss of shear capacity will occur. A load transfer wearout function can be generated from this data as a component of a design process for CRC pavements based on 1 million-9 kip load applications. A function such as this should relate crack width ( $cw$ ), load cycles ( $N$ ), and shear

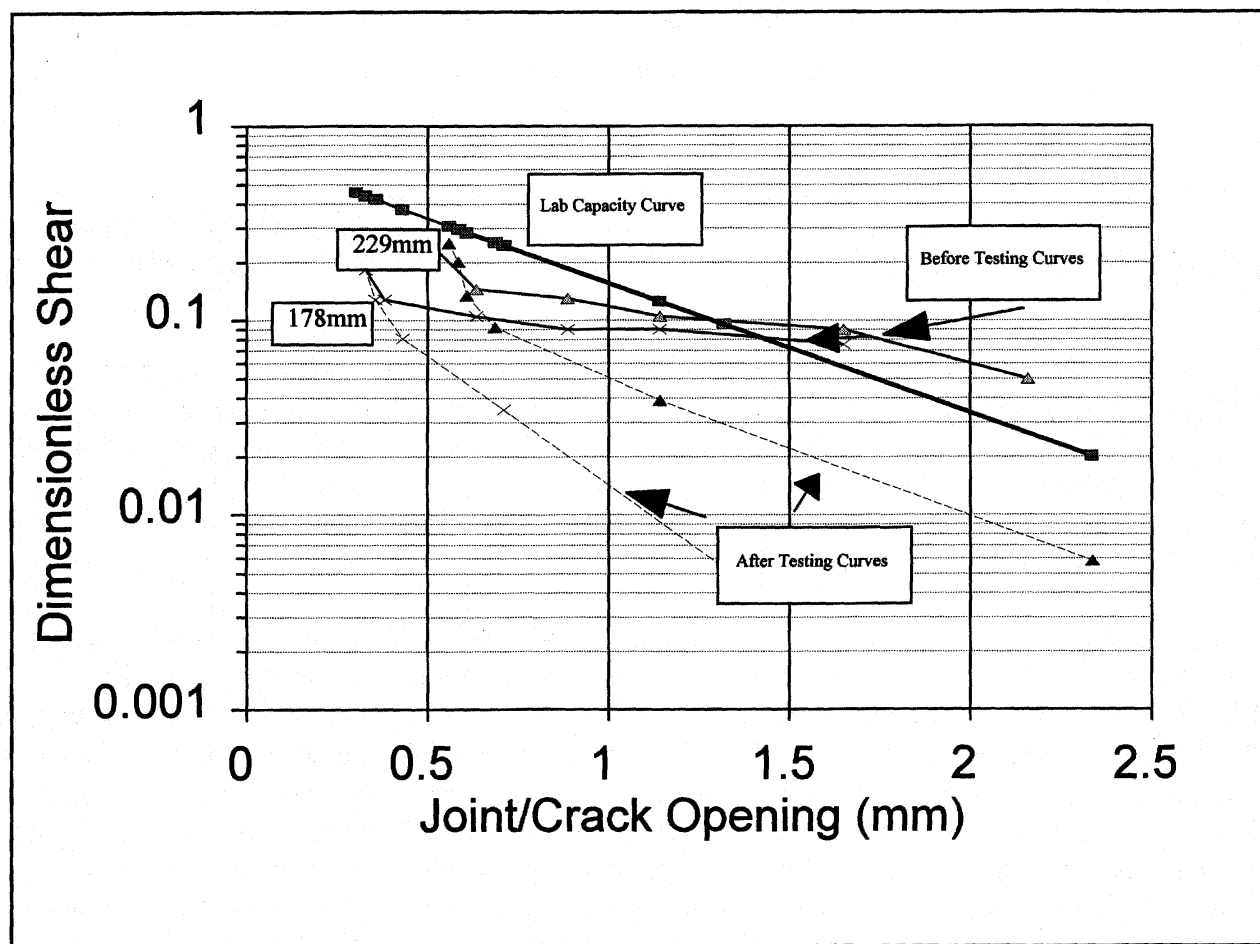


Figure 13. Shear capacity relationships based on PCA tests and laboratory test data.

stress to the loss in shear stress capacity ( $\tau h^2/P$ ). The PCA and laboratory test results referred to above have universal applicability to concrete pavement systems through the dimensionless shear parameter where it is unique to each pavement type.

### Thickness Design Procedure

The emphasis of the thickness design procedure is to maintain a high level of load transfer efficiency and to limit fatigue cracking from resulting in premature punchout distress. Bending stresses associated with fatigue cracking are closely tied to load transfer efficiency and the degree of support at each transverse crack. As previously pointed out, load transfer efficiency is a function of the crack width and shear capacity of the transverse cracks. The crack width depends upon the crack spacing, the thermal coefficient of expansion of the concrete, and the design steel percentage. This means that the spacing between individual transverse cracks is of vital interest to the pavement design engineer since maintaining a high level of load transfer will be largely dependent upon the width of individual transverse cracks.

In the design of CRC pavements, if the crack spacing pattern occurs randomly and is assumed to be normally distributed over a given range of cracking intervals (and since crack width is relative to crack spacing), a certain amount of variability can be assigned to the crack width and the load transfer across the transverse cracks. In fact, the crack width variability can be expressed relative to the variability of the crack spacing, concrete strength, and maximum temperature drop from curing temperature at the time of construction.

Based on recent developments in CRC pavement construction technology relative to improved crack patterns discussed in chapter 4, the crack pattern can be positively controlled through the use of early-aged sawcutting to preselected intervals or allowed to occur randomly as is the current practice in CRC pavement construction technology. In the case of the latter, the mean crack spacing may be used to estimate the mean crack width (subsequently discussed); otherwise, the design crack spacing as generated from the incorporation of early-aged sawcutting technology is used to estimate the crack width. It should be pointed out that there is also a considerable reduction in crack width and crack spacing variability (and consequently, pavement performance) associated with this case that should be accounted for in the assessment of the variability associated within the thickness design process.

The basic design process can focus on the prediction of longitudinal cracking prerequisite to the formation of punchout distress in the form of a Weibull-related distribution cracking function:

$$\%C = 100 \cdot e^{-\left(\frac{D}{\alpha}\right)^{\beta}} \quad (6)$$

where  $D$  is the accumulated fatigue damage (due to slab bending in the transverse direction) and  $\alpha$  and  $\beta$  are cracking calibration constants. The fatigue damage due to wheel load and environmentally related stress can be accumulated according to Miner's Damage Hypothesis<sup>(18)</sup> by summing the damage over the entire design period. The damage equation is:

$$D = \sum_{k=0}^{k=P} \sum_{j=1}^{j=3} \sum_{i=1}^{i=m} \frac{n_{ijk}}{N_{ijk}} \quad (7)$$

where

- $D$  = total accumulated fatigue damage over the design period occurring at the critical fatigue location in the slab,
- $n_{ijk}$  = number of applied axle load applications of the  $i^{\text{th}}$  magnitude over environmental gradients or conditions for the number of occurring  $k$  values over the design period,
- $N_{ijk}$  = number of allowable axle load applications of the  $i^{\text{th}}$  magnitude over the identical cases for  $N_{ijk}$ ,
- $i$  = a counter for the magnitude of load,
- $j$  = a counter for daytime and nighttime temperature gradients or conditions,
- $k$  = a counter for the particular case of  $k$  value, and
- $m$  = total number of single axle load groups.

The applied traffic  $n_{ijk}$  is computed using traffic data for the design period. Load equivalency ratios are applied (in terms of EDR values - discussed later) to the seasonal and daily breakdown of the traffic to obtain the number of load applications (bending) for design analysis. This method is similar to that used to calculate the accumulated fatigue damage for jointed concrete pavement. The allowable axle load applications ( $N_{ijk}$ ) are estimated using:

$$\text{Log } N_d = 17.61 - 17.61 * R \quad (8)$$

where

- $N_d$  = number of allowable load applications, and
- $R$  = ratio of applied wheel load stress to modulus of rupture (stress ratio =  $\sigma_{\text{tot}}/\text{MOR}$ ).
- $\text{MOR}$  = Modulus of Rupture

The applied stress used in the above equation is the total of wheel load stress and environmentally induced stress, which will vary depending on the base type, shoulder configuration, the level of LTE, crack spacing, and other factors to be elaborated later in this chapter.

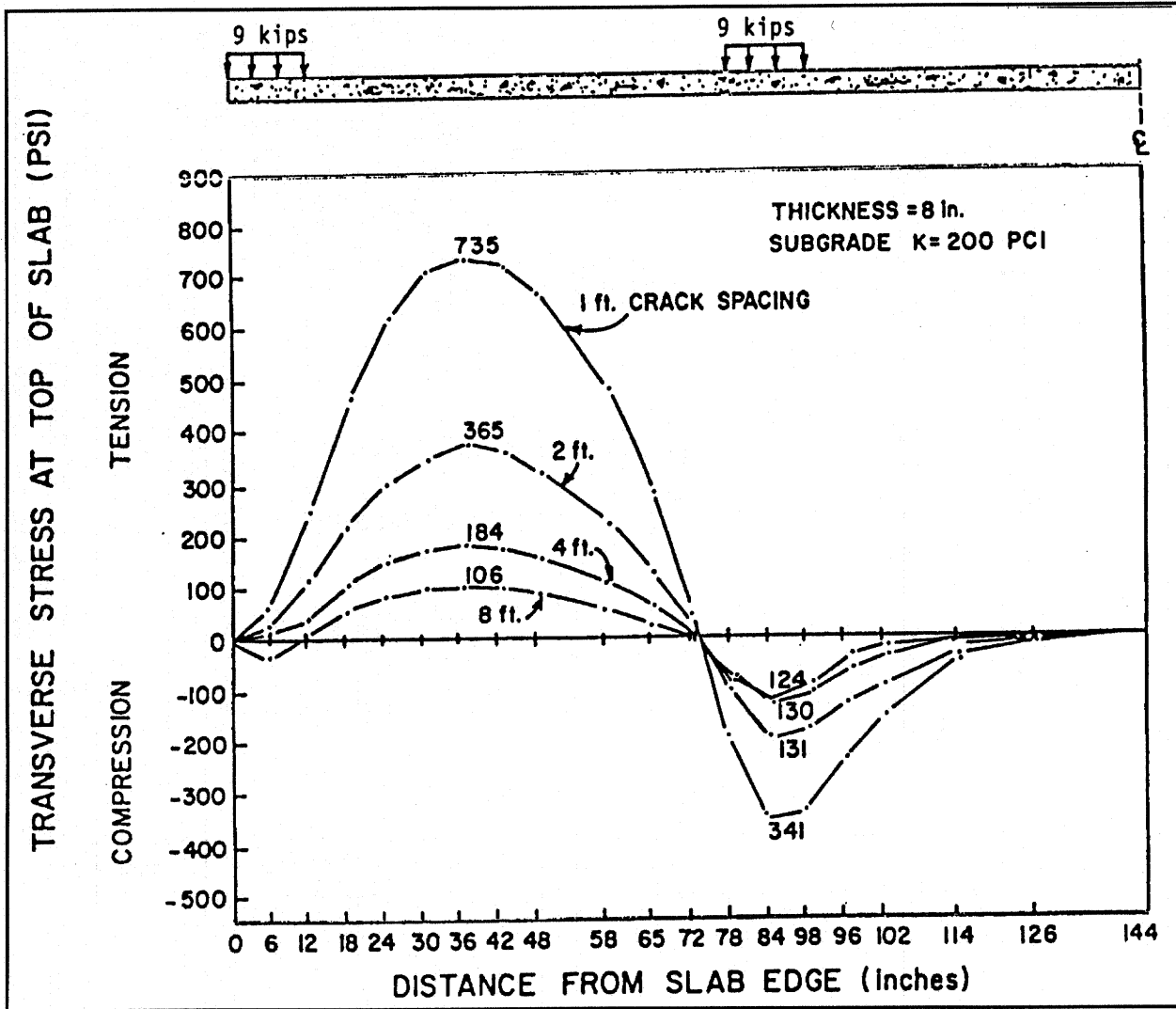
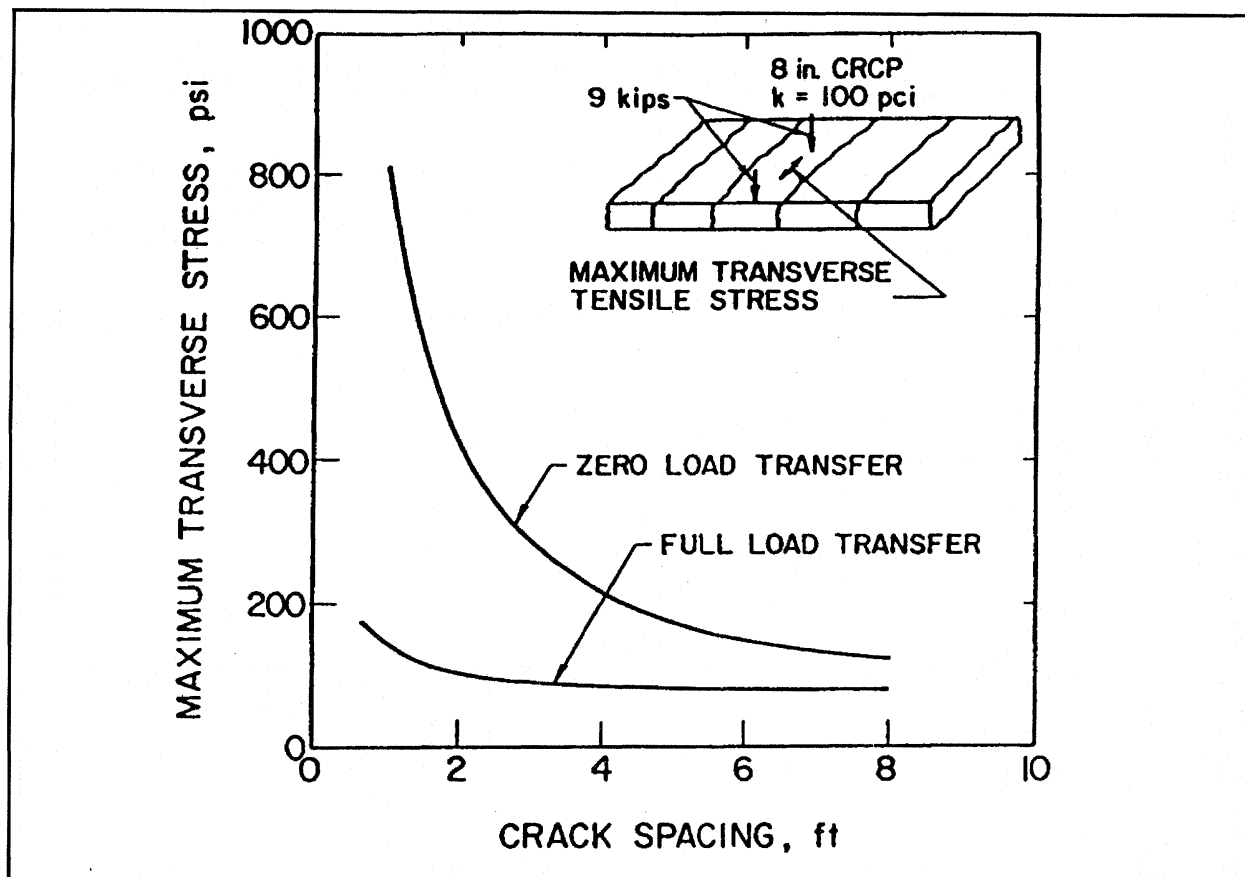


Figure 14. Effect of crack spacing on maximum tensile stress (0 percent LTE).<sup>(23)</sup>

### Transverse Bending Stresses

The formation of longitudinal cracking (towards the development of punchout distress) by lateral stresses due to wheel load has been thoroughly reviewed by others.<sup>(23)</sup> Crack spacing has been shown to significantly affect the magnitude of the lateral stresses illustrated in figure 14 and as shown, the longitudinal stresses also decrease with decreasing crack spacing. However, a more important parameter is the load transfer across the crack shown in figure 15. Transverse bending stresses ( $\sigma_x$  illustrated in figure 16) are low at high load transfer efficiencies LTE and are high at low LTE's. Obviously, the location of the maximum transverse bending stress is in between the wheel load positions (approximately 0.8 m (30 in) from the pavement edge) for a bituminous shoulder type. These stresses are significant below a LTE of 80 percent. In



1 psi = 6.89 kPa, 100 pci = 27.1 kPa/mm, 9 kips = 40 kN, 1 in = 25.4 mm, 1 ft = 0.305 m

Figure 15. Effect of load transfer efficiency across transverse cracks on maximum transverse stress in CRC pavement.<sup>(23)</sup>

comparison, the longitudinal bending stresses ( $\sigma_b$ ) are relatively low but may contribute to some extent to further transverse cracking as part of the overall cracking pattern. Interestingly enough, analysis tends to indicate that the effect of loss of support by itself on  $\sigma_a$  and  $\sigma_b$  stresses is surprisingly small. However, if LTE is diminished because of excessive shear stresses induced by poor or nonuniform support, then these stresses are significantly affected. This means that loss of support acts as a catalyst precipitating the loss of LTE, particularly since punchouts observed in field studies were always accompanied with severe erosion and loss of support. Consequently, loss of load transfer is really the dominant effect of excessively high bending stresses, which are accelerated due to loss of support and are relatively unaffected by environmentally induced slab curling and warping. Coupled with loss of load transfer, curling and warping effects will contribute significantly to longitudinal cracking stresses. However, loss of load transfer is the most significant factor, which reemphasizes the importance of the aggregate wearout function previously discussed.

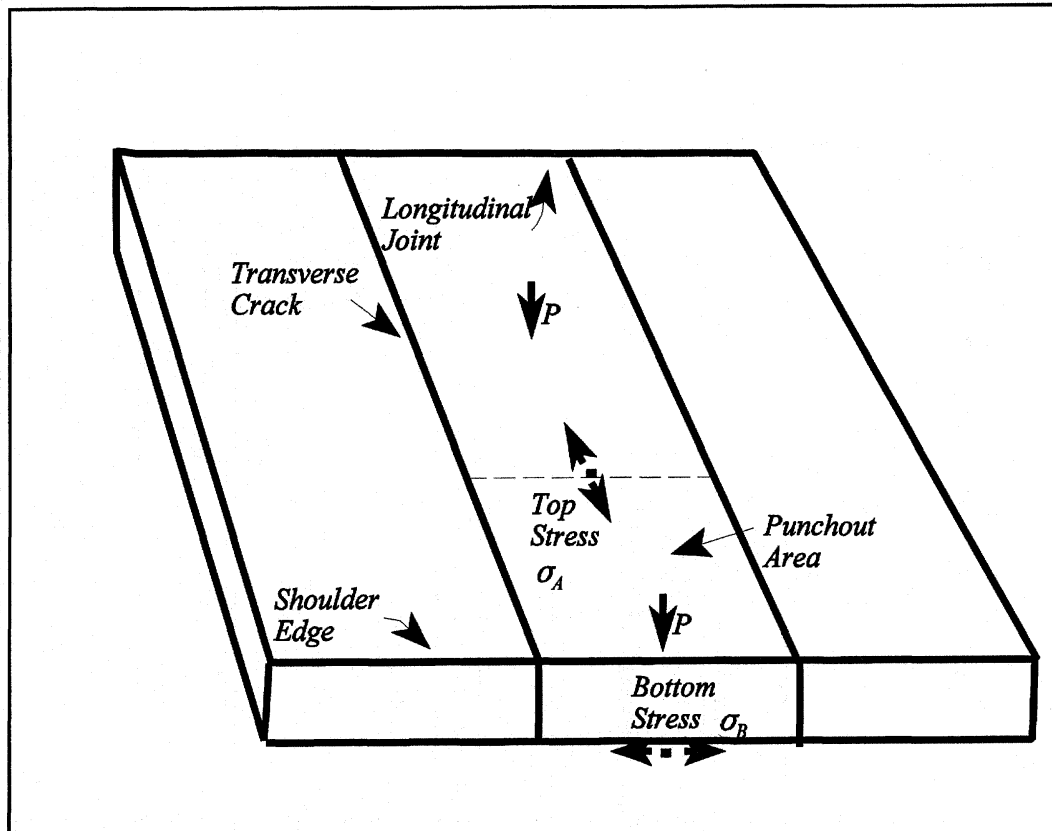
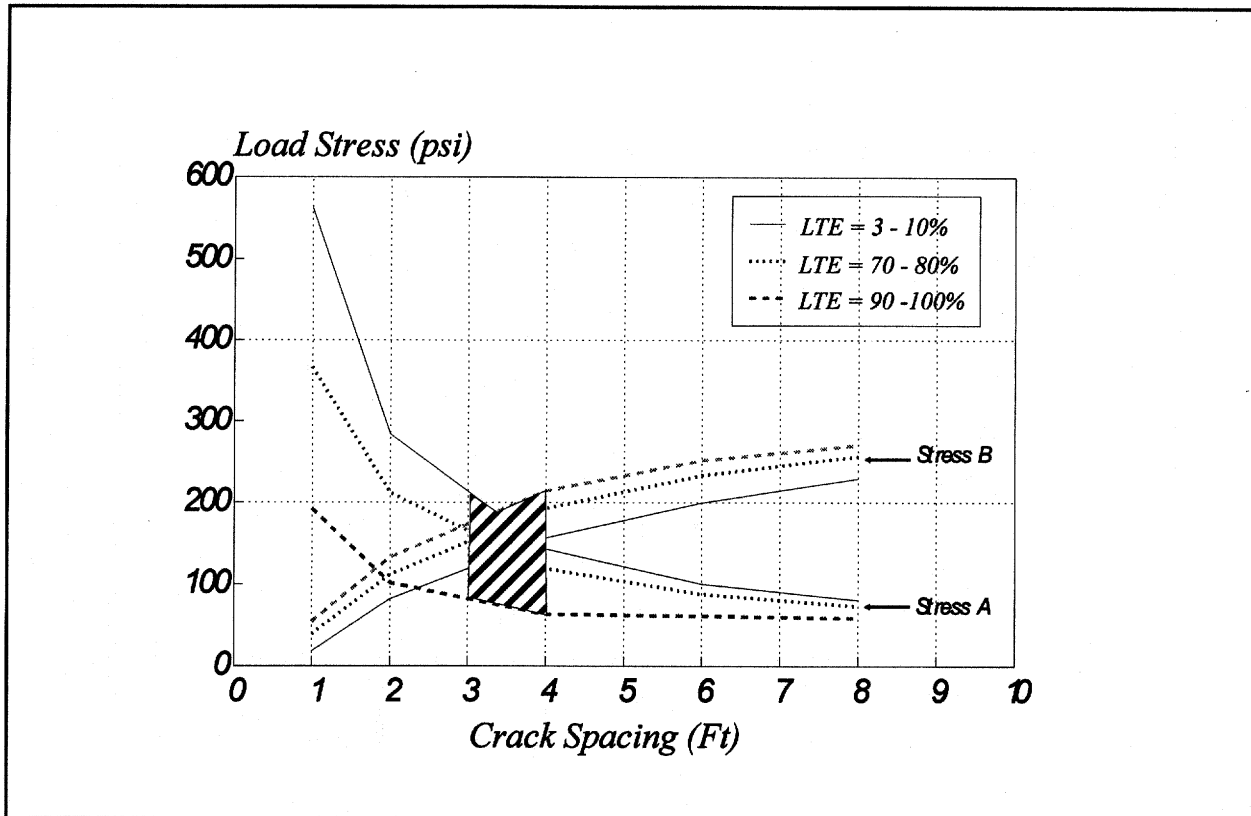


Figure 16. Wheel load stresses in a loaded CRC pavement system.<sup>(2)</sup>

Figure 17 illustrates a comparison between  $\sigma_a$  and  $\sigma_b$  shown in figure 16 that provides some basis for selection of optimal design crack spacing. The  $\sigma_b$  stress decreases with decreasing crack spacing as long as the load transfer remains high. For a bituminous shoulder and a given level of aggregate wearout and loss of load transfer, a crack spacing between 0.9 to 1.2 m (3 to 4 ft) may be the most optimal crack spacing for design purposes. The reason being, within this cracking interval, if the LTE remains high,  $\sigma_b$  will always be greater than  $\sigma_a$  (notwithstanding the fact that neither of the stresses are excessive). However, if the LTE is lost, then these stresses will be approximately equal to each other and, interestingly enough, still lower than the level of  $\sigma_b$  at the high load transfer condition. Crack spacing outside of this range will cause higher stresses for any level of LTE leading to a less optimum fatigue life. The crack spacing range of 0.9 to 1.2 m (3 to 4 ft) provides a balance between the maximum stresses  $\sigma_a$  and  $\sigma_b$  causing the stresses to be somewhat independent of the load transfer. Loss of LTE can have a significant influence on the performance of CRC pavement segments on erodible bases dominated by 0.6 m (2 ft) crack spacings but would have less of an impact for 1.2 m (4 ft) crack spacings. A CRC pavement with a 0.6 m (2 ft) extended driving lane or a 3 m (10 ft) tied shoulder causes the optimum crack spacing range (for a balance between stresses  $\sigma_a$  and  $\sigma_b$ ) to increase to 1.5 to 1.8 m (5 to 6 ft). The stresses in the 0.9 to 1.2 m (3 to 4 ft) range for the 0.6 m (2 ft) extended shoulder case are approximately 5 to 6 percent less than the stresses for the bituminous shoulder case in the same range. The load behavior for a 3 m (10 ft) tied shoulder is similar to a 0.6 m (2



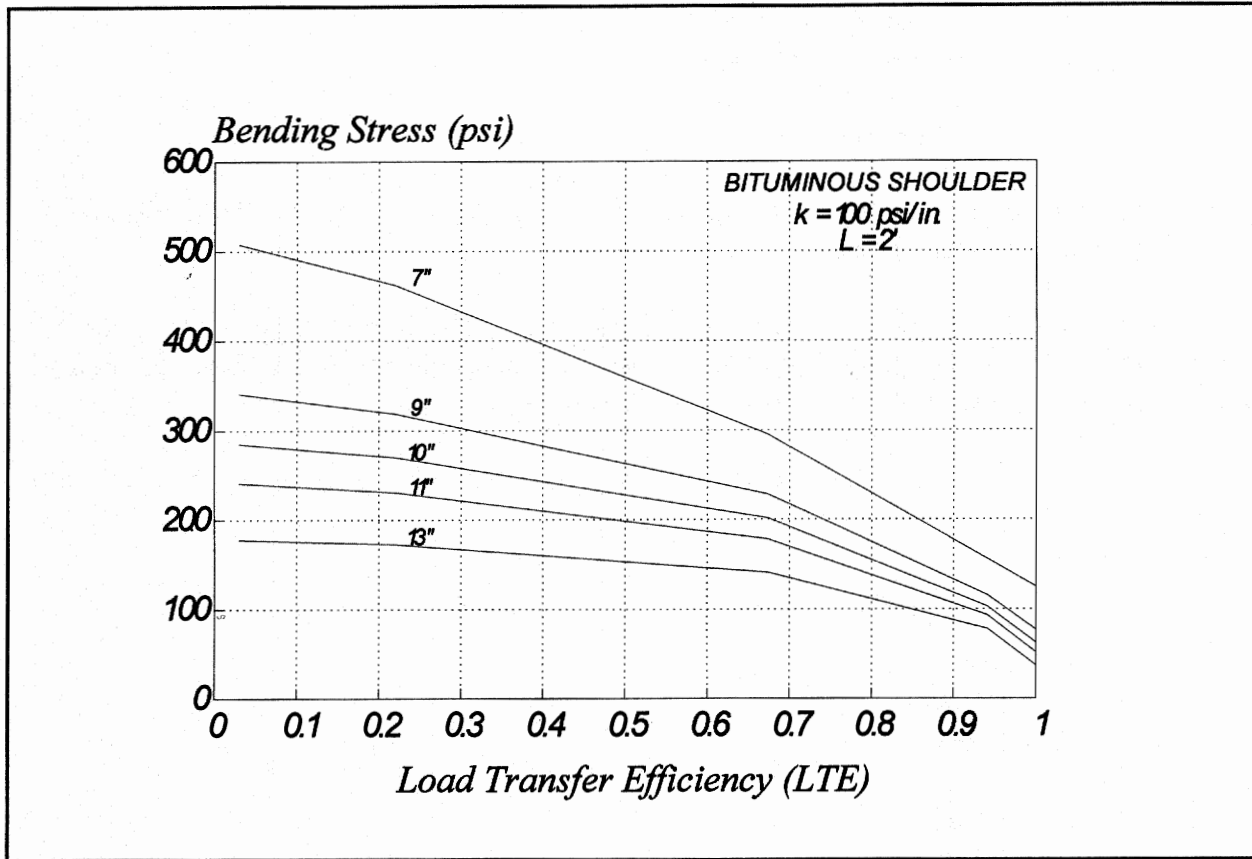
1 ft = 0.305 m, 1 psi = 6.89 kPa

Figure 17. Comparison of  $\sigma_a$  and  $\sigma_b$  with crack spacing for a 254 mm (10 in) pavement thickness. <sup>(2)</sup>

ft) extended driving lane except the maximum stresses with a tied shoulder are 138 to 207 kPa (20 to 30 psi) less. These stress comparisons do not include environmentally induced stresses.

Previous studies<sup>(2)</sup> have indicated that nonuniform supported conditions in CRC pavements seem to have a greater effect on transverse shear stresses than on transverse bending stresses. A greater shear stress condition will increase the rate of load transfer loss, which will result in increased bending stresses and greater potential for punchout distress. The shear stresses are reduced with either a 0.6 m (2 ft) extended or a 3 m (10 ft) tied shoulder if sufficient load transfer on the longitudinal shoulder is provided.

Transverse wheel-load stresses should be included in a thickness design process for CRC pavement systems. Using ILLISLAB<sup>(46)</sup> analysis, a database of maximum transverse wheel-load stresses was generated for a CRC pavement system (under a free edge condition) for a variety of thicknesses, load transfer efficiencies, and crack spacings. A typical pattern of maximum stresses is shown in figure 18. The contribution of bending stresses to fatigue damage is negligible prior to wearout of the aggregate interlock and concomitant loss of load transfer. The level of load transfer may also affect the maximum stress location in a CRC pavement system



2 ft = 0.6 m, 100 psi/in = 27.1 kPa/mm, 1 psi = 6.89 kPa, 1 in = 25.4 mm  
 Figure 18. Transverse bending stress: CRC pavement with bituminous shoulder.<sup>(2)</sup>

consisting of a bituminous shoulder and to a lesser degree with other shoulder types. The variation of wheel load stress with load transfer efficiency and thickness illustrated in figure 18 is based upon a cracking interval of 0.6 m (2 ft). Transverse wheel-load stresses in a CRC pavement system are therefore, at a minimum, a function of crack spacing and shoulder configuration. A stress function for transverse wheel-load stresses can be configured (independent of environmental transverse stresses—discussed later) for a CRC pavement with a bituminous shoulder as follows:

$$s = \{a + b \ln(L/\ell)\}^{-1} \quad (9)$$

where

- a =  $\exp(-0.930 + 2.84\{1 + \exp[-(LTE - 96.4)/24.6]\}^{-1})$
- b =  $(0.427 + 9.73 \times 10^{-7} LTE^3)^2$
- L = mean crack spacing (L)
- $\ell$  = radius of relative stiffness (L)
- LTE = load transfer efficiency (%)

- s = dimensionless stress ( $\sigma_{wls}h^2/P$ )
- $\sigma_{wls}$  = wheel load stress ( $FL^{-2}$ )
- h = pavement thickness (L)
- P = wheel load (F)

Total stresses will include  $\sigma_{wls}$  along with curl and warping-related stresses, which are discussed later in this chapter in greater detail.

A load transfer function is necessary to characterize the relationship shown in figure 12 to incorporate the effects of aggregate wear on load transfer efficiency. Relating deflection load transfer and joint stiffness<sup>(15,30)</sup> is shown in the following expression:

$$LTE (\%) = (a + cx + ex^2 + gx^3)/(1 + bx + dx^2 + fx^3) \quad (10)$$

where

- x =  $\ln(\text{Agg}/k\ell)$
- a = 45.973
- b = -0.00855
- c = 19.588
- d = 0.056
- e = 2.785
- f = -1.205 e-05
- g = 0.130

and demonstrates a relationship between the stiffness of the transverse crack and the deflection LTE across the crack.

The relationship between dimensionless shear stress (s) of the transverse crack and the stiffness of the transverse crack as a function of the degree of load transfer offered by a tied concrete shoulder is illustrated in figure 19. As the degree of load transfer across the concrete shoulder joint increases, the dimensionless shear stress on the transverse crack decreases as characterized in the following equation form for a specific crack spacing:

$$s = \frac{a + c \cdot \text{Log} \left( \frac{\text{Agg}}{k\ell} \right)_T}{1 + b \cdot \text{Log} \left( \frac{\text{Agg}}{k\ell} \right)_T}$$

where

- a =  $a_1 - a_2 \ln (\text{Agg}/k\ell)_s$
- b =  $b_1 + b_2 \exp (-\text{Agg}/k\ell)_s$
- c =  $c_1 - c_2 \ln (\text{Agg}/k\ell)_s$

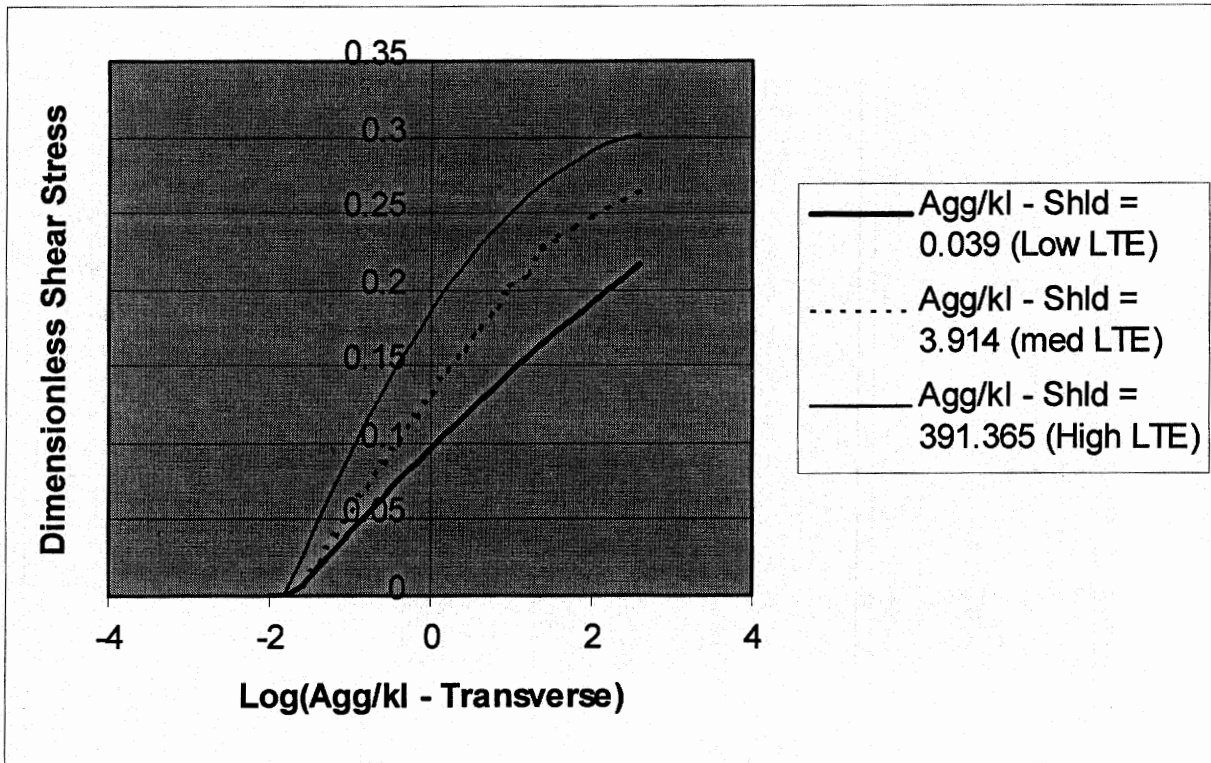


Figure 19. Shear stress as a function of load transfer efficiency provided by a concrete shoulder.<sup>(1)</sup>

Note: T: load transfer on the transverse crack; S: load transfer on the longitudinal joint. It is recommended that the coefficients be determined for a 0.61 m (2 ft) cracking interval.

Shear stress also depends upon the distance between cracks, and decreases as the crack spacing increases. Figure 20 depicts dimensionless shear stress as a ratio ( $s_x/s$ ) of the shear stress for a crack spacing of 0.61 m (2 ft). Therefore, the dimensionless shear stress ( $s_x$ ) can be determined for a wide range of crack spacings in CRC pavement in terms of the dimensionless shear stress ( $s$ ) for 0.61 m (2 ft) cracking interval in the form of :

$$\frac{s_x}{s} = a_1 + a_2 \cdot \ln\left(\frac{Agg}{kl}\right) + \frac{a_3}{\left(\frac{Agg}{kl}\right)^{1/2}}$$

where

$$a_i = b_1 + \frac{b_2}{\ln L} + \frac{b_3}{L^{3/2}} + \frac{b_4}{e^L}$$

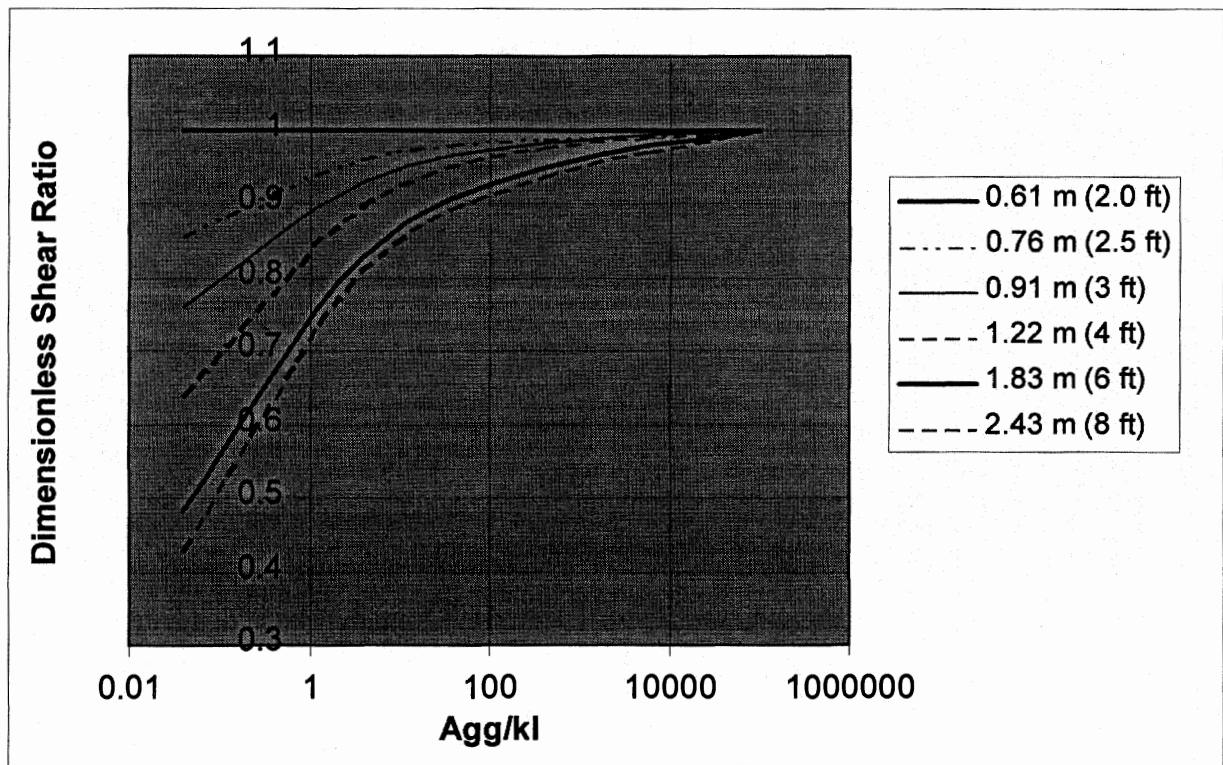


Figure 20. Adjustment of dimensionless shear stress for crack spacing.<sup>(1)</sup>

and

L = Crack spacing (ft)

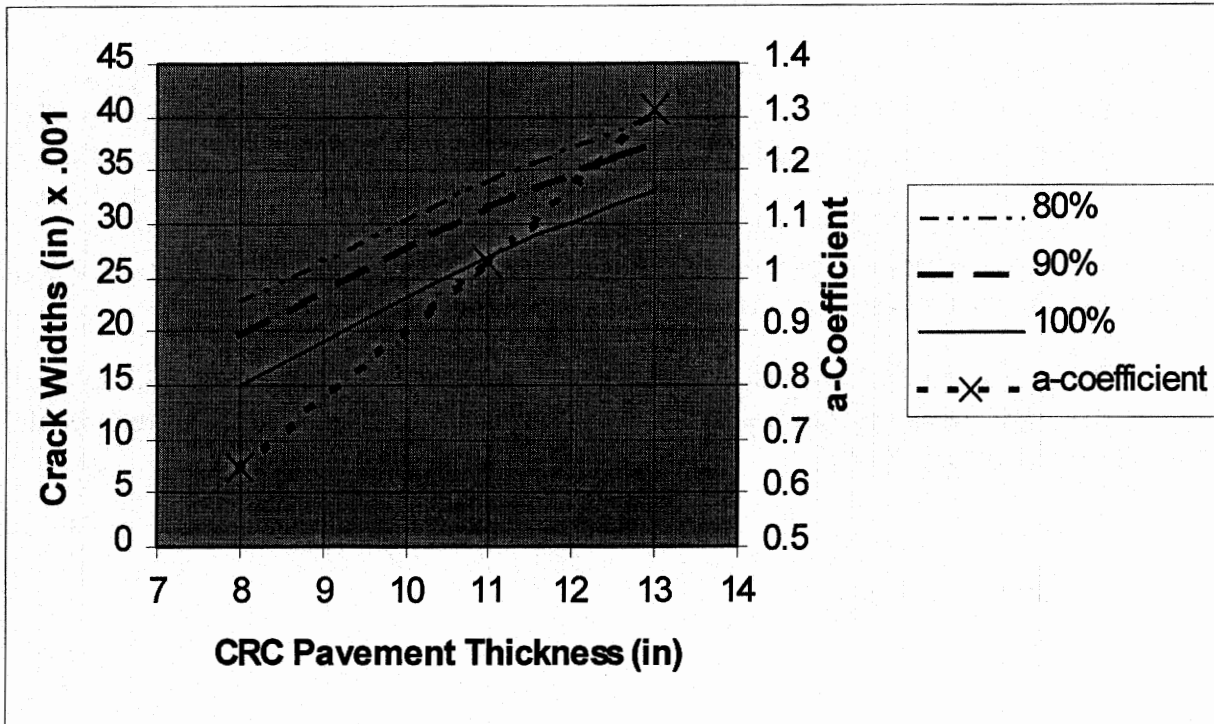
b = Coefficients based on a specific cracking interval (0.61 m is recommended)

It should also be noted that shear capacity is a function of the width of the transverse crack as illustrated in figure 13 and is characterized in the following form:<sup>(15)</sup>

$$S_{\text{capacity}} = \tau h^2 / P = a e^{-0.039 cw} \quad (11)$$

where  $cw$  = crack width. The value of 'a' ranges from .55 to 1.3 as a function of thickness as shown in figure 21. This figure demonstrates crack width requirements relative to slab thickness and load transfer requirements. It should be noted that the limits shown in figure 21 fall between those recommended by PIARC (0.5mm)<sup>(49)</sup> and those recommended by AASHTO (1mm).<sup>(54)</sup> Figure 21 suggests that the PIARC requirements are too conservative to typical CRC pavement thicknesses.

The loss of shear capacity ( $\Delta S$ ) due to wheel load applications is also characterized in terms of the width of the transverse crack based on a function derived from the PCA test data.



1 in = 25.4 mm

Figure 21. Maximum crack width limits based on shear capacity requirements.<sup>(1)</sup>

Such a function is important with respect to accounting for the effect of aggregate wearout in the prediction of performance of CRC pavement systems:

where  $N$  is the accumulated traffic,  $\tau_{\text{stress}}$  is the shear stress on the transverse crack (figures 19 and 20), and  $\tau_{\text{ref}}$  is a reference shear stress derived from the PCA test results. Figure 12 indicates that nonuniform support conditions can result in an increase in shear stress by a factor of two, which contributes to accelerated aggregate wearout. Shear stresses are calculated as:

$$\tau_{\text{stress}} = sP_i/h^2 \quad (12)$$

and

$$\tau_{\text{ref}} = s_{\text{pca}}(111.1)$$

$$\ln(s_{\text{PCA}}) = \frac{a+c \cdot \ln\left(\frac{AGG}{kl}\right)}{1+b \cdot \ln\left(\frac{AGG}{kl}\right)}$$

where the dimensionless shear is denoted as 's' and  $a = -2.60$ ,  $b = 0.14$ , and  $c = -0.085$ . Equation 12 demonstrates how shear capacity can diminish over time. This expression constitutes the wearout function that allows for the deterioration of the aggregate interlock to be considered in the performance estimate of CRC pavement systems. The coefficients of this function may vary for different aggregate types, but preliminary test results<sup>(15)</sup> indicate little differences in the shear wearout behavior of mixes made with different coarse aggregate types. Further research should be conducted to verify this finding. However, all the expressions introduced above combine together to characterize how the load transfer efficiency (and consequently, the fatigue stress) can change throughout the performance period of a CRC pavement system.

Equation 13 is the final expression that forms the basis of the CRC pavement thickness design process. This equation, shown below, is useful for determination of a design crack width in terms of certain design parameters.

$$\overline{cw} = L (z + \alpha_c t_{max}) + \frac{f_t}{E_c} \left( L - \frac{f_t d_b}{4up} \right) \quad (13)$$

where

- $\alpha_c$  = thermal coefficient of expansion
- $t_{max}$  = maximum drop in pavement temperature
- $d_b$  = reinforcing steel bar diameter (L)

and the terms have been previously defined. Subbase friction effects, although not directly included in equation 13, are reflected in the percentage of steel (p) requirements, to be discussed later. Equation 13 will also be useful in assessing the design reliability associated with this suggested design process (also to be discussed later) and, as pointed out in chapter 4, the variability in crack width will be affected by the method employed to control the pattern of the crack spacing.

The basic design steps discussed above can be used (as summarized below) to generate maximum crack width-thickness requirements for design purposes. The crack width capacity coefficient 'a' is also shown in figure 21 as a function of thickness. These limits are suggested to ensure adequate load transfer and shear capacity throughout the performance period of the pavement. The design process is as follows:

- (1) Determine the mean crack width (equation 13).
- (2) Determine the shear capacity of the CRC crack pattern (equation 11) and determine the associated mean stiffness of the transverse crack pattern.
- (3) Determine the associated level of load transfer efficiency (equation 10).
- (4) Determine the associated wheel load stress and level of fatigue damage based on current traffic increment (equation 9).

- (5) Determine level of loss in shear capacity due to load and support conditions for same traffic increment (equation 12 and figures 19 and 20) ( $\text{New } S_{\text{capacity}} = \text{Old } S_{\text{capacity}} - \Delta S$ ).
- (6) Repeat steps (3) through (6) using average LTE and wheel load stress for the given increment of traffic to determine a new level of fatigue damage (equations 7 and 8).
- (7) Assess the level of cracking (equation 6).

The design of the reinforcing steel in a CRC pavement system is discussed later in some detail, but it has been found to contribute very little to the load transfer capability of the pavement due to problems associated with the first failure mode.<sup>(2)</sup> However, load transfer in CRC pavement is function of the crack width and the intensity of the shear loading and is related to the pavement thickness in terms of performance. Therefore, a thickness design should be based upon the level of crack width, and consequently, the load transfer over the design period as is evidenced throughout the suggested design process.

### Environmentally Induced Stresses

Curl and warping behavior in the transverse direction in CRC pavement should be considered in the design process because of the effect they have on transverse stresses and the load-related fatigue damage contribution provided by them and because of the erosive action associated with such behavior. The effect of erosion on nonuniform support has been previously discussed but fatigue damage due to these effects can increase if load transfer begins to diminish. To estimate these effects in a logical manner, curl and warping stresses can simply be superimposed on the wheel load stresses to determine total load stresses and are considered repetitively in fatigue damage analysis. Load and environmentally induced stresses superpositioning is justified until more sophisticated methods can be developed that consider crack growth on a mechanics and materials basis.

Curl and warping stress distribution in the transverse direction across the traveled lane is due to the weight of the slab, the associated climatic gradient, and the stiffness of the pavement system. These stresses are dependent on the foundation support modulus ( $k$ ), pavement thickness ( $h$ ) temperature, or moisture gradient ( $G$ ) as a function of the transverse position on the slab. The curl stress in the transverse direction is also a function of the lane width and the shoulder type (i.e., 3 m (10 ft) tied concrete shoulder, 0.6 m (2 ft) extended shoulder, etc.). Curling stress can be derived from daily temperature cycles and warping stress from seasonal moisture variations.

Curling stress for a pavement can be calculated using the well known Westergaard equation for slab stresses under thermal gradients.<sup>(19)</sup> This solution will not be elaborated here. However, a similar approach can be taken for slab stresses caused by moisture gradients. The maximum curling stress ( $\sigma_c$ ) in a concrete slab based on Westergaard's analysis predicts the stress condition under certain slab edge boundary conditions and is:

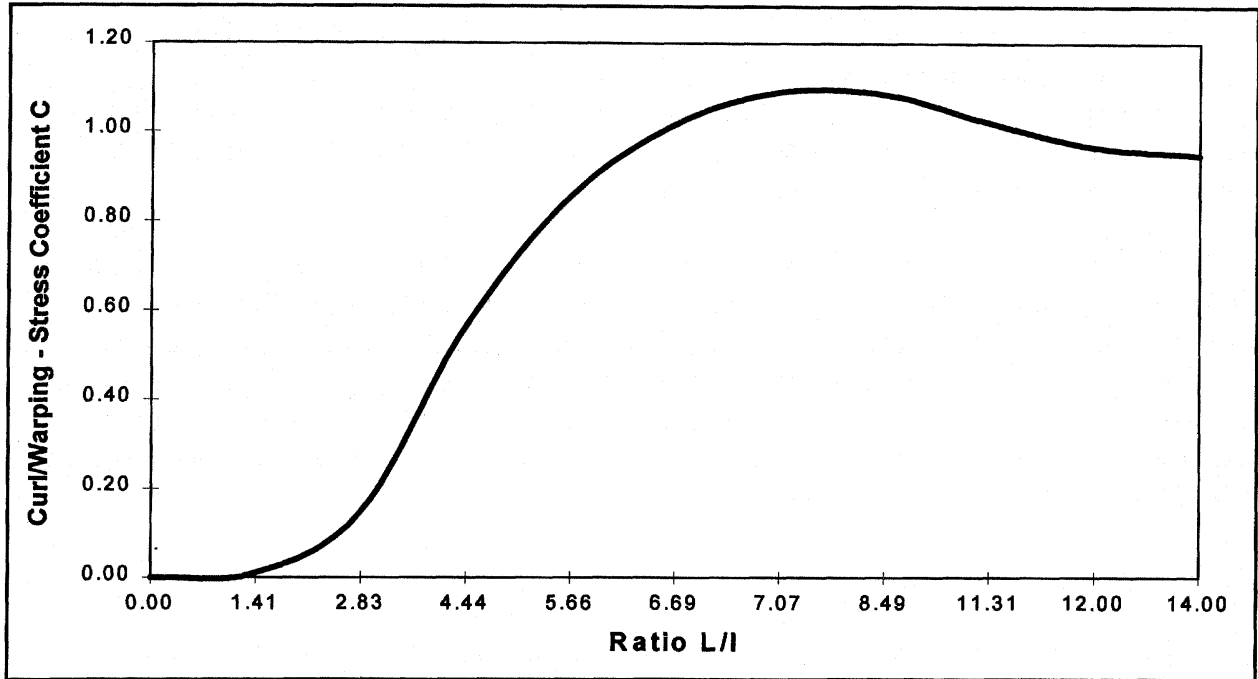


Figure 22. Curling stress coefficients.<sup>(20)</sup>

$$\sigma_0 = \sigma' = \frac{E_c \alpha t}{2(1-\nu)} = \frac{E_c}{2(1-\nu)} \epsilon'$$

where

- $\alpha$  = thermal coefficient of expansion ( $^{\circ}\text{C}$ )
- $t$  = temperature change or drop
- $\epsilon'$  =  $\alpha t$

Bradbury<sup>(20)</sup> developed coefficients based on the Westergaard solution as applied to slabs of practical dimensions. The coefficients are shown in figure 22 and are used in the following equations:

**Edge stress:**

$$\sigma = \frac{CE_c \alpha t}{2} = C(1-\nu)\sigma'$$

### Interior stress:

$$\begin{aligned}\sigma &= \frac{E_c \alpha t}{2} \left( \frac{C_1 + \nu C_2}{1 - \nu^2} \right) = \left( \frac{C_1 + \nu C_2}{1 - \nu^2} \right) \sigma^t (1 - \nu) \\ &= \sigma^t \left( \frac{C_1 + \nu C_2}{1 + \nu} \right)\end{aligned}$$

If  $C_1 = C_2 = C$  then  $\sigma = C\sigma^t$

The coefficient  $C_1$  is the desired direction, whereas  $C_2$  is for the direction perpendicular to this direction.  $L_x$  and  $L_y$  are the free length and width, respectively. However, in the design of CRC pavement systems, the length of interest is in the transverse direction (same direction as  $\sigma_a$  in figure 16).

### Warping Stresses

Similarly, the interaction of drying shrinkage ( $\epsilon^{sh}$ ) of concrete and pavement restraint can induce warping stresses in a concrete slab. The calculation of strain due to drying shrinkage of concrete has been suggested in the form of a model as a function of the relative humidity ( $h$  or  $rh$  to avoid confusion with slab thickness) and  $\epsilon^{sh\infty}$  (as a material parameter, which is the ultimate concrete shrinkage at the reference  $rh = 50$  percent).

In an infinitely large concrete slab, the middle portion is fully restrained against shrinkage or temperature-induced deformation. The shrinkage-induced stresses ( $\sigma^{sh}$ ) in the middle portion are:

$$\sigma_x = \sigma_y = \frac{E_c}{1 - \nu} \epsilon^{sh}$$

Moisture measurements in actual field slabs, using instrumentation described by others,<sup>(39)</sup> have indicated that the drying process tends to occur to some extent throughout the concrete slab. These measurements have also indicated the nonlinearity of the humidity profile vertically through a pavement slab during wetting and drying cycles. One would expect that such variations will result in similar profiles or distributions of moisture-induced warping stresses. If it is assumed that the shrinkage stress distributes linearly through the thickness of the slab, varying from  $\sigma^{sh}$  at the top to zero at the bottom, the solutions provided by Westergaard<sup>(19)</sup> and Bradbury<sup>(20)</sup> can be implemented by only replacing  $\epsilon^t$  in all previously noted curl equations by  $\epsilon^{sh}$ . The parameter  $\epsilon^{sh}$  is the free shrinkage at the top surface of the pavement, which may be estimated as described below. Moisture loss from the concrete can be converted into shrinkage strains using the following equation:<sup>(21)</sup>

$$\epsilon_{sh} = \epsilon_{sh\infty}(1-h^3)$$

where  $h$  is previously defined, and the ultimate concrete shrinkage ( $\epsilon_{sh\infty}$ ), which is a material parameter of the concrete. The following formula is used to compute  $\epsilon_{sh\infty}$ :<sup>(21)</sup>

$$\epsilon_{sh\infty} = 1330 - 970y$$

where

$$y = (390z^{-4} + 1)^{-1}$$

and

$$z = 0.381 \sqrt{f_{cyl28}} \left[ 1.25 \sqrt{\frac{a}{c} + 0.5 \left( \frac{g}{s} \right)^2} \right]^3 \sqrt{\frac{1 + \frac{s}{c}}{\frac{w}{c}} - 12}$$

where

- $a/c$  = total aggregate/cement ratio
- $g/s$  = coarse aggregate/cement ratio
- $s/c$  = fine aggregate/cement ratio
- $w/c$  = water/cement ratio

The above parameters related to the concrete mix design.

Temperature and moisture gradients in the pavement (which cycle both daily and seasonally), are useful in finding the environmentally induced stresses as a function of time and season. Normally, it is expected that environmentally induced stresses should be broken down on a monthly, daytime, and nighttime basis to coincide with characteristic patterns in the truck traffic. Although, the discussion here is based on linear temperature and moisture gradients, the framework presented can be adopted to non-linear gradients using the approach suggested by Hansen.<sup>(52)</sup>

In addition to the other factors discussed above, the actual location of the pavement design stresses will vary depending upon the pavement shoulder type as illustrated in figure 23. The maximum (design) wheel load stress location changes as a function of the shoulder type and consequently may affect the location of where curl and warping stresses are determined. For a bituminous shoulder condition, maximum load stresses occur between 1.06 and 0.76 m (42 and 30 in) from the pavement edge (between the wheel loads). The associated curl and warping

stresses are calculated at the 1.06 m (42 in) location. The maximum or the design load stress location moves to the inner wheel load position for pavements with an extended driving lane or a 3 m (10 ft) tied shoulder (if the shoulder is effectively tied).

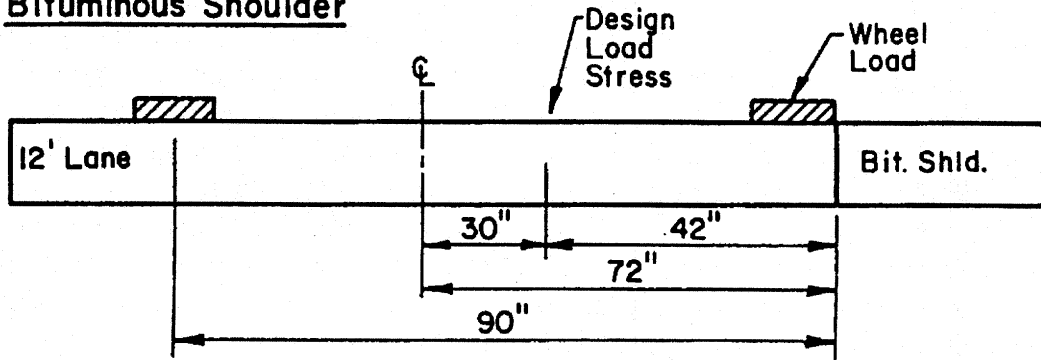
Fatigue damage analysis is facilitated by the use of equivalent damage ratios<sup>(22)</sup> for CRC pavement. Equivalent damage ratios (EDR) are useful in determining the percentage of traffic applied to the design wheel load location to cause the equivalent amount of fatigue damage as that caused by the entire distribution of traffic. The EDR values were determined from computation of the fatigue damage distribution across the traffic lane for incremental positions of the traffic distribution. A similar approach was used in the determination of EDR values for jointed concrete pavement<sup>(22)</sup> where the EDR values were defined in terms of a mean distance from the pavement edge to the outer edge of the wheel load (D). The EDR values for the bituminous shoulder type are typically the lowest since the load stresses are greater than stresses in pavements with other shoulder types (figure 24). The stresses in a CRC pavement with an 2.44 m to 3 m (8 to 10 ft) tied shoulder are more uniformly distributed causing fatigue contributions from a broader portion of the traffic distribution than for a 0.6 m (2 ft) extended driving lane which leads to smaller EDR values. It should be pointed out that the EDR values for the 0.6 m (2 ft) extended and an 2.44 m to 3 m (8 to 10 ft) tied shoulder configurations were based on a maximum or design stress location at the inner wheel load while EDR values for the bituminous shoulder configuration was based on the maximum stress occurring between the wheel loads. Consequently, comparisons between EDR values of these two groups of shoulder configurations may be limited.

Fatigue analysis reveals that the accumulated damage due to bending prior to the loss of load transfer is negligible. However, the rate of fatigue damage changes significantly as aggregate wearout occurs. Therefore, fatigue damage for transverse bending should be adjusted according to the level of LTE. The level of LTE, as previously shown, will vary as a function of the crack width and aggregate interlock wearout. Erosion of the subbase will increase aggregate wear out and loss of LTE. The traffic should also be broken down according to the judgment of the design engineer, but the smaller the traffic increments the more accurate will be the determination of fatigue damage.

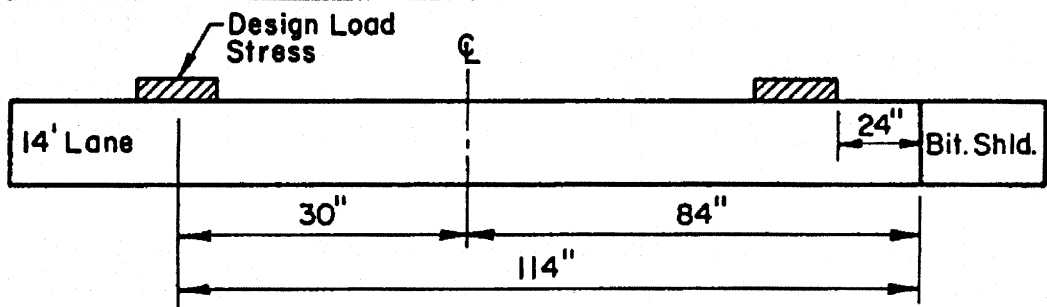
#### Design Reliability for CRC Pavements

Variability in design parameters and material properties can affect the degree of variability in the performance of CRC pavements. In order to improve the quality of the design process, the effect of variabilities inherent in the quantities relevant to material characteristics should be quantified in the form of design reliability. Therefore, design reliability constitutes the effect of variability in design parameters and material properties with respect to the design process.

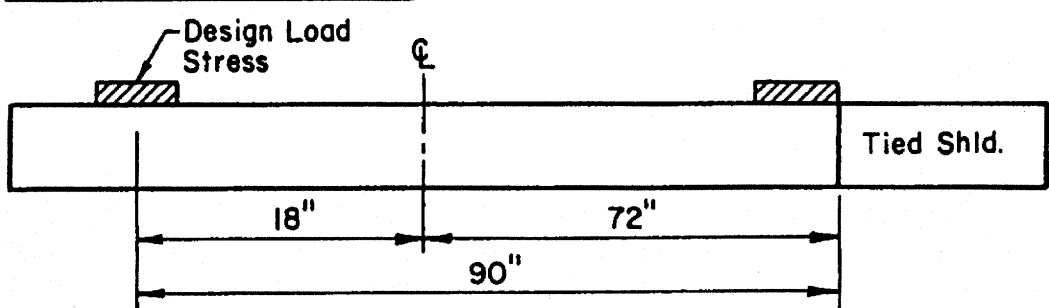
**Bituminous Shoulder**



**Two-Foot Extended Shoulder**

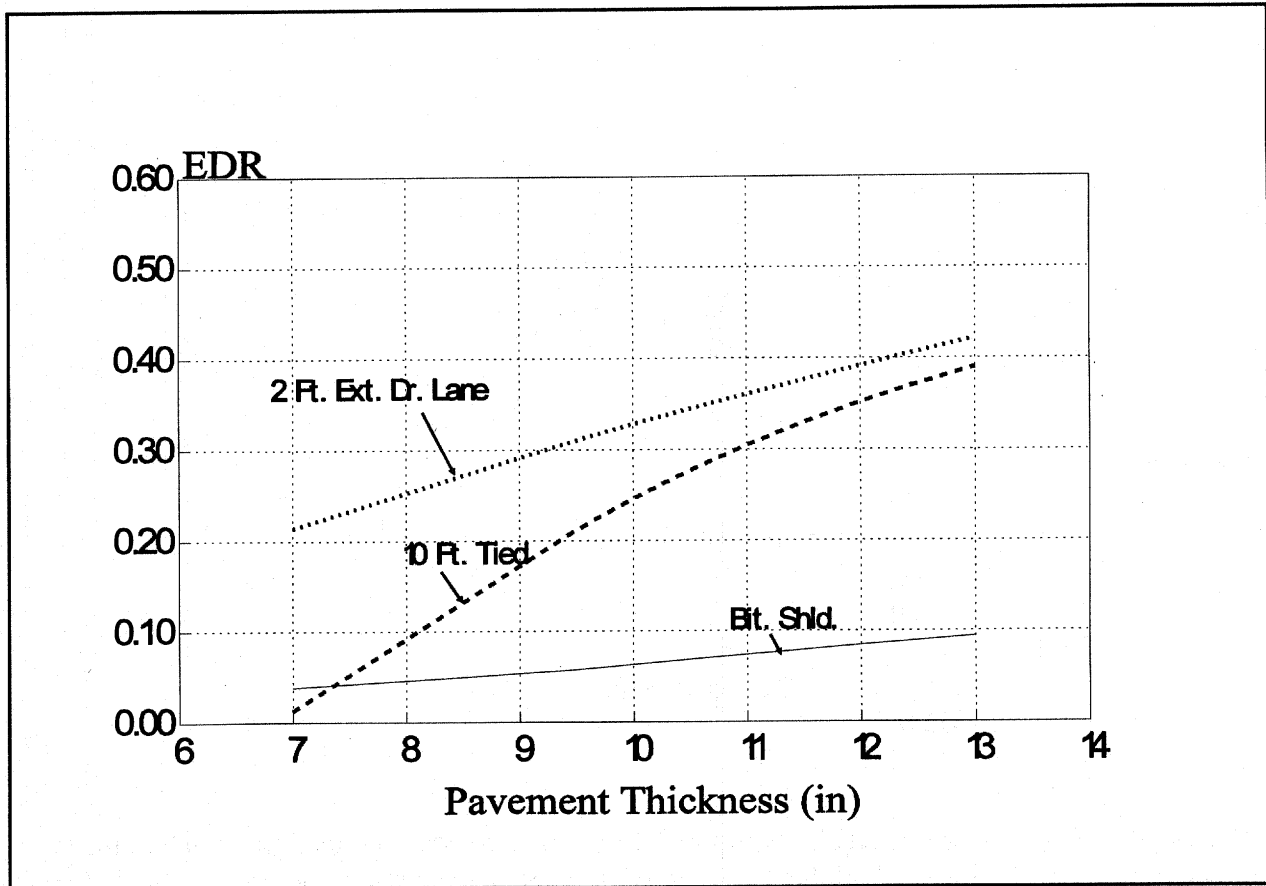


**Ten Foot Tied Shoulder**



1 in = 25.4 mm, 1 ft = 0.305 m

Figure 23. Suggested design stress locations as a function of a typical pavement/shoulder configuration.<sup>(2)</sup>



2 ft = 0.6 m, 10 ft = 3 m, 1 in = 25.4 mm

Figure 24. Transverse bending equivalent damage ratios (0.46 m (18 in) from pavement edge).<sup>(2)</sup>

An approach to including the effect of variability of crack spacing, crack width, concrete strength, etc., in the design process can be framed within the variability or variance of cracking (or punchout distress):

$$Var(C) \approx \sum_{i=1}^n c_i^2 Var(X_i) + \sum_{i=1}^n \sum_{j=1}^n c_i c_j Cov(X_i, X_j)$$

where

- $c$  = partial derivative  $\partial C / \partial X_i$  of the functional cracking relationship
- $Cov(X_i, X_j)$  = covariance of the parameters  $X_i$  and  $X_j$
- $Var(X_i)$  = variance of the cracking equation parameter
- $C$  = percent cracking

Further development allows for an expression for  $c$  to be generated:

$$\frac{\partial C}{\partial X_i} = -\%C \cdot \frac{\beta}{\alpha} \cdot v^r \left[ \frac{\partial D}{\partial X_i} \right]$$

and

$$\frac{\partial D}{\partial X_i} = \frac{\partial \left( \frac{1}{N_i} \right)}{\partial X_i} \cdot n_i$$

where

- $X_i$  =  $k_1, k_2, \text{MOR}, h, E_c, k, \partial\sigma/\partial X_i$
- $X_i$  =  $h, E_c, k, \text{LTE}, L, cw$
- $k_i$  = fatigue coefficients
- MOR = modulus of rupture
- D = accumulated fatigue damage
- v =  $(D/\alpha)^\beta$
- r =  $(\beta-1)/\beta$

The variability in cracking is related to the variability in damage accumulation, which in turn is affected by the variabilities of all the listed material properties relative to fatigue damage. The derivatives of D are developed from equations 7 to 14 and are dependent upon many variables that are included in these expressions. As an example of how these derivatives are developed, an abbreviated form of the variance of crack width (cw) (Var[cw]-as it pertains to  $\partial\sigma/\partial X_i$ ) is shown below:

$$\text{Var}(cw) \approx c_1 \cdot \text{Var}(f_t) + c_2 \cdot \text{Var}(L) + c_3 \cdot \text{Var}(t_{max}) + c_4 \cdot \text{Var}(z)$$

where

$$c_1 = \frac{1}{E_c} \left( L - \frac{df_t}{2up} \right)$$

$$c_2 = \left( z + \alpha_c t_{max} + \frac{f_t}{E_c} \right)$$

and  $c_3 = \alpha_c L$ ,  $c_4 = L$ . Using the variability in crack width, the crack width reliability ( $R_{cw}$ —as an example of how design reliability may be formulated) can be defined as one minus the probability ( $P$ ) that the crack width will exceed a minimum design crack width ( $cw_{min}$ ) associated with the crack width variance ( $V(cw)$ ):

$$R_{cw} = 1 - P = 1 - Prob(cw \geq cw_{min})$$

$$cw_{design} = \overline{cw} - Z_r \sqrt{Var(cw)}$$

where

$$\begin{aligned} Z_r &= \text{value of the variate corresponding to } R_{cw} \\ cw_{design} &= \text{Design crack width} \end{aligned}$$

The reliability in cracking can be formulated in the same manner except the probability of cracking exceeding a certain level of cracking (selected by design) is substituted in place of the crack width shown above.

### CRC Pavement Reinforcement Considerations

A major factor in the crack development of CRC pavement is the percentage of longitudinal reinforcement expressed as the ratio of area of steel reinforcement to the area of concrete ( $A_s/A_c$ ). The percentage of steel reinforcement has been listed as one of the most significant factors affecting crack spacing. As previously noted, many CRC pavements in the U.S. contain reinforcement in a range of 0.5 to 0.7 percent. In some northern regions, percentages in the higher end of the range has been used. The unfortunate problem associated with cracking is that environmental and construction conditions can many times dominate how the reinforcement interacts with the concrete pavement cracking behavior. Many punchout distresses may be a function of crack width in which crack spacing is considered to have a major influence on crack width. Although the principal purpose of the reinforcement is to maintain tight crack spacing and good aggregate interlock, little information is available as to the actual role the reinforcement plays in the load transfer developed in CRC pavement.

### *Percentage of Reinforcement*

Most theoretical relationships for the determination of reinforcement are based on the yield strength of the steel ( $f_y$ ). Vetter<sup>(5)</sup> originally developed two expressions for the percentage of reinforcement ( $p = A_s/A_c$ ) in reinforced concrete under fully restrained conditions for

volumetric changes. One expression is in terms of drying shrinkage and the other is in terms of temperature drop, respectively:

$$p = f_t / (f_y + zE_s - nf_t) \quad (14)$$

and

$$p = f_t / (f_y - nf_t) \quad (15)$$

where

$$\begin{aligned} f_t &= \text{concrete tensile strength} \\ f_y &= \text{yield strength of steel reinforcement} \end{aligned}$$

The above equations were developed for unbonded or low friction subbase interfaces. They have been modified (using a multiplication factor of  $1.3 - 0.2\mu$  where  $\mu$  is the coefficient of friction) to account for other coefficients of subbase friction other than a coefficient of friction of 1.5, which was apparently associated with unbonded subbase conditions. The advantage of using the multiplication factor is to increase the percentage of reinforcement under longer crack spacings which may result from lower values of friction coefficients. However, the affect of subbase friction on the design percent of steel is rather insignificant and experience has indicated that the percentages predicted by these expressions are suitable for friction coefficients up to 3.0. On this premise, a multiplication factor of  $1.3 - 0.1\mu$  may more be appropriate. Since it is recommended that subbase interfaces with friction coefficients greater than 3.0 be avoided, any further adjustments to the design percent of steel based on subbase friction is not warranted.

Vetter rationalized that the above expressions formed the basis for minimum reinforcement. He showed that the maximum shrinkage that can be sustained by the concrete without cracks forming (ignoring creep) is  $z = S_t / E_c$ , where  $S_t$  is the tensile strength of the concrete; upon substitution in the first of the two above equations, the sum of the last two terms of the denominator is zero and  $p$  becomes equal to  $S_t / f_y$ . Equation 15 represents the minimum limit of steel requirements if the shrinkage is zero and the temperature drop ( $T$ ) does not exceed a critical amount in which the total bond development length is greater than the crack spacing. In such case:

$$p = S_t / 2(f_y - T\alpha_s E_s) \quad (16)$$

Under minimum steel conditions ( $f_t = S_t$ ), equation 16 is equivalent to equation 15. Equation 16 only pertains to the case where the crack spacing is less than or equal to two times the bond development length. The percentage of steel calculated by equation 16 assumes the steel to be at the elastic limit and gives results greater than those determined by equation 15 as long as the steel stress is below the yield strength at a crack spacing of twice the bond development length or less. Consequently, equation 16 is not frequently applicable since these conditions (crack spacing and temperature drop combined) are rarely met.

The role of the stress in the concrete and the reinforcement is demonstrated in the above equations in which the amount of reinforcement is minimized if yielding of the reinforcement occurs. Equations 14 and 15 are also useful in determining the level of stress in the reinforcement (at the crack) given the percentage of reinforcement (p):

$$f_s = f_t(1/p + n) - zE_s$$

The stress equation for temperature drop independent of shrinkage is found by dropping out the shrinkage term. A Vetter type equation can be developed for a combination of shrinkage contraction and temperature drop by accounting for a difference in thermal coefficients for the concrete and the steel reinforcement (shown previously):

$$f_s = f_t(1/p + n) + E_s\{(t_m\alpha_s - t_t\alpha_c) - z\}$$

where

$$t_m = \text{temperature drop at mid-depth of slab}$$

$$t_t = \text{temperature drop}$$

McCullough<sup>(47, 48)</sup> developed a regression equation for the stress in the steel at the crack (fitting CRCP-2 computer results), which includes a parameter for wheel load stress:

$$f_s = 47300(1 + t/100)^{0.425} \times (1 + f_t/1000)^{4.09} \times (1 + \sigma/1000)^{-3.14} \times (1 + 1000z)^{-0.494} \times (1 + p)^{-2.74}$$

where  $r^2 = 0.926$  and  $SEE = 9570$ .

Analysis and experience have indicated that rebar bond area to volume of concrete (Q) will affect the crack spacing in CRC pavement and that the parameter Q is related to the time of year of construction. As a result, minimum Q values of 0.03 for summer construction and 0.04 for fall or winter conditions are recommended. Although no guidelines are available, it is suggested that these factors be increased 10 percent for epoxy coated reinforcement. It is pointed out, however, that one study indicated epoxy coated reinforcement has little affect on CRC pavement crack patterns.<sup>(51)</sup> Past AASHTO design guides have recommended a limiting stress criteria for the reinforcement of 75 percent of the ultimate tensile strength of the steel.<sup>(24)</sup> Based on stress predictions of in service CRC pavements which have shown good performance, it was concluded that yielding of the steel occurs. This has led to a reconsideration of the criteria to allow for a small amount of permanent deformation in the steel reinforcement. McCullough<sup>(24)</sup> suggested maximum rebar stresses based on the premise of allowing some permanent deformation and increased crack width of 0.25 mm (0.01 in). The plastic strain deformation was calculated for a gauge length corresponding to the stress range that exceeds the yield stress. This resulted in a relationship for maximum allowable stress as a limiting criteria as:

$$\sigma_{\max} = (0.19E_s\sqrt{f_c}/d_b2f_y) + (f_y \times 0.75)$$

However, it should be pointed out that other limiting crack width criteria have been suggested by McCullough based on spalling, steel corrosion, and subgrade erosion induced by excessive crack widths. The crack widths should be limited to 0.61 mm (0.024 in) for spalling considerations and to 0.20 to 0.25 mm (0.008 to 0.010 in) to minimize steel corrosion. These were considered to be too conservative for reasonable reinforcement design. Therefore, it was suggested the limiting design criteria should be based upon the selection of a temperature drop below the construction temperature corresponding to a crack width of approximately 0.64 mm (0.025 in). This temperature drop should not be exceeded 95 percent of the time. The 1986 AASHTO Design Guide allows a design crack width of 1.02 mm (0.040 in), which suggests that some corrosion of the reinforcement may be expected.

The purpose of transverse reinforcement is:

- (1) to support longitudinal steel at the correct depth and to maintain its spacing interval.
- (2) to act as tie-bars across longitudinal joints and random cracks to minimize the crack or joint opening.

Paving construction methods are used, such as tube placement, which allow embedment of the reinforcing bar into the concrete pavement without the use of transverse reinforcement. The design for transverse steel (if needed), as suggested by the AASHTO design guides, is based upon the subgrade drag theory:

$$A_s = Wlf/2f_s$$

where

- W = weight of the concrete slab per unit area
- l = distance between contraction joints
- f = coefficient of friction
- f<sub>s</sub> = yield strength of reinforcement

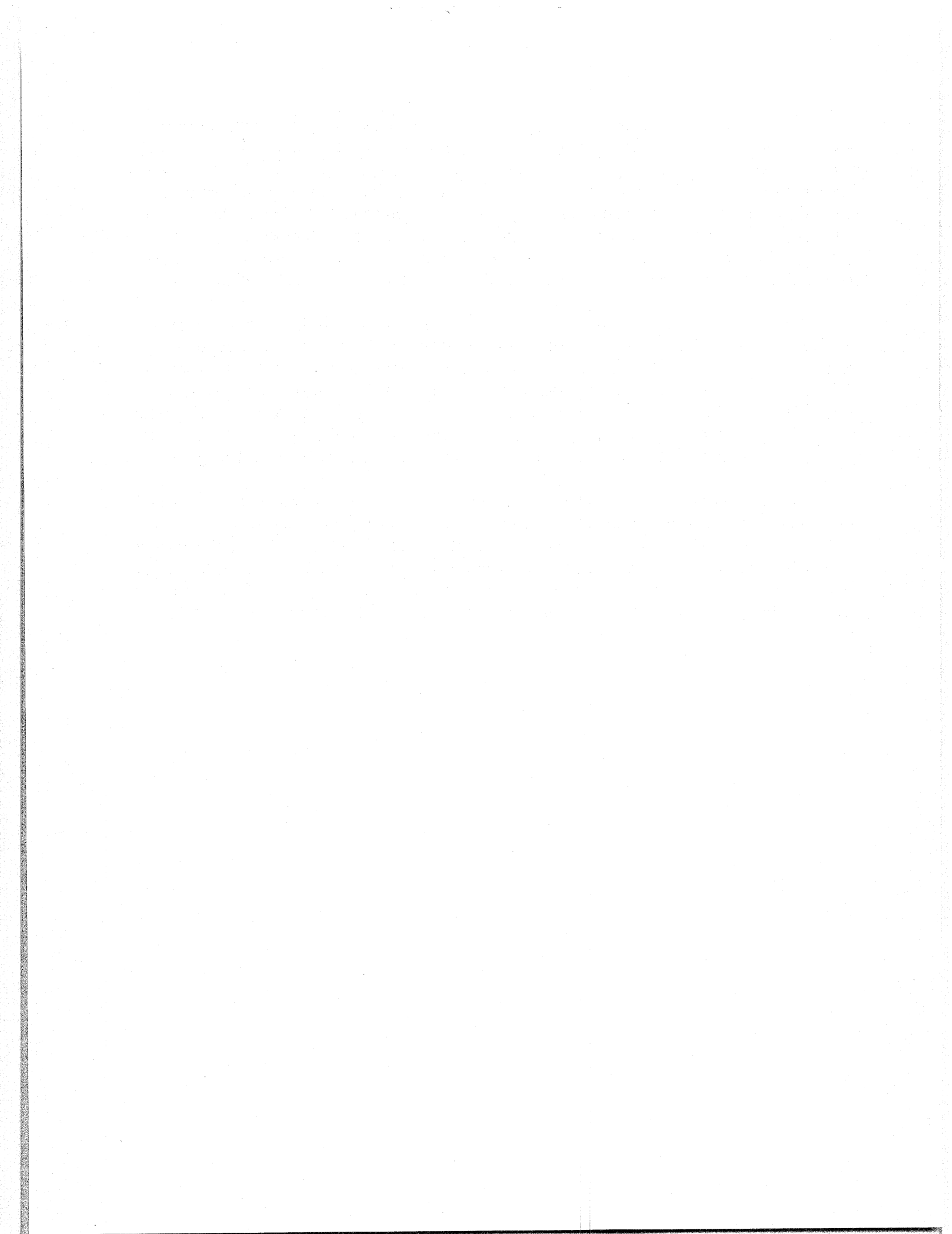
### Summary

The emphasis of a thickness design procedure should be to maintain a high level of load transfer efficiency and to limit fatigue cracking from developing into premature punchout distress under uniformly supported conditions. Loading under nonuniformly supported conditions will accelerate the wearout of the load transfer and the accumulated fatigue damage due to bending stresses. It has been established that load transfer efficiency is a function of the crack width and that the crack width depends upon the crack spacing and that limiting crack widths are clearly a function of pavement thickness, loading conditions, and the required performance conditions. Use of a constant crack width requirement for all designs may rarely be adequate and is therefore not recommended for design practice. Crack width variability can be considered in design as outlined in this chapter.

Crack spacing may be assumed to be normally distributed over a given range; however, a large amount of variability is associated with any given crack space distribution. This variability should be accounted for in design but can be significantly reduced based on recent construction developments (discussed later) to positively control cracking to induce a predesigned crack pattern. The crack width variability can be expressed with a probability level on the basis of the variability of the crack spacing, concrete strength, and maximum temperature drop from the curing temperature at the time of construction and concrete shrinkage. The pavement thickness is determined as a function of the load transfer efficiency and the crack width variability.

Design analysis of transverse bending and climatic stresses can be considered in terms of load transfer. Analysis and field data indicate that the load transfer efficiency remains high as long as crack spalling is at a minimum and crack widths are maintained within the limits shown in figure 21. Under these conditions, bending stresses will be maintained at a relatively low level. Therefore, if load transfer efficiency decreases due to aggregate wearout or widening crack widths, the total stresses will increase. The design pavement thickness is consequently a function of the load transverse efficiency, the design crack width, and accumulated fatigue damage.

Design reliability can be implemented in terms of selected design parameters with an end result of an increased overall reliability in the pavement performance as long as uniformly support conditions exist. Given a crack space distribution, a consistent level of reliability may be applied to the design in terms of crack spacing, crack width, and material characteristics. As data are made available, pavement performance may be correlated to the accumulated fatigue damage due to longitudinal cracking leading to punchout distress for different regions of the country.



## CHAPTER 4 - CONSTRUCTION METHODS TO IMPROVE CRC PAVEMENT CRACK PATTERNS

Continuously reinforced concrete (CRC) pavement is characterized by the presence of longitudinal reinforcing steel placed continuously throughout its length that, technically speaking, has no intentionally placed transverse joints other than construction joints in the pavement. However, the continuity of the concrete in the pavement is interrupted by a great number of transverse cracks caused by volumetric changes in the concrete due to shrinkage and temperature changes. When a transverse crack occurs, the stress distributions in concrete and the reinforcing rebar change greatly from point to point in the pavement. Experience has indicated that pavement performance is significantly linked to the resulting transverse crack pattern or post-cracking behavior of CRC pavement. For example, short crack spacings coupled with pavement locations where poor support conditions exist have shown a strong correlation with a high frequency of punchout distress. On the other hand, long crack spacings can lead to large crack openings, which may result in crack spalling, steel rupture, and poor LTE. Once load transfer has diminished to a certain extent, punchout distress or faulting may be evident particularly where loss of support exists under the pavement. Even crack initiation, unto itself, can lead to the development of undesirable surface defects, such as 'Y' cracks, which eventually may require maintenance. Some advantage does exist by controlling the crack pattern, for a given set of conditions and materials, to minimize crack widths, spall development, and poor crack patterns and surface defects thereby extending the pavement life. Therefore, the positive control of the crack pattern and the initiation of cracking in CRC pavement by initiating or inducing the transverse crack at a desirable crack location and orientation and crack pattern may be an efficient way to improve the performance of CRC pavement. Since cracking in CRC pavement is, in practical terms, unavoidable it should be employed or induced to the advantage of the design engineer.

In the 1986/1993 AASHTO Guide for Design of Pavement Structures, a procedure is set forth that considers crack spacing, crack width, and steel stress at a crack in the design of CRC pavement. The design percentage of longitudinal steel is selected in such a way that the results from the analysis satisfy the desired range in crack spacing, allowable steel stress, and crack width. This analysis is a function of predetermined parameters such as concrete tensile strength, thermal coefficients of steel and concrete, rebar diameter, concrete tensile stress due to wheel load, concrete shrinkage, and design temperature drop based upon predictive formulas. This design method suggests providing an appropriate percentage of steel reinforcement to distribute transverse cracks, so that instead of a few wide cracks, there are numerous cracks consisting of small widths.

During construction, it is expected that the final crack spacing will fall into the desirable range due to the above mentioned design parameters. Unfortunately, it is difficult to eliminate 'Y' cracks and other defects such as closely spaced transverse cracks by only adjusting the amount of longitudinal steel, primarily because of the variability of material properties, construction factors, and environmental conditions that are to some extent outside of the

contractor's control. Moreover, the early aged cracking behavior of CRC pavement is not only affected by the previously noted design parameters but also by the vertical location of the longitudinal and transverse steel reinforcement, coarse aggregate type, and ambient temperature condition at the time of paving. This has been a concern for some time, and efforts are underway to develop a greater knowledge base of these factors and their influence during construction on CRC performance. (Current research efforts at the Texas Transportation Institute (TTI) and the Center for Transportation Research (CTR) are addressing the influence of the above factors in field test sections on crack development in CRC pavement and developing models to consider these factors in an effort to provide and advance new concepts in the technology of CRC pavement construction.) The sections that follow will briefly describe these efforts and some of the experimental concepts to be considered to improve how CRC pavements perform.

### **Experimental Pavement Sections to Improve Crack Patterns**

A CRC pavement test section examining coarse aggregate effects on pavement crack patterns in light of different crack control and curing methods was constructed on Highway 290 in Cypress, Texas. The information from this section is to provide a basis to modify specifications for construction. This test section was useful in examining the factors that affect cracking behavior of CRC pavement under hot climate conditions since the construction took place in August of 1992. Therefore, the findings and conclusions that were developed from this section are applicable to concrete pavement construction under hot weather conditions as they would occur in areas of Texas. This test section included a variety of variables related to crack initiation under field conditions in CRC pavement. These methods are as follows:

- Saw cutting a swallow notch in the pavement surface.
- Metallic crack inducers placed in various configurations.
- Transverse reinforcement.

Saw cutting techniques and crack inducers were used to control, on an experimental basis, the transverse crack locations at different prescribed intervals. Transverse rebar and inducer locations were documented prior to concrete paving operations.

Four different concrete mix designs with different types or amounts of coarse aggregate were used in the Cypress test site. Also, different curing methods were used in experiments at the test site to investigate the effect that method or type of curing may have on crack development in CRC pavement. Concrete temperature and relative humidity were measured by thermocouples and specially modified (commercially available) humidity sensors.

The Cypress test section consisted of 330 mm (13 in) pavement thickness, and contained a double layer of steel reinforcement. The test section, which was constructed under a temperature range from 32 to 38°C (90 to 100°F), also consisted of four different mix designs systematically placed in two separate areas of the paving construction. The mix designs for the test sections are summarized in table 3. The Cypress test section also included three different

Table 3. Four mix designs used in Cypress test section.

Composition lb per cubic ft	Mix 1 100% LS	Mix 2 67% LS, 33% RG	Mix 3 67% RG, 33% LS	Mix 4 100% RG
Coarse Aggregate	277	185.7/96.4	195.8/91.5	292.2
Water	35	35	35	35
Cement	65.8	65.8	65.8	65.8
Fly Ash	23	23.1	23.1	23.1
Fine Aggregate	233	232	232	231
Entrained Air (%Vol.)	4.5%	6.4%	5.5%	4.6%
W/C Ratio	0.39	0.39	0.39	0.39
Cement Factor (SK/CY)	6	6	6	6
Coarse Aggregate Factor	0.652	0.652	0.652	0.652
Maximum Coarse Aggregate Size (in)	1.5	1.5/1.5	1.5/1.5	1.5

curing mediums (polyethylene film, double coat of wax-based membrane curing compound, and single coat of wax-based membrane curing compound). All experimental crack control and early aged surface notching techniques were employed in specially designated sections to induce pavement cracking at 0.9 m (3 ft), at a combination of 1.2 and 1.5 m (4 and 5 ft) pairs, 1.8 m (6 ft), and 2.7 m (9 ft) crack spacings. Metallic crack inducers, shown in figure 25, were placed in both single and stacked layer configurations and were anchored to the double layer of longitudinal reinforcement to provide support against the flow of the fresh concrete during the paving operations.

A variety of devices were installed in both test sections to instrument the test pavements for temperature, moisture, and shrinkage variations as a function of the curing conditions. These devices consisted of thermocouples, monitoring points for specially modified relative humidity (RH) sensors, and D-Mec points embedded in the pavement section while the concrete was in a fresh state. Immediately after paving, a series of field measurements and crack surveys were conducted. A sample of results from the field surveys of the collected data is given in the following sections of this report with respect to the concrete temperature and relative humidity

measurements and the methods for control of cracking in CRC pavement. A summary of primary findings and discussions is also provided.

#### Measurement of Pavement Temperature and Relative Humidity

Previous field studies of CRC performance in Texas concluded that the formation of transverse cracks result from a drop in pavement temperature following the rise in temperature due to the

evolution of the heat of hydration. However, at this very early-age, it is expected that both pavement temperature and moisture changes affect the development of transverse cracking, particularly at the pavement surface where a certain amount of shrinkage due to moisture loss combined with the temperature effects in the concrete near the surface of pavement may be the primary factors that initiate cracks at the pavement surface. After the concrete material achieves a level of maturity and strength, the drying shrinkage may make less of a contribution to later transverse crack development which continues for a year or more after placement of the pavement. Typically, 80 to 90 percent of the transverse crack develops in the first 180 days after paving.

Typical concrete pavement temperature distribution with depth at early ages indicated that the temperature variation at the pavement surface was larger than that at the pavement bottom. A maximum pavement temperature condition occurred, in many instances, during day 2 and day 3 after paving. The maximum temperature difference between the top and the bottom of pavement ( $T_{\text{top}} - T_{\text{bottom}}$ ) was a minus 12°C (20°F), which occurred at 7 a.m. in the morning and a plus 13.2°C (22°F) at 4 p.m. in the afternoon, respectively, on day 2 after paving. However, the maximum temperature difference over the time period from day 2 to day 4 was 25.2°C (42°F) at the pavement surface and 16.8°C (28°F) at the bottom of the pavement.

Generally speaking, the distribution (in both time and space) of initial pavement temperature depended on the ambient temperature conditions and the mix proportioning of the concrete. In order to account for the moisture effects on the cracking behavior in concrete pavement, moisture history and distribution through the slab thickness was measured. A small relative humidity sensor was used to measure the relative humidities interior to the concrete

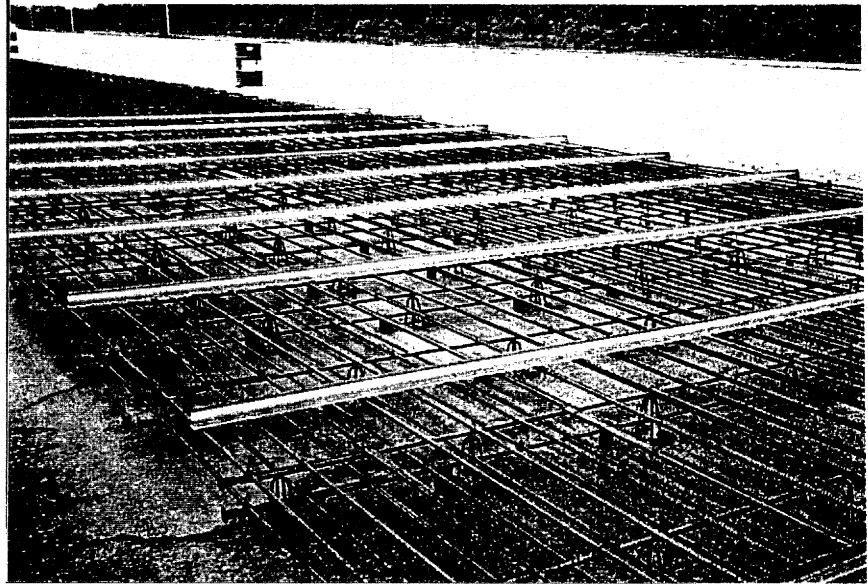
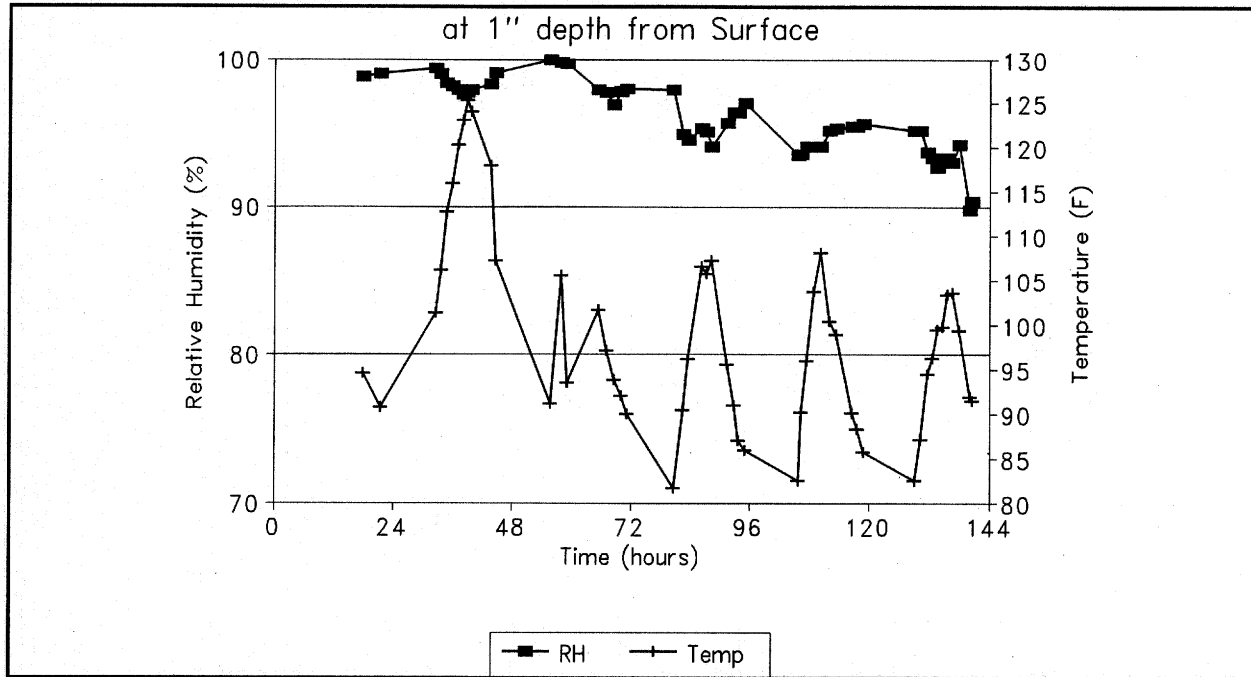


Figure 25. Metallic crack inducer located on the top of longitudinal rebar.



$^{\circ}\text{F} = 32 + 1.8^{\circ}\text{C}$ , 1 in = 25.4 mm

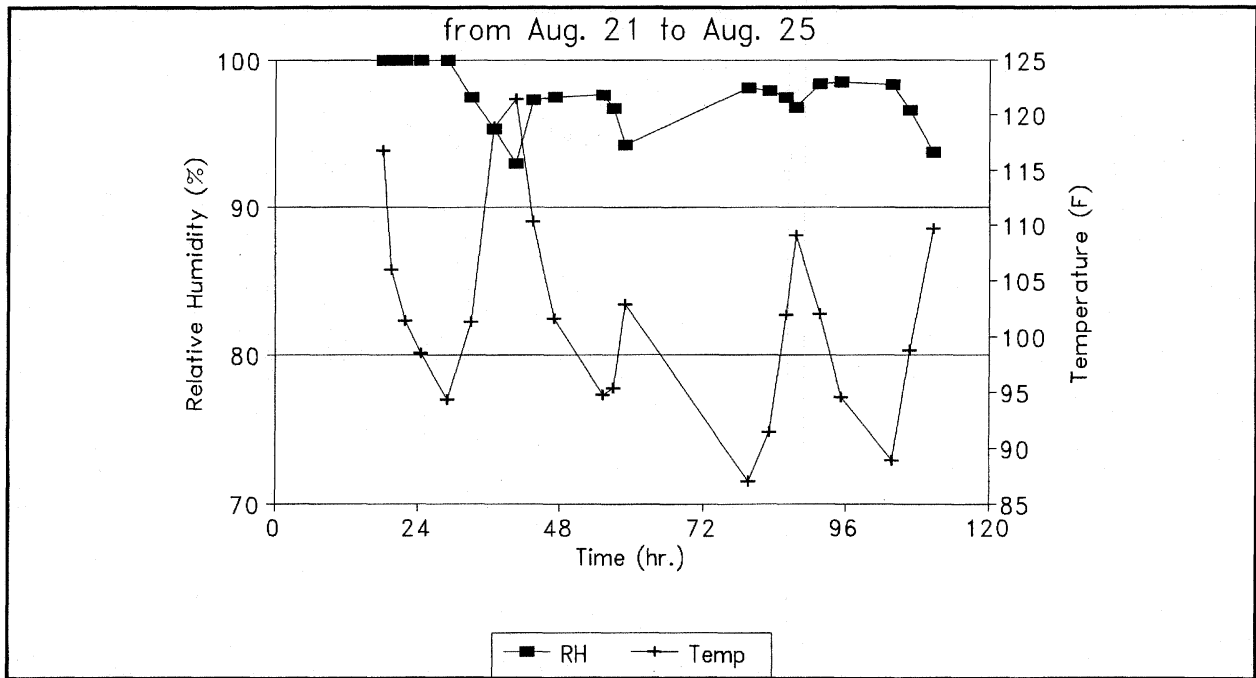
Figure 26. Typical relative humidity variation with time at 25 mm (1 in) from the surface of the pavement.

placed in the field test sections. The most common sensor in use is the thin-film capacitance type humidity sensor. These sensors comprise parallel electrodes on a glass substrate covered by a thin film of a hygroscopic polymer. The sensor monitors the change in capacitance of the thin polymer film as it absorbs water vapor. The full response of the probe can be achieved within a few seconds at relative humidities below 80 percent but at higher humidities the response becomes inconveniently slow.

Relative humidity measurements were taken at depths from the pavement surface ranging from 12.5 mm (0.5 in) to 292 mm (11.5 in) at 63.5 mm (2.5 in) intervals. The field installation was configured to protect the sensors while monitoring hardening concrete. The temperature and relative humidity were measured simultaneously at various concrete ages.

With the use of specially prepared relative humidity/temperature (RHT) sensors, the interior relative humidity in concrete pavement was successfully measured. Several observations were noted with respect to variation in relative humidity within the pavement section. Typical relative humidity variation during the first day of paving as measured from the Cypress test section is shown in figure 26.

The interior relative humidity in concrete pavement tends to vary with daily temperature variation. In other words, when temperature increases the relative humidity decreases and vice



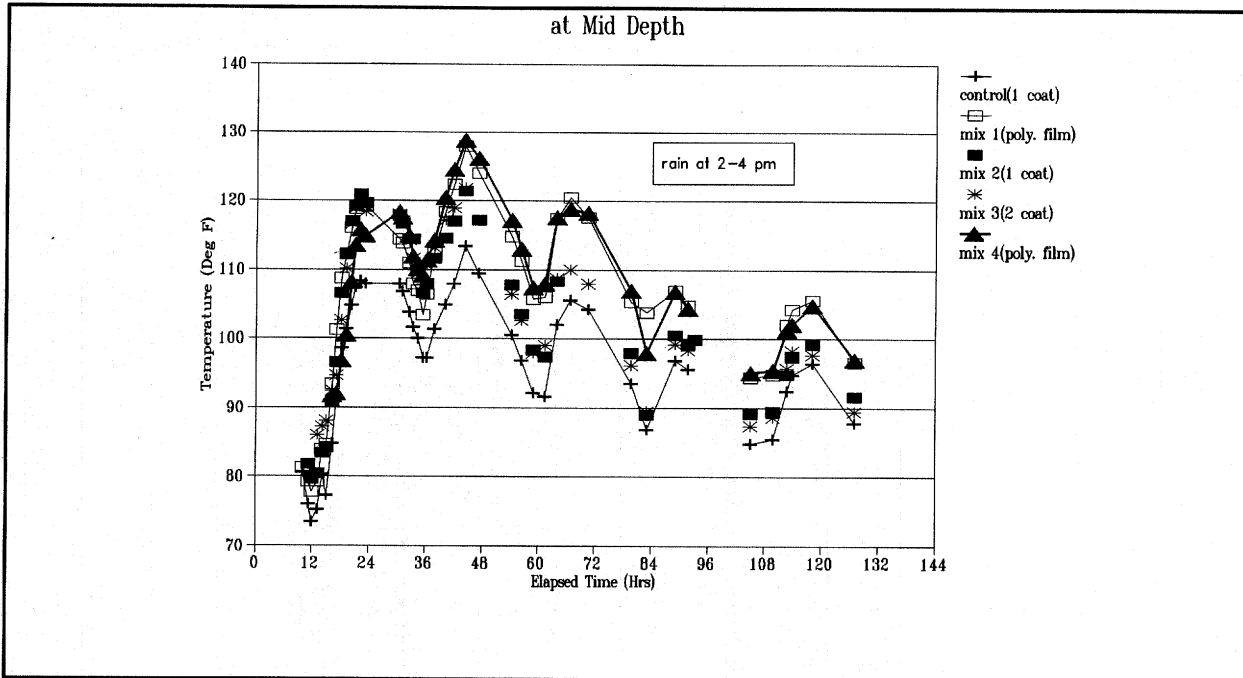
°F = 32+1.5°C

Figure 27. Relative humidity in the section cured by polyethylene sheet.

versa. This indicates that the interior relative humidity in concrete is a function of interior concrete temperature. However, after the hardening process, the overall tendency of relative humidity variation was to decrease with time. A similar characteristic was not as evident in Cypress pavement sections cured by polyethylene sheeting (shown in figure 27) in comparison to those in the sections cured by single coating of Type II curing compound (shown in figure 26). Polyethylene sheeting curing also affects the initial pavement temperatures particularly under hot paving conditions. This is illustrated in figure 28 where the newly placed concrete pavement covered by polyethylene sheeting developed greater maximum temperatures than pavement sections cured with membrane curing.

The moisture profiles in the second day and first 5 days after are greater than those in the control sections, which contained 100 percent limestone as the coarse aggregate. Figure 29 shows the effect of different curing methods on interior relative humidity in concrete measured on day 29.

From the viewpoint of preventing moisture loss, polyethylene film is more effective than a double coating of Type II curing compound at early ages. However, during the later stages of curing, a double coating of Type II curing compound is equivalent to the effectiveness provided by the polyethylene film. Both are more effective than a single coat of Type II curing compound.



$$0^{\circ}\text{F} = 32 + 1.8^{\circ}\text{C}$$

Figure 28. Temperature variations in the sections with different curing methods.

In contrast to temperature variation at the pavement surface, the loss of relative humidity at the surface is larger than that at the bottom of pavement. With respect to the combined effects of moisture and temperature, no pavement cracking was observed in the Cypress crack control sections until the morning of the third or fourth day after placement of the pavement. The noted variation in temperature and moisture with time and with depth apparently must achieve a certain level prior to crack initiation since transverse cracks did not occur (in the crack control section) until the early morning of day 3. (It should be pointed out that these observations were verified by greater crack openings at the pavement surface than at the bottom of pavement.) From the viewpoint of crack control under variations of this nature, crack initiation may be better served from notching at the pavement surface.

A series of field test specimens was prepared to determine concrete strength properties as they varied after the construction of the Cypress pavement sections. Table 4 shows the flexural strengths of concrete for four Cypress mix designs. It is clear from table 4 that the flexural strength of concrete with 100 percent river gravel as coarse aggregate is less than the others at early ages. At day 28 concrete paved with 100 percent river gravel has the highest flexural strength among the four mix designs.

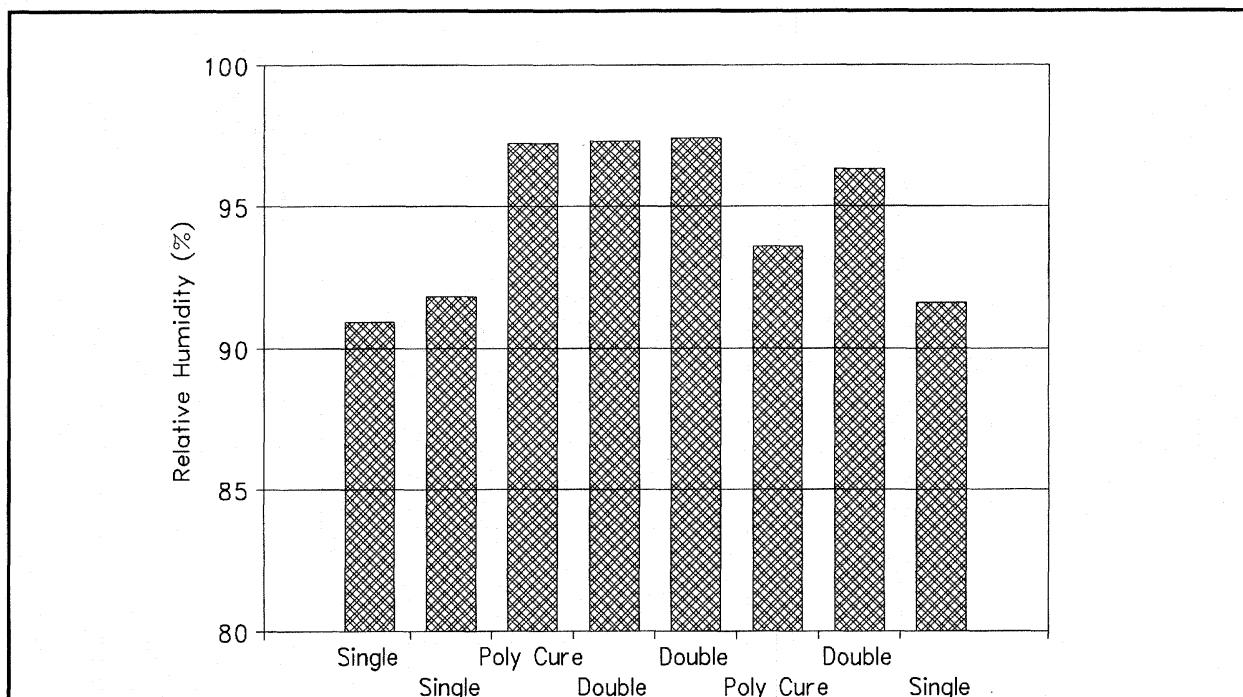


Figure 29. Effect of curing method on relative humidity in concrete pavement.

### Crack Control Methods

Cracks in the Cypress test sections were allowed to occur randomly or were controlled by inducers at prearranged locations. The crack induction was achieved by the use of swallow saw cut notches in the surface of the pavement or by the use of specially made and placed metallic crack inducers previously described. It also interesting to note that several cracks were unintentionally controlled by the transverse reinforcement typically placed as a part of the normal pavement reinforcement to support the longitudinal reinforcement in position. Some sections were placed with skewed transverse steel with reduced crack initiation on the transverse bar by approximately 50 percent. In any case, longitudinal reinforcement can be designed for CRC pavement so that the resulting crack spacings and widths are limited to certain ranges. The objective of the longitudinal reinforcement in the pavement structure is to maintain transverse crack widths tightly closed (within the limits shown in figure 21) as previously noted, but current CRC pavement design methods deal only with the latter approach in terms of crack control. But it is worth noting that the location of early aged cracks cannot be completely controlled by longitudinal reinforcement alone because of the previously noted propensity of early aged cracks to initiate at the pavement surface or the location of transverse steel, particularly when placement is done under summer or hot weather conditions. Another factor worth considering is the vertical position of the steel reinforcement, which may affect the transverse crack spacing and in turn affect the crack width.

Table 4. Third point loading concrete flexural strengths (psi).

Concrete Age	Mix 1 100% LS	Mix 2 67% LS 33% RG	Mix 3 67% RG 33% LS	Mix 4 100% RG
1 Day	370.8	369.6	395.85	308
3 Day	610.05	610.8	608.64	531.6
7 Days	678.9	682.1	730.43	636
14 Days	752.085	737.3	750.43	688.7
28 Days	798.5	818	769	842.5

1 psi = 6.89 kPa

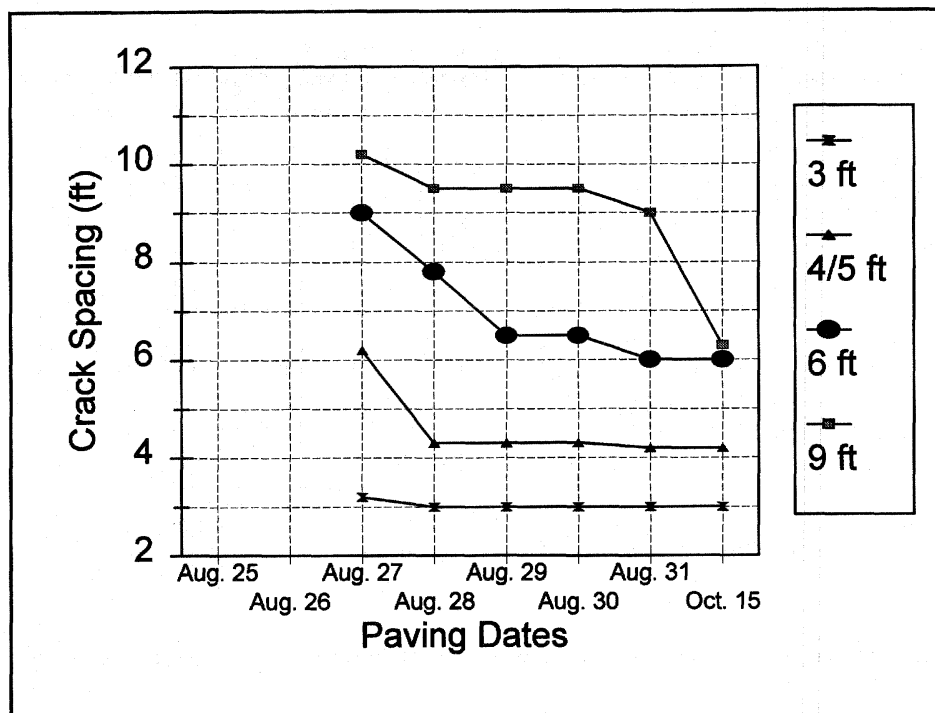
Two methods were considered in the test sections constructed in Cypress, Texas, for initiating cracks in CRC pavement. Early-aged saw cutting techniques were used (consisting of a light and portable saw cut machine as shown in figure 30) for surface notching, while the second method consisted of crack inducers placed to initiate cracking at the interior of the pavement thickness. In the Cypress test section, a similar pattern was followed where the longitudinal contraction joint was notched to a nominal depth of 25.4 mm (1 in) in selected paving segments.



Figure 30. Early-aged saw cutting technology.

The length of the transverse crack control section consisted of approximately 365.8 m (1200 ft). Notches were made about 4 h later after placement with 0.9 m (3 ft), 1.2 and 1.5 m (4 and 5 ft) combinations, and 1.8 m (6 ft), and 2.7 m (9 ft) intervals.

Experience in early-aged saw cutting practice has indicated that notches should be made between initial and final setting of the concrete. Timing is a very important factor to achieve the goal of artificial crack induction particularly at swallow notch depths. Results from crack surveys conducted on these test sections has indicated that surface notches placed early (shortly



1 ft = 0.305 m

Figure 31. Cracking development at saw cut locations.

after initial set has occurred) show very positive results and that cracking can be largely controlled by these notches. In comparisons made in figure 31, it is noted that nearly 100 percent cracking occurred in the notches spaced at 0.9 m (3 ft) and at 1.2/1.5 m (4/5 ft) notch combinations approximately 3 days after paving the Cypress test sections. However, in the 1.8 m (6 ft) and 2.7 m (9 ft) saw cut interval sections, it took 6 days to reach 100 percent cracking at the notches after placement. As noted in figure 31, secondary cracking occurred (after day 20) in the 2.7 m (9 ft) saw cut interval sections. A similar pattern was noted in the internally induced crack control sections that were similarly spaced. This may indicate that either the designed length of saw cut interval or the design percent of steel reinforcement should be reduced as long as the desired crack widths are maintained (a 10 percent reduction in steel content offsets the cost of the saw cutting). If the above-mentioned results are compared with the uncontrolled cracking Cypress sections, it can be found that it took several months to reach an average crack spacing of 1.8 m (6 ft) or even more to reach average crack spacing 0.9 m (3 ft).

Unlike the notching technique used to initiate cracking on the surface of pavement, crack inducers were used to initiate cracking from interior portions of pavement. It is seen from table 5 that a greater percentage of cracks occurred at the double crack inducers than at the single crack inducers. However, the incidence of cracks that occurred at the internal crack inducers is much less than at the surface notches. Under the paving and weather conditions that prevailed during the placing of the Cypress test sections, there appeared to be a number of cracks not controlled by the internal crack inducers. It was interesting to note that several cracks, in both the LaPorte (another test site) and the Cypress test sections, were found to coincide with the location of the transverse reinforcement. Therefore, it stands to reason that the design engineer may be able take advantage of the positioning of the transverse steel in the control of transverse cracking. It is anticipated that if interior crack inducers are embedded closer to the surface of pavement (and

Table 5. Percentage of crack initiated at crack inducer.

Location	No of Coatings	Spacing	Total No. of Crack	No of Crack at Inducer	Total %
Part III B1	Double	4 ft / 5 ft	14	8	57.14%
	Single	4 ft / 5 ft	15	6	40.0%
Part III B2	Double	6 ft	17	8	47.06%
	Single	6 ft	14	6	42.85%
Part III B3	Double	9 ft	15	6	40.0%
	Single	9 ft	25	-	-

1 ft = 0.305 m

that corrosion potential is not a concern), a greater percentage of cracks will be initiated due to greater stress intensity at the notch tip caused by increased restraint to induced displacement initiated by temperature drop and drying shrinkage.

As previously alluded to, transverse rebar in CRC pavement is used (1) to support the longitudinal steel reinforcement at the desired vertical location during the construction process, and (2) to maintain the spacing of the longitudinal steel during placing operations. However, field surveys of the test sections in the first 30 days found that there is a certain percentage of cracks initiated by the transverse reinforcement, as previously noted. These surveys have indicated that the percentage of cracks initiated by the transverse rebar is about 50 percent, and at even greater percentage in concrete pavements constructed with river gravel as the coarse aggregate type (see figure 32). A greater percentage of edge cracks initiated by the transverse rebar was noted in the LaPorte test section (constructed under winter conditions) as evidenced in a comparison of figures 32 and 33.

Apparently, based on the above limited observations, surface crack initiation using early-aged notching techniques, is more effective than interior crack initiation (i.e., crack inducer or transverse reinforcement) in controlling the crack pattern. Usually, the notch width is larger than initial random crack opening which may suggest that the notches should be sealed after saw cutting, to reduce the possibility of spalling around the notches; however, spalling of this nature has not been observed in the early-aged notches. Whether the transverse crack is initiated by crack inducers or notches, it is expected that crack width or the crack opening could be minimized as a result of this process.

In the Cypress test section that consisted of the uncontrolled cracking section, four mix designs were included. Mix designs 1 to 4 contained 100 percent limestone, 67 percent

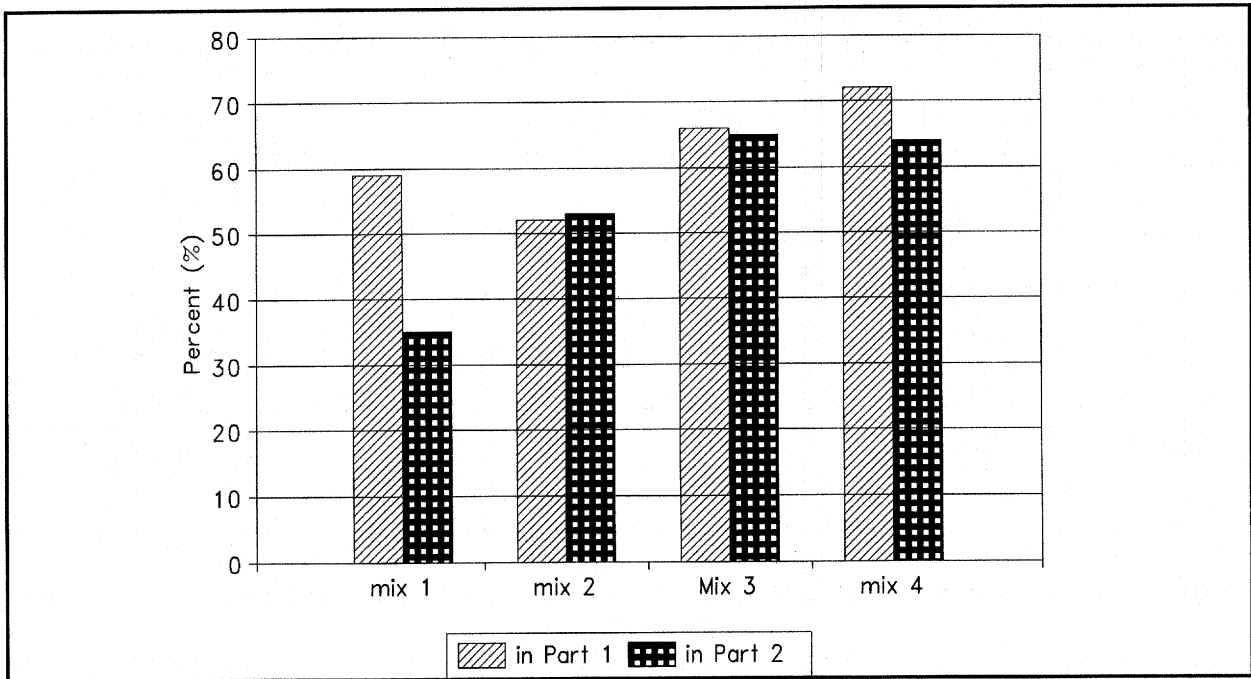


Figure 32. Percentage of cracks that occurred at rebar in Cypress section.

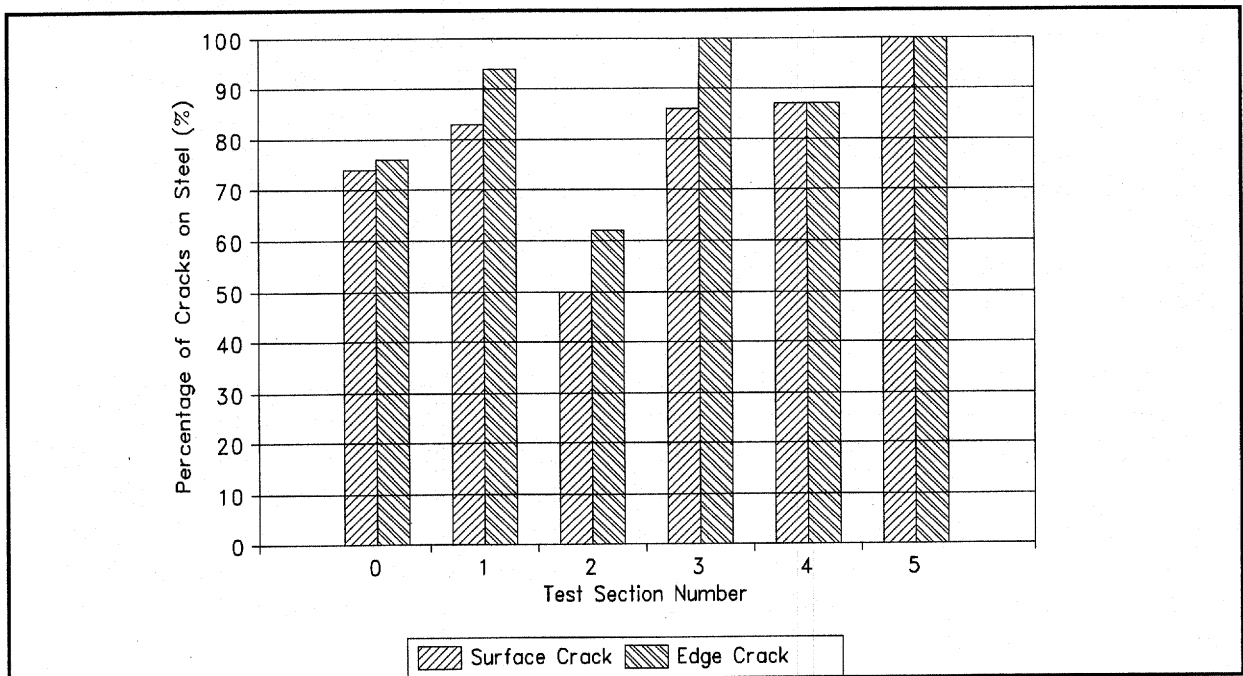
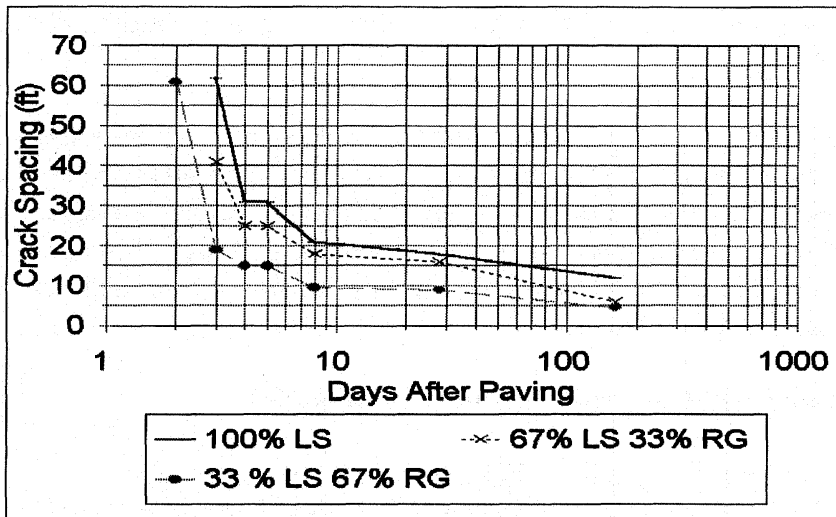


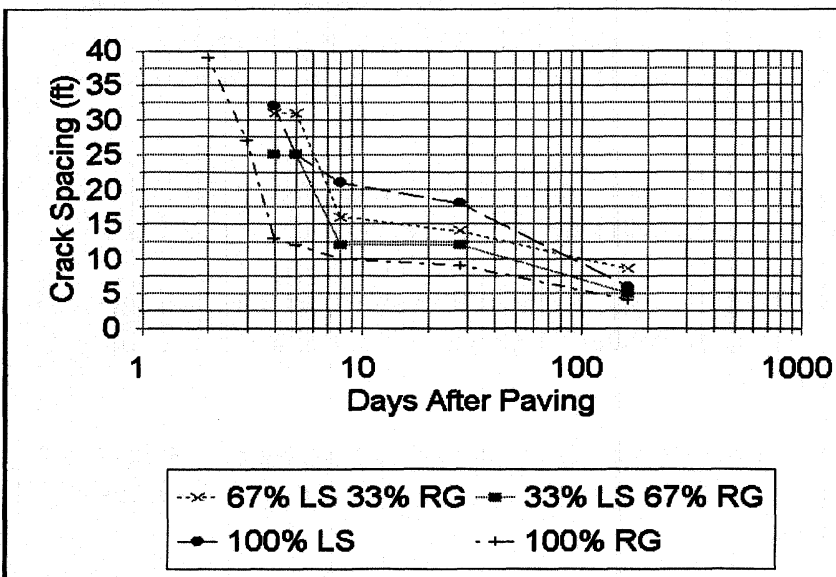
Figure 33. Percentage of cracks that occurred at rebar in LaPorte section.



1 ft = 0.305 m

Figure 34. Uncontrolled cracking test sections placed in morning hours.

afternoon before 4 p.m. Concrete with more river gravel as coarse aggregate had less uniformly distributed cracks and smaller average crack spacing than concrete with more limestone. More cracks tended to occur at early age in concrete with river gravel than concrete with limestone as the coarse aggregate.



1 ft = 0.305 m

Figure 35. Uncontrolled cracking test sections placed in afternoon hours.

limestone and 33 percent river gravel, 67 percent river gravel and 33 percent limestone, and 100 percent river gravel, respectively, as previously indicated. Paving at the Cypress test section started in the early morning of August 20th. Figures 34 and 35 show the crack spacing variation in each mix design as a function of the time of placement (morning versus afternoon). Not only the time of initial crack occurrence was delayed but also initial crack spacing was reduced for all mix designs when paving occurred in the

The field results indicated that under the same environmental conditions, CRC pavement using limestone as the coarse aggregate results in a larger average crack spacing than CRC pavement using river gravel as the coarse aggregate. Typically, the crack spacing ranged from 1.5 to 11.2 m (5 to 37 ft) with an average of 3.6 m (12 ft) for limestone concrete and ranged from 0.6 m to 3 m (2 to 10 ft) with an average

of 1.2 m (4 ft) for river gravel concrete. If 2.4 or 3.6 m (8 or 12 ft) is chosen as the designed sawcut interval, it may be achieved (0.3048 m = 1 ft) in concrete pavement with limestone under some conditions, but it may not be achieved in concrete pavement with river gravel, particularly if constructed in the summer months.

It was found that the visible depth of most initial vertical cracks observed from the edge of pavement was more than four-fifths of pavement thickness when they were first observed on the early morning of the third or fourth day after paving. The width of early developing cracks (all were less than 0.38 mm (15 mils)) are larger than that of later developing cracks. This indicates that the history of crack formation development may affect the structural responses of CRC pavement and its associated long-term performance.

### **Suggested Guidelines for CRC Pavement Construction and Crack Control**

As a result of the Cypress test section and others similar to it, a set of construction guidelines were devised. Appropriate CRC pavement design and construction procedures need to recognize and consider the effects of coarse aggregate type selection, curing practice, and weather conditions on performance. Coarse aggregate type selection can be determined in terms of physical properties such as the thermal expansion and the bonding characteristics of the aggregate. The bonding toughness can be characterized in terms of all fracture toughness (using a modified ASTM C496) of the concrete mixture determined at an early age of 1 day and the chemical makeup of the aggregate. Although coarse aggregate type may affect drying shrinkage to some extent, this factor is considered insignificant in aggregate type selections.

Coarse aggregate type selection should be made in terms of categories of the thermal characteristics of the concrete mixture or the aggregate itself and upon the engineering and chemical properties of the coarse aggregates used in the mix. The proposed categories are as follows:

- |                     |  |
|---------------------|--|
| <b>Category #1)</b> | Coarse aggregate coefficient of thermal expansion $< 4.0 \mu\epsilon$ and mixture fracture toughness at 1 day of age $> 31.3 \text{ mPa}\cdot\text{mm}^{1/2}$ . <sup>(32)</sup>          |
| <b>Category #2)</b> | Coarse aggregate coefficient of thermal expansion $> 4.0$ but $< 6.0 \mu\epsilon$ and mixture fracture toughness at 1 day of age $< 31.3$ but $> 24.3 \text{ mPa}\cdot\text{mm}^{1/2}$ . |
| <b>Category #3)</b> | Coarse aggregate coefficient of thermal expansion $> 6.0$ but $> 8.0 \mu\epsilon$ and mixture fracture toughness at 1 day of age $< 24.3$ but $> 17.4 \text{ mPa}\cdot\text{mm}^{1/2}$ . |
| <b>Category #4)</b> | Coarse aggregate coefficient of thermal expansion $> 8.0 \mu\epsilon$ and mixture fracture toughness at 1 day of age $< 17.4 \text{ mPa}\cdot\text{mm}^{1/2}$ .                          |

Aggregates in a concrete mixture may be blended to improve the engineering properties of the mixture. Blending can also be considered to improve workability, strength, fracture toughness, and thermal behavior characteristics. Drying shrinkage is largely controlled by the quality of curing.

### Summer Versus Winter (or Nighttime) Placement :

#### *Summertime Placement (air temperature < 33°C)*

- Enhance random crack control by skewing the transverse reinforcement (at a 60° angle) to minimize the incidence of transverse cracking at the location of the transverse bar for sections using *category #1 and #2* coarse aggregate mixtures.
- Positively control the crack spacing and reduce the potential for spalling in pavement sections consisting of *categories #3 and #4* coarse aggregate mixtures with swallow, transverse saw cut notches (made with the early-aged saw cut method) placed at specified intervals in the pavement surface. Also, use the transverse steel (in an unskewed configuration) to supplement induction of the crack at the surface notches. The percent of steel should reflect the percentages established by suitable analysis that specifies the percentage of steel reinforcement according to *the mixture category*. *Category #3 and #4* mixtures require less reinforcement to achieve the desired crack spacing and should be designed according to the coarse aggregate properties. The crack pattern can also be satisfactorily controlled with the use of positive control measures on alternating crack locations.
- Use as a minimum a combination of any two of the following curing methods.
  - a. One coat of Type I curing compound,
  - b. One coat of Type II curing compound, or
  - c. Polyethylene Sheeting

#### *Summertime Placement (air temperature > 33°C)*

- Same as above, but use two coats of Type II compound for placements made with *category #1 and #2* mixtures and polyethylene sheeting (with a coat of Type I compound) for placements made *with category #3 and #4* mixtures.

### Winter Placements

- Use a combination of one coat of Type I and Type II curing compounds and adjust the percent of fly ash to prevent long delays in initial set times.

- Use early-aged transverse saw cutting to minimize the incidence of delamination in *category #4* mixture placements in combination with mid-depth crack inducers (i.e., alignment of double layer transverse steel with the sawcut notches). *Category #4* mixture placements should use inducers placed at mid-depth since crack initiation is much greater at this location in the slab under winter placing conditions.

Concrete strength is not directly considered in these guidelines since its effect is reflected in the aggregate/paste bond strength at an early concrete age.

### **Conclusions**

Based on the limited experience and observation gained from the test sections constructed in LaPorte and Cypress, Texas, the following preliminary conclusions are offered.

Early-aged sawcutting practice in the Cypress test section suggests that surface crack initiation is more efficient than interior crack initiation (i.e., crack inducer and transverse rebar). It is recognized that sawcutting should be performed between initial and final setting of the concrete. Under some conditions, early-aged sawcutting techniques (in combination with the transverse reinforcement location) may be entirely sufficient to control the crack pattern, where for other conditions, the use of interior crack inducers may be warranted.

Control of crack pattern in CRC pavement can be affected by several factors other than those relative to the technique of crack induction. Good mix design (in terms of workability and crack susceptibility), reinforcement steel design, and construction practice will ensure that crack interval will develop as expected. In traditional design analysis of CRC pavement, the average crack spacing and crack width is derived as a result of the longitudinal steel design, the tensile strength of the concrete, and the design temperature drop. This approach assumes when the stress induced by a drop in temperature and drying shrinkage exceeds the tensile strength, a crack is assumed to form in concrete pavement. Naturally, a great degree of variation is expected (and does occur as surface defects) in the actual crack patterns, which, if can be significantly reduced, will result in more economical CRC pavement designs providing greater performance lives.

## CHAPTER 5 - ADVANCEMENTS IN THE EVALUATION OF CRC PAVEMENT PERFORMANCE

An approach to the evaluation of existing CRC pavement should take into account two factors relative to the performance of CRC pavement: uniformity of the crack pattern and structural adequacy of the transverse cracking and pavement support system. Characterization of the crack pattern can be accomplished from analysis of crack spacing data. Poor crack pattern characteristics such as 'y' cracks, divided cracks, close crack intervals, etc., can be included in parameters derived from analysis of the cracking data. Poor characteristics noted above can increase the potential for punchout distress if poor support conditions develop or wide cracks. Therefore, the effect of the crack pattern should be included as part of the evaluation process of CRC pavement.

An approach to the structural evaluation of CRC pavement should take into consideration the development of pavement distress from two different aspects in terms of fatigue cracking and pavement support. The type of distress that typically occurs in CRC pavement and is often of the most concern to highway engineers is punchout distress. The mechanism associated with the development of this distress, which has been previously noted and summarized<sup>(2)</sup> and will not be elaborated here. However, it is recognized that the failure aspects pointed out above are entirely encompassed within the framework of the punchout mechanism.

Pavement support, uniformly distributed, has been recognized for several years as the key to long-term performance of CRC pavements (particularly for CRC overlays). However, the consequence of lack of uniform support appears to have been only indirectly considered in the design of CRC pavements in terms of the erodibility of the subbase surface. Recent experience in Pennsylvania,<sup>(25)</sup> Wisconsin,<sup>(26)</sup> and Arkansas<sup>(44)</sup> has indicated a need to consider nonuniformly supported conditions for CRC pavements, especially those placed as overlays on jointed concrete systems. Concentrated shear stresses (which can be very intensive) that result in punchout distress are difficult, if not impossible, to account for in design and are generally caused by unsupported subbase conditions. A design for these conditions may warrant crack and seating the original pavement system prior to overlaying. The characterization and analysis of the support under a CRC pavement (or overlay) is based upon initial stiffness (at the transverse cracks) of the pavement system and can be described in terms of nondestructive testing (NDT) results. It is noted that these results may depend upon several factors which are affected by the degree of pavement support and are therefore useful in characterizing subbase support. Associated with these factors are the inherent variabilities that should be accounted for to properly estimate the reliability associated with different levels of design (as discussed in chapter 4). Therefore, the focus of this chapter will be on the analysis and the process, which is mechanistic in nature, of the evaluation of CRC pavement behavior and support and its application to design.

## Crack Pattern Evaluation

The evaluation of the crack pattern can be broken down into three areas: crack condition, randomness of the crack pattern, and cluster cracking. Each of these areas is described in detail below.

A key factor in evaluation of the crack pattern is the condition of the transverse cracks. Table 6 is provided to assist in the visual evaluation of the transverse cracking condition. The crack classification categories listed in table 6 are broken down into four groups. C-1 and C-2 cracks are typically considered to be cracks in good condition and exhibit a high degree of stiffness. The crack width categories are based on widths at the surface of the pavement but typically are much narrower within a short distance below the pavement surface. C-3 and C-4 cracks are typically associated with punchouts in the later stages of development and exhibit low stiffness characteristics. Consequently, it is possible to generally associate the crack classifications with NDT evaluation of different transverse cracks.

### Randomness of Cracks

Cracks in CRC pavements can have various shapes. Some cracks might be straight and some are curved or meandered in shape. Cracks that meander (shown in figure 36) increase the probability of secondary cracks, which result in punchouts, the major form of distress of CRC pavements. The randomness of the crack can be found by rating the individual crack.<sup>(29)</sup>

The Randomness Rating (RR) concept was developed by McCullough et al.<sup>(29)</sup> Accordingly, RR is the mean of the individual randomness ratings. An individual randomness rating is a subjective rating of the randomness of a specific crack by an individual rater. The rating scale used was similar to the scale associated with the Present Serviceability Rating.<sup>(29)</sup> The scale is:

- (5.0) Very Good (almost straight crack)
- (4.0) Good
- (3.0) Fair
- (2.0) Poor, and
- (1.0) Very Poor (very meandering).

A mathematical model of the Randomness Index (RI) is derived by correlating the RR with objectively measured values taken from the corresponding cracks. The RI model can be used to obtain an estimate of the RR for any crack without the need for any further rating. The RR of a crack is represented by:<sup>(29)</sup>

$$RR = RI + \epsilon$$

where

$\epsilon$  = the residual not explained by mathematical model.

Table 6. CRC pavement classification systems.  
CRCP Crack Classification (modified AASHTO Road Test - Report 5)

- 
- C-1: Fine crack not visible under dry surface conditions at a distance of 4.5 m (15 ft). (Tight)
  - C-2: A crack that can be seen at 4.5 m (15 ft), but exhibits only minor spalling. The opening at the surface is 0.8 mm (30 mils) or less. (Open)
  - C-3: The crack is opened at the surface 0.8 mm (30 mils) or more for any portion of the crack length. The crack exhibits low to medium spalling. Amount of faulting is noted.
  - C-4: The crack is either very wide (> 1.6 mm) (60 mils) or sealed and exhibits medium to severe spalling. Amount of faulting is noted.
- 

In order to determine the randomness, the curve length of the crack (L), the lane width (W), and the number of concrete blocks (N), which are associated with the crack and enclosed by secondary cracks, are measured. These parameters are chosen because they are simple to measure, and the effects of secondary cracks, which form Y-cracks or punchouts, are reflected by the number of separated concrete blocks (N). Randomness (R) is represented by the following equation:<sup>(29)</sup>

$$R = \frac{L - W}{W} \times 100$$

where

- R = randomness
- L = curve length of the crack
- W = lane width

Using the general linear model procedure, a mathematical model for the RI, which is a function of R and N, was developed (29):

$$RI = \frac{5.463}{(R + 1)^{0.259} (N + 1)^{0.510}}$$

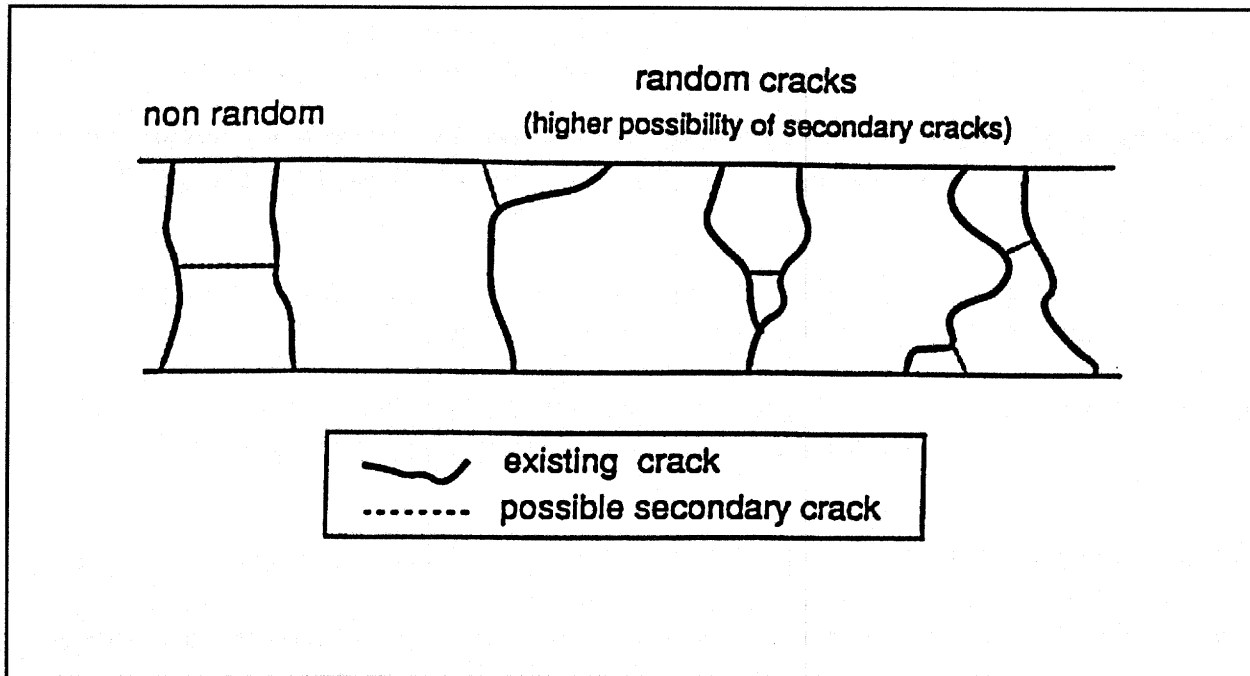


Figure 36. Shapes of cracks and possible cracks on random cracks.<sup>(29)</sup>

### Cluster Cracking

It is generally recommended in design that the crack spacing for CRC pavement should result in crack widths small enough to minimize the entrance of water into the crack and to provide the necessary load transfer through aggregate interlock. Consequently, cracking design criteria have evolved over time to include shorter cracking intervals. Early recommendations suggested design crack spacing should be between 1.5 and 2.4 m (5 and 8 ft) based on deflection test results and steel corrosion studies. Most recently the minimum crack spacing recommendation has changed to as low as 0.9 m (3 ft) based on load transfer and pavement stiffness requirements.<sup>(9)</sup> The maximum crack spacing recommended to minimize spalling at the transverse cracks is a range between 1.8 to 2.4 m (6 to 8 ft). As pointed out previously, punchout distress may occur at a greater frequency in pavement sections with crack spacing of 0.3 to 0.6 m (1 to 2 ft). In spite of noted reinforcing steel effects in design, a certain percentage of crack spacing usually falls below the specified minimum crack interval. Consequently, a very short cracking interval (which may occur in clusters) has been recognized as an undesirable feature, especially in combination with poor support conditions. Pavements with high steel percentages will develop crack intervals that average less than 1 m (3 ft) will provide adequate performance as long as good support exists and the crack widths are within the range shown in figure 21.

Therefore, it is of interest to characterize the occurrence of "cluster-cracking" in a CRC pavement system in terms of the percentage frequency of cracks occurring in clusters. The crack spacing frequency distribution can provide an indication of the level of cluster cracking. Cluster

cracking is a type of "distress" in CRC pavements. Consequently, as previously pointed out, cluster cracks typically will act as a locus for punchout development under repeated application of traffic loads. Shear stress may also be higher in these groups of cracks possibly leading to excessive wearout of the aggregate interlock and contributing to a greater rate of punchout distress at these locations. Generally speaking, cluster cracks occur within a distance of 0.3, 0.6, or 0.9 m (1, 2, or 3 ft) intervals. The probability of two, three, or four consecutive cracks occurring within a range of distances can be chosen as a basis to evaluate the evidence of cluster cracking within a particular pavement segment. Cluster cracking is found from crack spacing distribution data with respect to the probability that a specified number (say two) consecutive cracks occurring within less than a 0.3 m (1 ft) distance, a 0.6 m (2 ft) distance, etc., in which a simple algorithm can be developed to calculate the associated probability of cluster cracking as:

PROB (distance between two consecutive transverse cracks < Distance X) =

$$\sum \frac{\text{Number of two crack group (clusters) spaced at an interval within distance X}}{\text{Total number at two crack clusters within entire crack distribution}} =$$

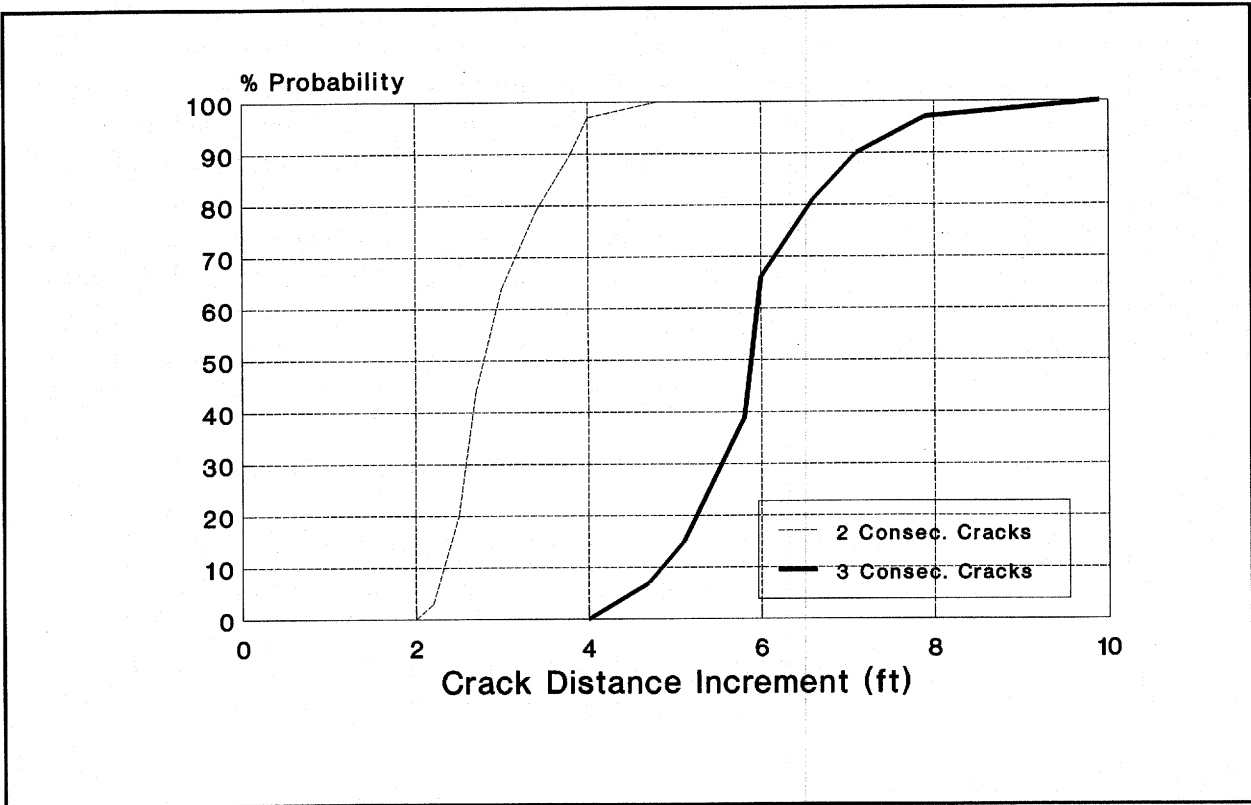
$$\sum \frac{\text{Number of two crack groups (clusters) spaced at an interval within distance X}}{\text{Total number cracks included in entire crack distribution} - (r - 1)}$$

where:  $r =$  two cracks

The denominator of this algorithm actually represents the total number of combinations of possible consecutive crack combinations in a given population of cracks. The number of combinations is calculated by deducting  $(r - 1)$  from the total number of cracks where 'r' is the number of consecutive cracks under consideration.

Therefore, the probability of cluster cracking is the total number of instances that a certain group of consecutive cracks (say two consecutive cracks occurring at random intervals) lie within a specified distance (say 4 m) divided by the total number of crack groups consisting of three consecutive cracks, that exist in the pavement cracking pattern distribution.

It should be noted that cluster cracking for ideal CRC pavement cracking distributions (where the pavement cracking is uniformly distributed) is illustrated in figure 37 (based on two and three crack clusters spaced at 0.6 m (2 ft) intervals). A characteristic of an ideal crack spacing distribution would be reflected in the degree of similarity between the curve for two consecutive cracks and the curve for three consecutive cracks (at the same intervals) if they were superimposed upon each other by doubling the two consecutive crack distance interval at any level of probability. In other words, the curve for two consecutive cracks can, so to speak, be converted into a curve for three consecutive cracks by shifting the curve to the right the interval distance associated with the interval between two consecutive cracks.



1 ft = 0.305 m

Figure 37. Ideal CRC pavement cluster cracking probability.

Elaborating further, the concept illustrated in figure 37 for a given set of data can be used to determine a "cluster ratio" to serve as a measure of cluster cracking manifest by a particular crack pattern. The cluster ratio is determined by dividing the ideal crack distance interval for three consecutive cracks (by doubling the crack interval distance associated with any probability along the curve for two consecutive cracks) by the actual distance between three consecutive cracks at the same probability that corresponds to the curve distance (associated with three consecutive cracks) and subtracting this quantity from one as shown below:

$$\text{Cluster Ratio} = 1 - \frac{2 * X_1}{X_2}$$

where  $X_1$  and  $X_2$  are the crack distant intervals for two and three consecutive cracks, respectively. An ideal crack spacing distribution exhibits a cluster ratio of zero by the above formation. The lower the cluster ratio, the lower the evidence of cluster cracking in the crack pattern. Good performing CRC pavements typically manifest cluster ratios less than 20 percent.

## **Characterization of Pavement Support Conditions**

In the characterization of pavement support conditions, the following types of field information regarding the existing pavement structure are found to be necessary:

- a. Foundation modulus or k-value,
- b. Thickness and elastic modulus of each layer, and
- c. Falling weight deflectometer (FWD) data (tests normally conducted in the morning hours) at cracks, joints, and other locations in the existing CRC pavement.

The use of FWD data plays a key role in this approach to CRC pavement evaluation. The sensor deflections can be used to calculate the basin area and provide important information for the pavement support analysis. The FWD data are used to calculate the basin area and the LTE across each joint or crack, which are used in the analysis to characterize support conditions as provided by the pavement system. Whether the FWD data is collected at the pavement edge or at an interior location will affect how the back calculation is conducted. However, either position is appropriate as long as it is consistent with the analytical approach. It is unlikely that edge curling or warping will significantly affect assessment of stiffness across a crack in CRC pavements consisting of C-1 and C-2 cracks.

### Foundation Modulus or Subgrade k-Value

The k-value of a soil or its modulus of subgrade reaction is indicative of the support provided by the subgrade and is important along with its associated variability or coefficient of variation (cv) in a thickness design process. The conventional method of using the plate-bearing test may be used to determine the modulus of subgrade reaction, but may not be practical in some instances particularly in the case of the construction of a pavement overlay. Various strength tests performed on the subgrade soils in which correlations to k-values for the soil are available may be used to characterize the subgrade k-value. Nondestructive testing (NDT) may also be used to determine a subgrade k-value at center slab locations by back-calculation methods based upon Westergaard's-type formulations. This approach can provide acceptable foundation support data. When a subbase or a stabilized subbase is used under the pavement, the k-value determined by NDT represents the entire foundation support as a composite layer.

### Thickness and Modulus of Each Layer

The type, thickness, and the modulus of each layer in the existing pavement section must be known so that effective modeling of the system layer configuration is possible. From the as-built plans and profiles of the existing subgrade, details of the thickness of each layer in the pavement section are typically available. The type and the thickness of the subbase material may also be noted. The elastic modulus of the existing concrete may be determined from the testing of available cores taken from the original slab or other means and used as an input to the NDT analysis. The modulus of the subbase is also determined using compression tests on field or laboratory samples depending upon the type of stabilizer used.

## Load Transfer Efficiency

Joints have been recognized as a major focal point for pavement distress in jointed concrete pavements and, consequently, transverse cracks are in many instances the source of problems that develop in CRC pavement (and overlays placed on jointed pavement systems). Data related to slab deflections and LTE are obtained during testing and are a primary way of characterizing support conditions under the original pavement. Results of the FWD testing may be described in part with respect to the plate deflection ( $D_0$ ) and the LTE. The LTE may be defined as the deflection on the unloaded side of the crack divided by the deflection on the loaded side of the crack (figure 38):

$$\text{LTE} = \Delta_L / \Delta_A \times 100 \%$$

where

$\Delta_L$  = unloaded deflection

$\Delta_A$  = loaded deflection

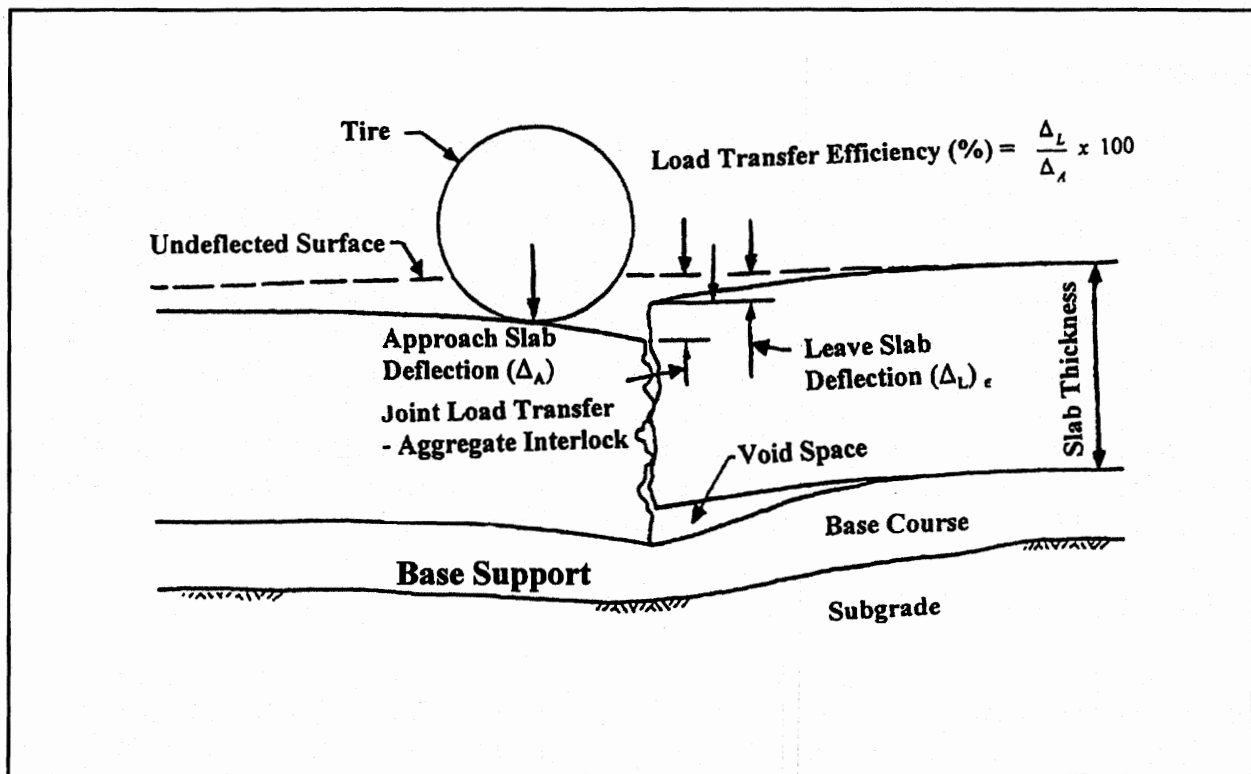


Figure 38. Load transfer efficiency.

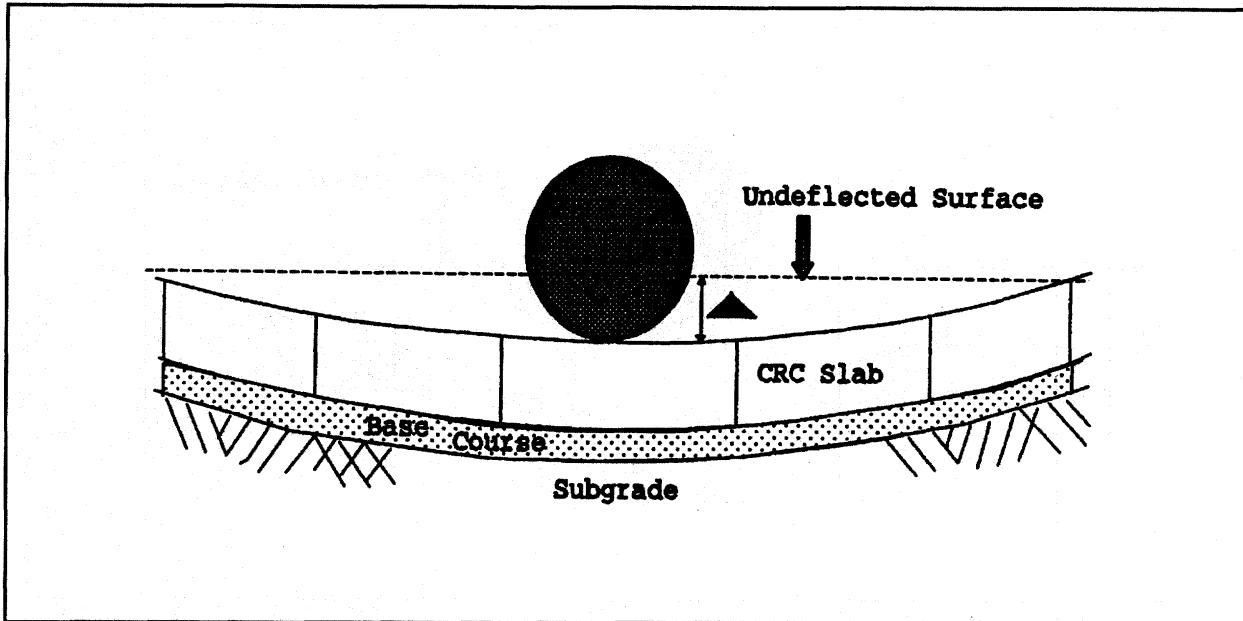


Figure 39. Shape of deflection basin under a slab of high stiffness and weak subgrade support.

The LTE of a transverse crack has a tremendous effect on the stresses that are developed in a CRC pavement and therefore on the degree of performance under repetitive loading. A perfectly efficient system for transferring load from one side of a crack to the other can significantly reduce the deflection which would occur from a free edge condition. The objective of a perfectly efficient system for transferring load is to minimize tensile stresses and, in the case of CRC pavements and overlays, the deflections in the pavement that result when loads are applied at (or between) transverse cracks in the pavement.

#### Basin Area

When any type of load is placed on a rigid pavement slab, the slab will deflect to form a basin. The deflected shape of that basin is a function of several variables, including the thickness and stiffness of the slab, the stiffness of the underlying materials, and the magnitude of the load. This may be depicted by the shapes of the basin area created by different strengths or types of subgrade material or different slab configurations as shown in figures 39 and 40.<sup>(27)</sup>

Basin area (figure 41) gives an indication of the deflection profiles measured using FWD, and may be calculated from sensor deflections as:

$$\text{Area} = 12/(2 \cdot D_0) [D_0 + 2\{D_1 + D_2 + \dots + D_{n-1}\} + D_n]$$

where

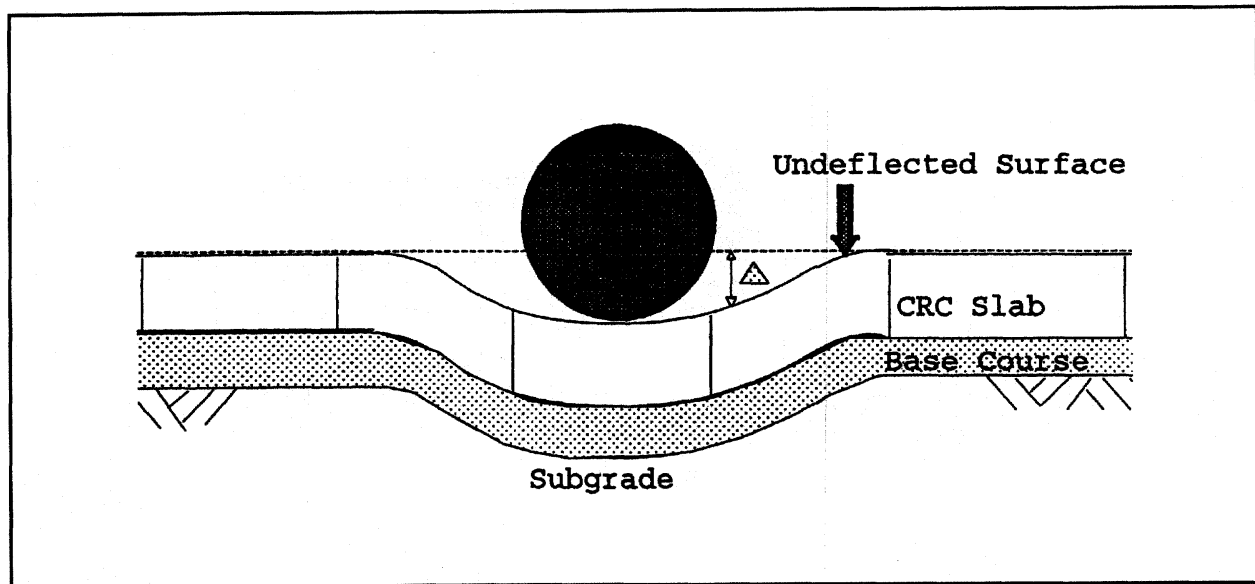


Figure 40. Shape of the deflected basin under a slab of low stiffness and subgrade support.

- Area = basin area,
- $D_i$  = measured sensor deflection
- $n$  = number of sensor (at 0.3 m (12 in) spacing) on one side of load plate minus one.

This area concept, illustrated in figure 41, combines all measured deflections in the basin into a single parameter. The area being determined is essentially one-half of the cross-sectional area of the deflection basin taken through the center of the load. Each deflection reading is normalized with respect to the maximum deflection  $D_o$ . Thus, the basin area has the units of length and is a function of the number and location of the sensors.

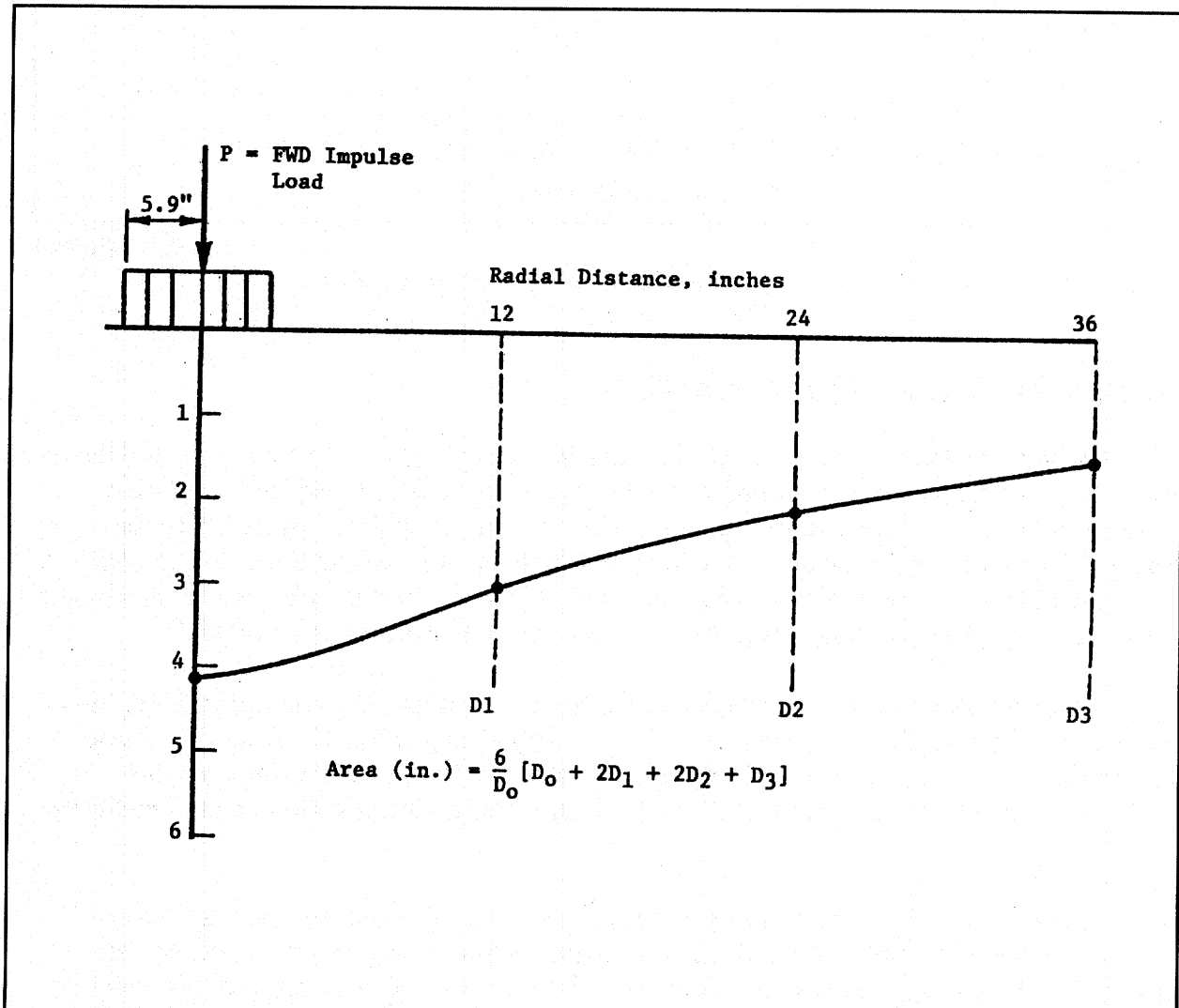
With respect to the evaluation process, all the measured basin areas are averaged to determine a mean basin area and the coefficient of variation. This information is used subsequently in the assessment of the variability of the remaining pavement life. For any given sensor arrangement, a relationship between the basin area and the radius of relative stiffness ( $\ell$ ) exists as illustrated in figure 42. This forms the basis of the representation of different load transfer conditions in the existing slab as explained later.

In the analysis of rigid pavements, one of the stress-inducing factors is the continuity of the subgrade support as affected by permanent deformations of the subgrade or loss of support. A concrete pavement slab deforms under load depending upon the position, magnitude, and area of contact of the load on the pavement surface. The resistance to deformation depends upon the stiffness of the supporting medium, as well as the flexural stiffness of the slab. This parameter, referred to above, is called the radius of relative stiffness ( $\ell$ ), and depends upon the properties of both the slab and the foundation. This relative stiffness may be defined as in the following equation:

$$l = \left( \frac{E h^3}{12 (1 - \nu^2) k} \right)^{\frac{1}{4}}$$

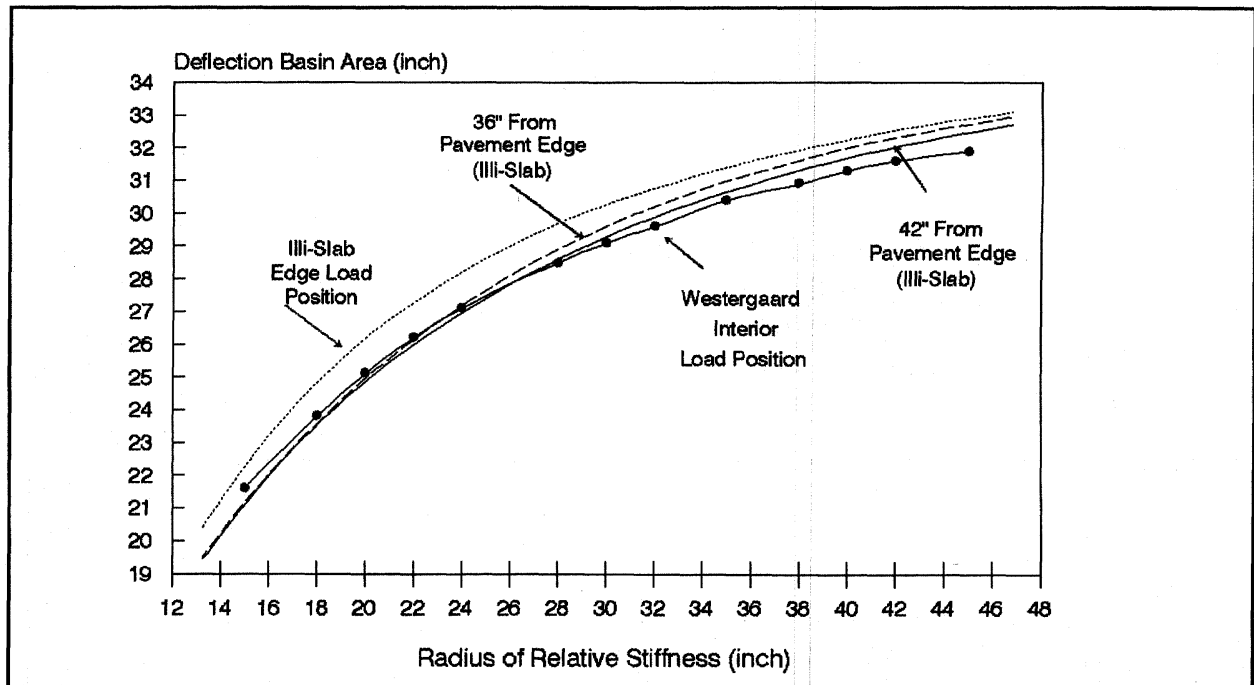
where

- E = concrete modulus of elasticity (psi)
- h = thickness (in)
- $\nu$  = Poisson's ratio
- k = foundation modulus (psi/in)



1 in = 25.4 mm

Figure 41. The deflection basin "area" concept.<sup>(27)</sup>



1 in = 25.4 mm

Figure 42. Variation of deflection basin area with  $l$ .<sup>(2)</sup>

### Characterization of Pavement Stiffness Conditions

Application of theoretically sound, mechanistic concepts to the structural evaluation of an existing CRC pavement has been prompted by the development of commercially available devices for nondestructive testing such as the FWD. This can be achieved by matching the theoretically predicted response of the system, typically in the form of a deflection basin, with corresponding behavior (as may be represented by an 'effective'  $l$ -value) observed *in situ* through the selection of appropriate system parameters such as layer thicknesses and moduli.<sup>(28)</sup>

Failure modes relating to punchout distress have been proposed as fundamental thickness design mechanisms for CRC pavements and CRC overlays (chapter 4). The analysis of these failure modes is based *a priori* on uniform support conditions.<sup>(2)</sup> Hence, it is important to incorporate a structural model that will allow matching of the deflection basin as measured in the field.

A deflection profile (and resulting pavement and material properties) for a loaded slab may be generated using the ILLI-SLAB finite-element computer program.<sup>(46)</sup> However, the closed-form solution suggested by Ioannides, et al.<sup>(28)</sup> for back-calculation purposes, is preferred. For this purpose, a slab with a joint/crack is characterized to represent field conditions with respect to support conditions and load transfer conditions of the transverse cracks. The purpose of this is to back-calculate either an effective layer modulus or a composite  $k$ -value as

determined by the collected field data. This information is used later in the determination of an "effective" stiffness of the transverse crack.

There are two different extremes that will arise when considering an existing pavement. The slab may either be bonded to the base or it may be unbonded. In either case, it is most appropriate to consider the base or the subbase as a part of the pavement system rather than part of the pavement support. For modeling an unbonded condition, a two layer analysis may be used where the existing pavement is modeled atop a stabilized base (if one exists) and the subgrade. This approach can provide a back-calculated k-value or an effective layer modulus (Ioannides, et al.).<sup>(28)</sup> In a bonded slab, the ILLI-SLAB program treats two layers as one equivalent layer with a composite layer thickness. If the existing slab has no stabilized base, two layer analysis is most appropriate.<sup>(53, 54)</sup>

A back-calculated k-value (whether the pavement is bonded or unbonded) as approximated from Westergaard analysis for an interior load condition is:

$$k = \frac{P}{8D_o(\ell_m)^2} \left[ 1 - \left( \frac{a}{\ell_m} \right)^2 0.217 - 0.367 \log \left( \frac{a}{\ell_m} \right) \right] \quad (17)$$

The effective elastic modulus, if of interest, ( $E_{eff}$ ), may also be back-calculated as:

$$E_{eff} = \ell_m 12 (1 - \nu^2) \frac{k}{h^3} \quad (18)$$

where

- P = load applied lb/in
- $D_o$  = maximum deflection under the load
- $\ell_m$  = radius of relative stiffness corresponding to the measured basin area
- $\nu$  = Poisson's ratio
- k = back-calculated subgrade modulus.

This approach of back-calculation can also be used to characterize the overall pavement behavior in terms of the structural parameters of the original pavement system. It may be shown that the overall pavement stiffness ( $E_c h_c^3$ ) can be defined in terms of the existing pavement system and an unbonded overlay as:<sup>(28)</sup>

$$E_c h_c^3 = E_1 h_1^3 + E_2 h_2^3 \quad (19)$$

where

- $E_c h_c^3$  = composite pavement stiffness,
- $E_i$  = flexural moduli of the pavement layers (1 = Overlay, 2 = Existing Slab),
- $h_i$  = thicknesses of the pavement layers.

The subscript c denotes the properties of the composite pavement system imagined to rest on the same foundation as the original pavement.

A similar approach may be applied to the case of a bonded overlay. In this case, the flexural stiffness of the composite pavement may be determined in terms of the properties of the original pavement system and a bonded overlay using the parallel axes theorem:<sup>(28)</sup>

$$\frac{E_c h_c^3}{12} = \frac{E_1 h_1^3}{12} + E_1 h_1 \left[ x - \frac{h_1}{2} \right]^2 + E_2 h_2 \left[ h_1 - x + \frac{h_2}{2} \right]^2 \quad (20)$$

The above equation involves the term x, which is the distance of the neutral axis of the composite system from the top of the pavement layer configuration. The depth to the neutral axis

$$x = \frac{E_1 h_1 \frac{h_1}{2} + E_2 h_2 \left( h_1 + \frac{h_2}{2} \right)}{E_1 h_1 + E_2 h_2} \quad (21)$$

is determined as follows:

It should be noted that an effective pavement stiffness ( $E_e h_e^3$ ) may also be determined based on a field measured  $l$ -value ( $l_m$ ) as:

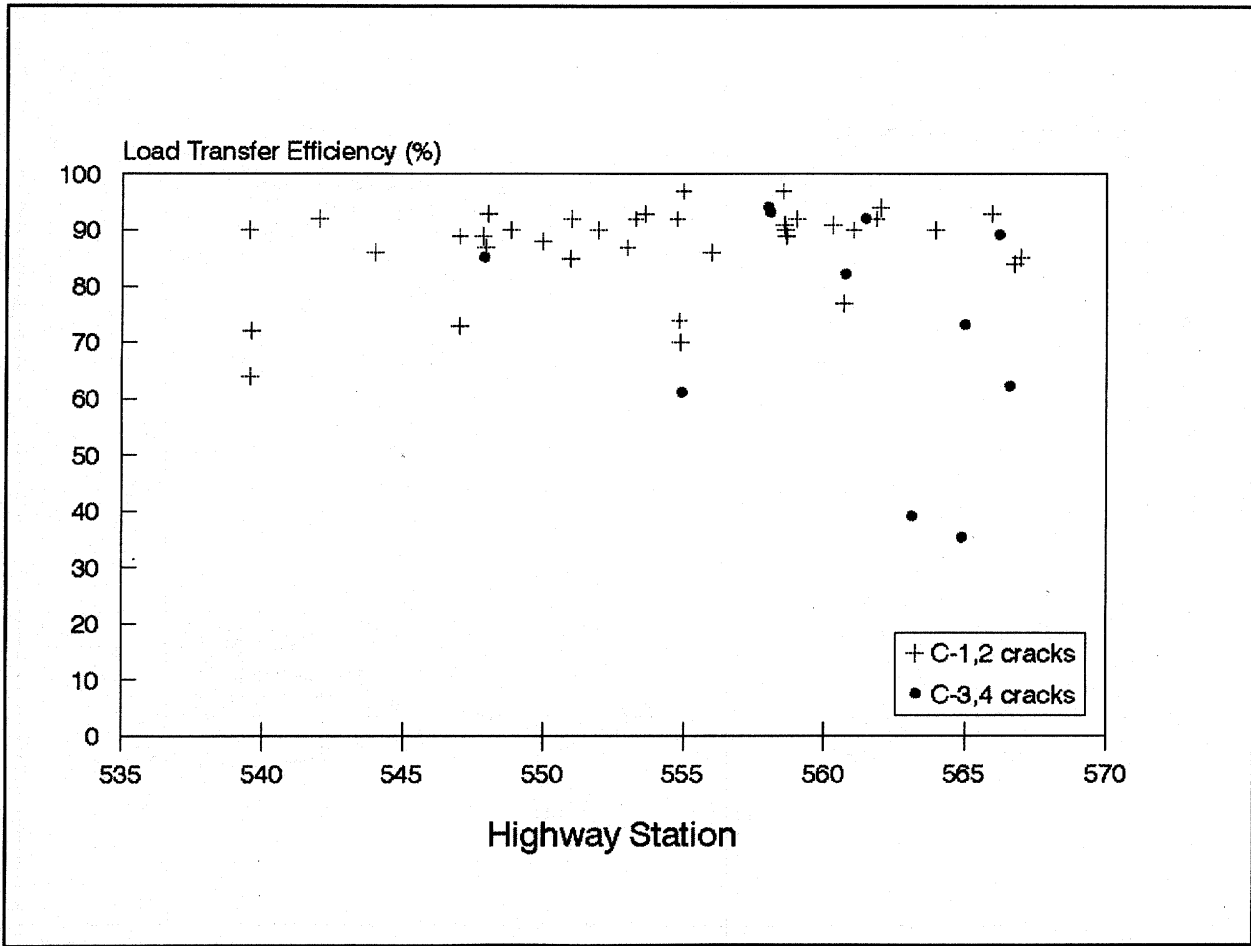
$$E_e h_e^3 = l_m^4 12 (1-\nu^2) k \quad (22)$$

and,

$$l_m = a_1 + a_2 \cdot \text{Area} + a_3 \cdot \text{Area}^2 \quad (23)$$

where  $a_1 = 74.32$ ,  $a_2 = -4.185$ , and  $a_3 = 0.003163$  are regression constants with  $r^2 = 0.9949$  and the SEE = 0.7548. This expression is applicable and dependent upon the configuration of the pavement system that exists at the time of the FWD testing, whether it be a single or two layer system. This value is used in equations 19 or 20 to calculate the composite pavement stiffness with an overlay.

Therefore, an overall stiffness ( $E_c h_c^3$ ) may be determined, for design purposes, for unbonded as well as bonded layer conditions relative to the basin area and to the radius of relative stiffness of the existing pavement system. For an unbonded system as shown above, the composite stiffness is given as in equation 19, and for a bonded system it is determined by equations 20 and 21.  $E_1$  and  $h_1$  are the elastic modulus and the thickness of the pavement surface (or overlay), and  $E_2$  and  $h_2$  are those of the lower pavement layer and may be considered to be effectiveness values since they may include the effectiveness of the transverse cracks and joints.

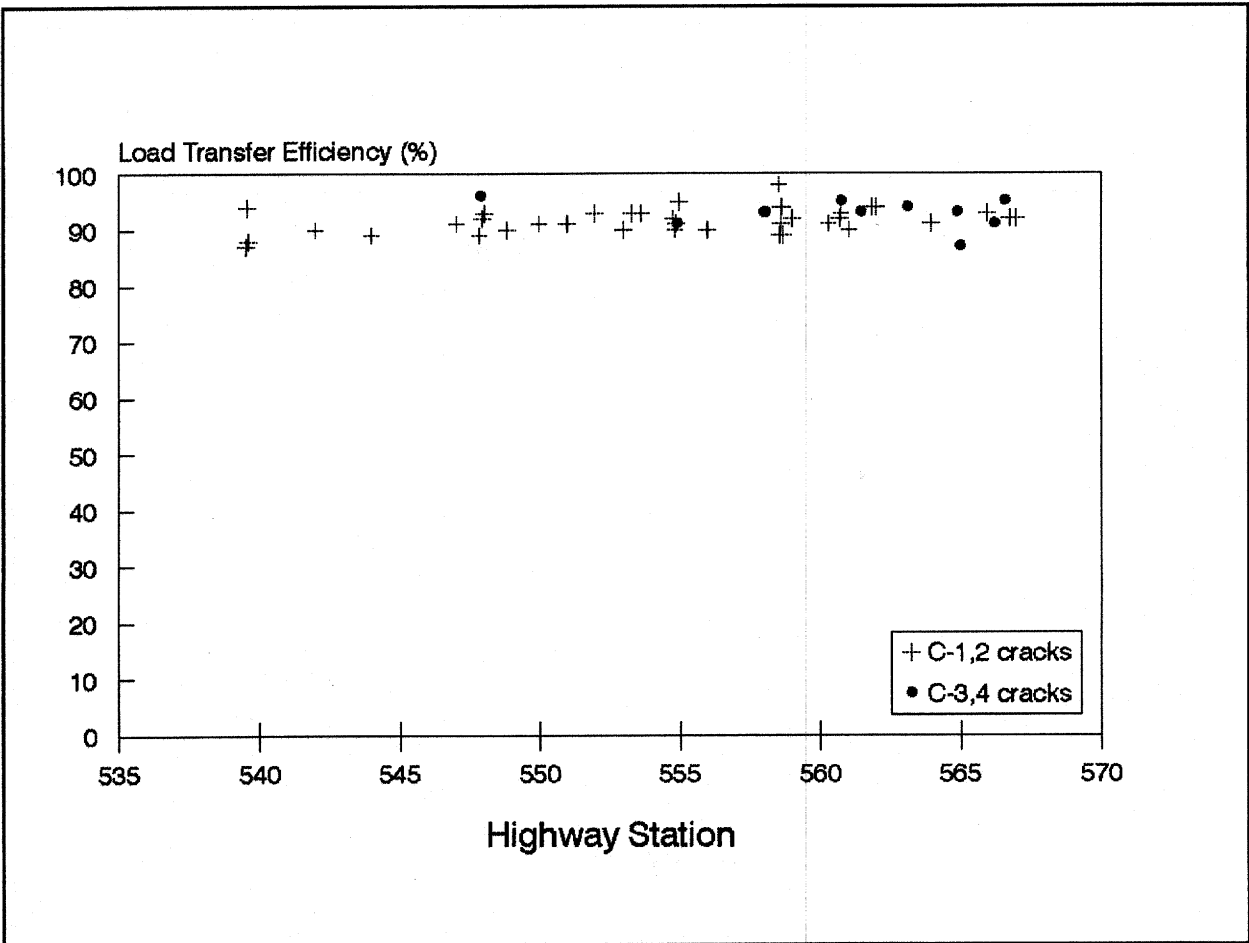


1 ft = 0.305 m

Figure 43a. NDT load transfer efficiency, morning results (Prior to 1000 h), I-72 WB.<sup>(2)</sup>

Interpretation of CRC Pavement NDT Data

As an example of the interpretation of CRC pavement NDT data, FWD deflection data obtained from a section of CRC pavement in Illinois<sup>(2)</sup> on I-72WB between MP 41.9 to MP 48.5 are shown in figure 43a and b. The data are shown in two groups according to the crack classification (table 6) for the approach and leave side of the transverse crack. Data for the approach side was obtained with the load plate of the FWD located on the side of the transfer crack from which the traffic approaches the crack. The leave side of the crack is the opposite side. Morning test results shown in figure 43a indicate that significant differences in LTE can exist between the two groups of cracks. These results are not surprising since C-3 and C-4 type cracks are spalled and has lost some load transfer capacity. Apparently, transverse cracks, categorized according to the crack classification, of this nature are tantamount to punchout distress. However, the load transfer differences between the two groups are less in the afternoon

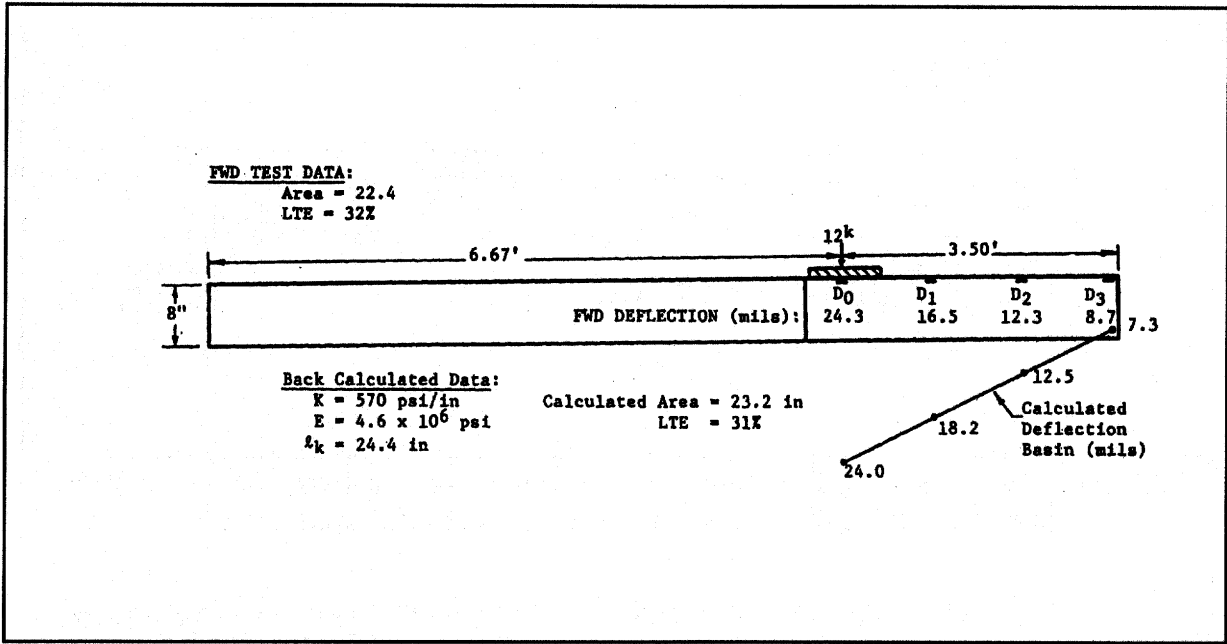


1 ft = 0.305 m

Figure 43b. NDT load transfer efficiency, afternoon results (after 1300 h), I-72 WB.<sup>(2)</sup>

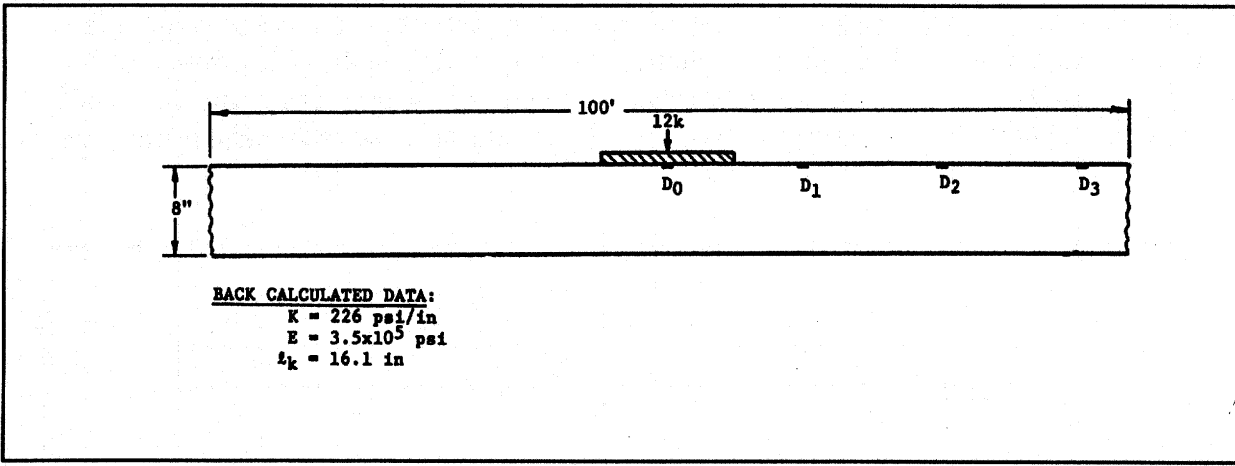
(figure 43b). The closing of the cracks due to an increase in the pavement temperature can cause a dramatic increase in LTE.

Load transfer data showed some correlation to crack widths measured at the pavement surface. In this same study, LTE increased in the afternoon due to a reduction in crack width. Some change in crack width occurred on the transverse cracks, which were very wide and spalled (C-3, 4 cracks). Even though only a small change in surface crack width occurred (relatively speaking), a very significant change in LTE occurred on these cracks. Apparently, the load transfer was carried by aggregate interlock below the spalled portion of the pavement. Thicker pavements tended to maintain a greater load transfer than thin pavements. Apparently, load-transfer-related problems in CRC pavements are more easily identified based on FWD data obtained in the morning as opposed to test data obtained in the afternoon. The same type of trends are noted with the plate deflection ( $D_0$ ) and the basin area results. Each of these parameters may be useful, in combination with visual observation, in evaluation of potential punchout distress. Since the C-3 and C-4 type cracks can be identified by observation,

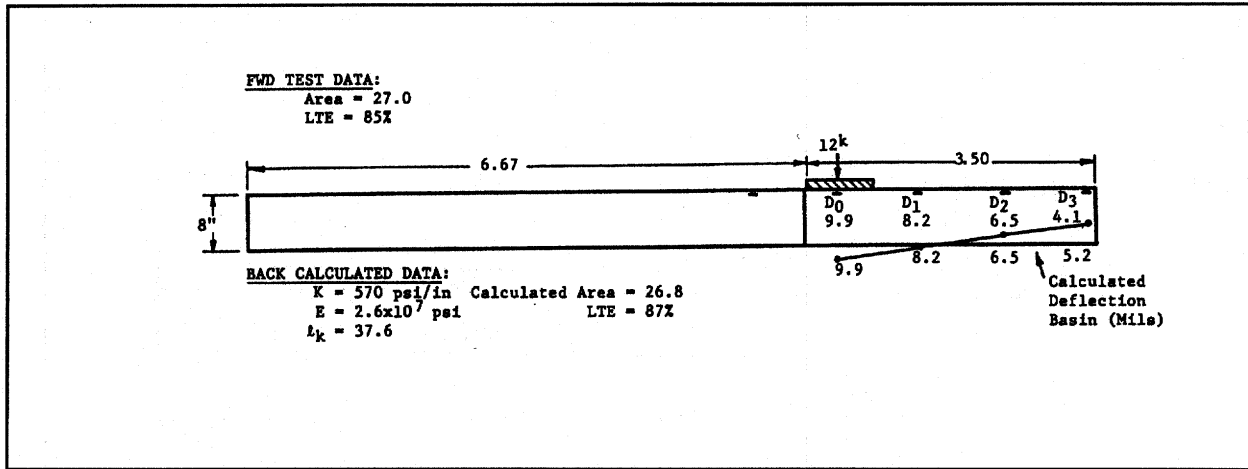


1 in = 25.4 mm, 1 psi = 6.89 kPa, 100 psi/in = 27.1 kPa/mm, 1 kip = 4.4 kN, 1 mil = 0.025 mm  
 Figure 44a. CRC pavement with transverse crack (morning case).<sup>(2)</sup>

NDT results should focus on potential problems developing with the C-1 and C-2 cracks. These problems are more readily evaluated using morning NDT results and at other time periods where the transverse cracks are open, such as during cold weather. Evaluation approaches of this nature would be appropriate for application of new and innovative methods of pavement evaluation.

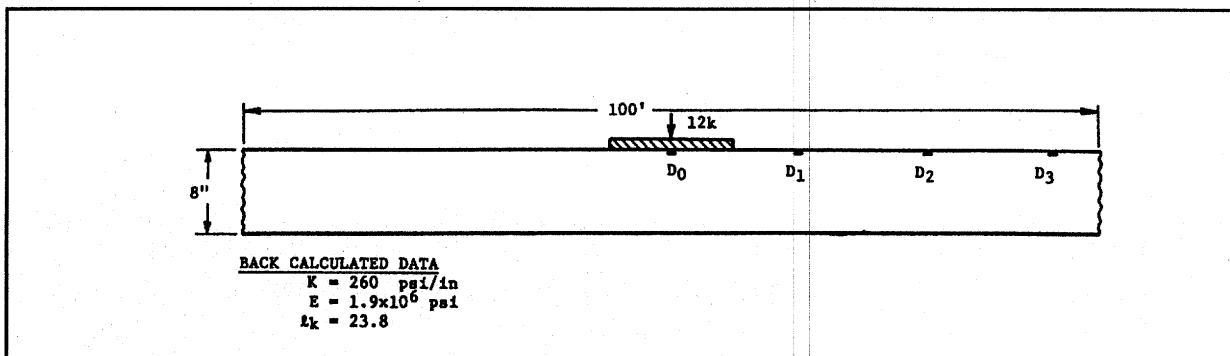


1 in = 25.4 mm, 1 psi = 6.89 kPa, 100 psi/in = 27.1 kPa/mm, 1 kip = 4.4 kN, 1 mil = 0.025 mm  
 Figure 44b. CRC pavement without transverse crack (morning case).<sup>(2)</sup>



1 in = 2.54 mm, 1 psi = 6.89 kPa, 100 psi/in = 27.1 kPa/mm, 1 kip = 4.4 kN, 1 mil = 0.025 mm  
 Figure 45a. CRC pavement with transverse cracks (afternoon case).<sup>(2)</sup>

As previously pointed out, the NDT results are also useful in back-calculating material properties of the pavement system such as the modulus of elasticity (E) and the modulus of subgrade reaction (k). Particular interest lies in back-calculated E values and the radius of relative stiffness ( $\ell_k$ ) at the transverse cracks. A method of back-calculation of these parameters based on deflection basin (data) has been discussed previously; however, little information is available relative to application of these methods to CRC pavement. One procedure is modeling the CRC pavement as a cracked system as shown in figure 44a (matching actual pavement crack spacing) with the load in the wheel path position for deflection basin data obtained from a section of I-57SB in Illinois.<sup>(2)</sup> The back-calculated E value is representative of actual concrete stiffness. The LTE of the case given in figure 44a is low for which an effective E value and  $\ell_k$  are of interest. Next, the effective E value is found from modeling the measured deflection basin of a CRC pavement as if it were a continuous slab of infinite length without joints shown in figure 44b (maintaining the same FWD sensor locations). The back-calculated E value from the morning test results given in the figure is less than 10 percent of the previously calculated value. The CRC pavement stiffness is expected to be low in this case since the load transfer was low.



1 in = 2.54 mm, 1 psi = 6.89 kPa, 100 psi/in = 27.1 kPa/cm, 1 kip = 4.4 kN, 1 mil = 0.025 mm  
 Figure 45b. CRC pavement without transverse cracks (afternoon case).<sup>(2)</sup>

The same cases are back-calculated again in figure 45 using data from the afternoon test. The back-calculated E value in part a is very high since the pavement system is responding in a stiff manner but is modeled with a joint. Modeling the same deflection basin with a continuous slab generates an effective E value which approaches the modulus of elasticity of normal concrete since the LTE is slightly low (85 percent).

The back-calculation can be accomplished for a range of thicknesses by using a deflection area basin-radius of relative stiffness relationship given in equation 23 (for an interior load position) and shown in figure 42. The edge and two-wheel path load location curves generated from ILLI-SLAB analysis are compared to the closed form curve obtained from the theoretical solution of a case of a circular load and a dense liquid foundation for an interior loading condition.<sup>(30)</sup> For a fully supported slab, the difference between the theoretical interior loading position and the wheel path loading positions is small enough for the most part so that the theoretical curve could possibly be used in place of the ILLI-SLAB generated curves. As stated earlier, the FWD wheel path testing position varied from 914 mm (36 in) to 1067 mm (42 in) from the pavement edge. Given the deflection basin area from the FWD test results, the radius of relative stiffness can be obtained from equation 23 for either the edge load or wheel path load positions for any pavement thickness. These distances are near the theoretical limits of any curling or warping effects.

Consequently, unique E and k values can be determined from  $l_k$  values obtained from equation 23 and Westergaard solutions<sup>(31)</sup> for slab-on-grade deflections at the edge and interior

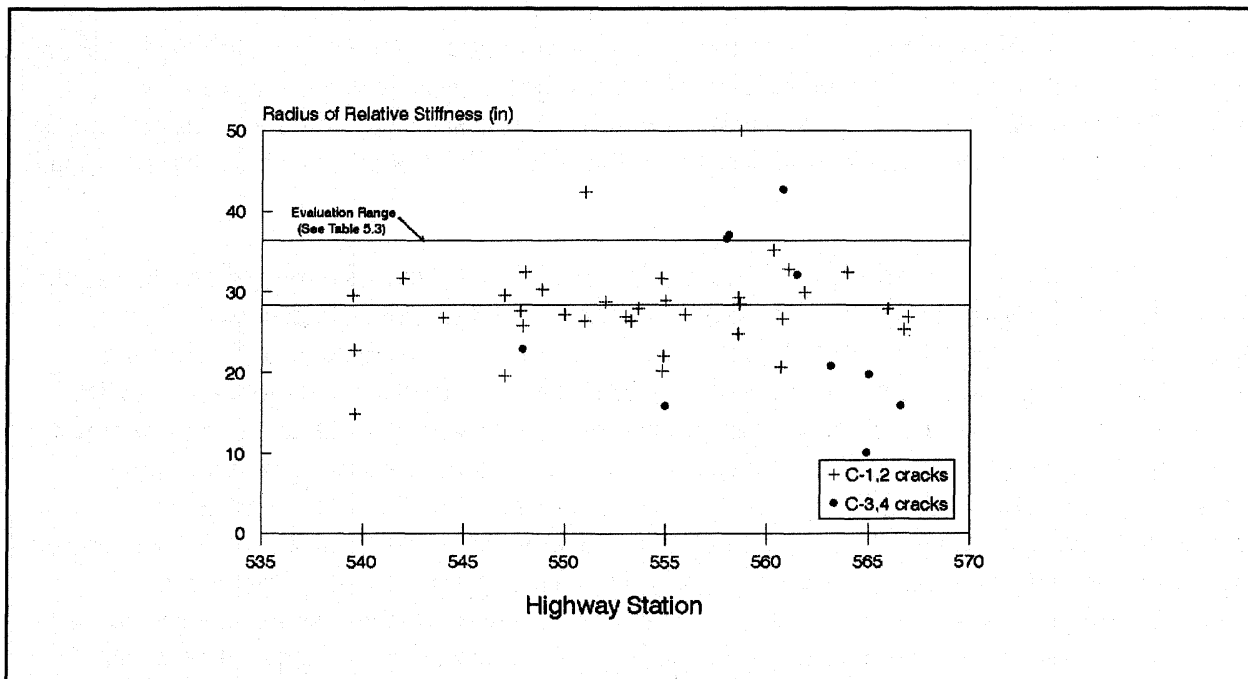


Figure 46a. Radius of relative stiffness, morning results (prior to 1000 h), I-72WB.<sup>(2)</sup>

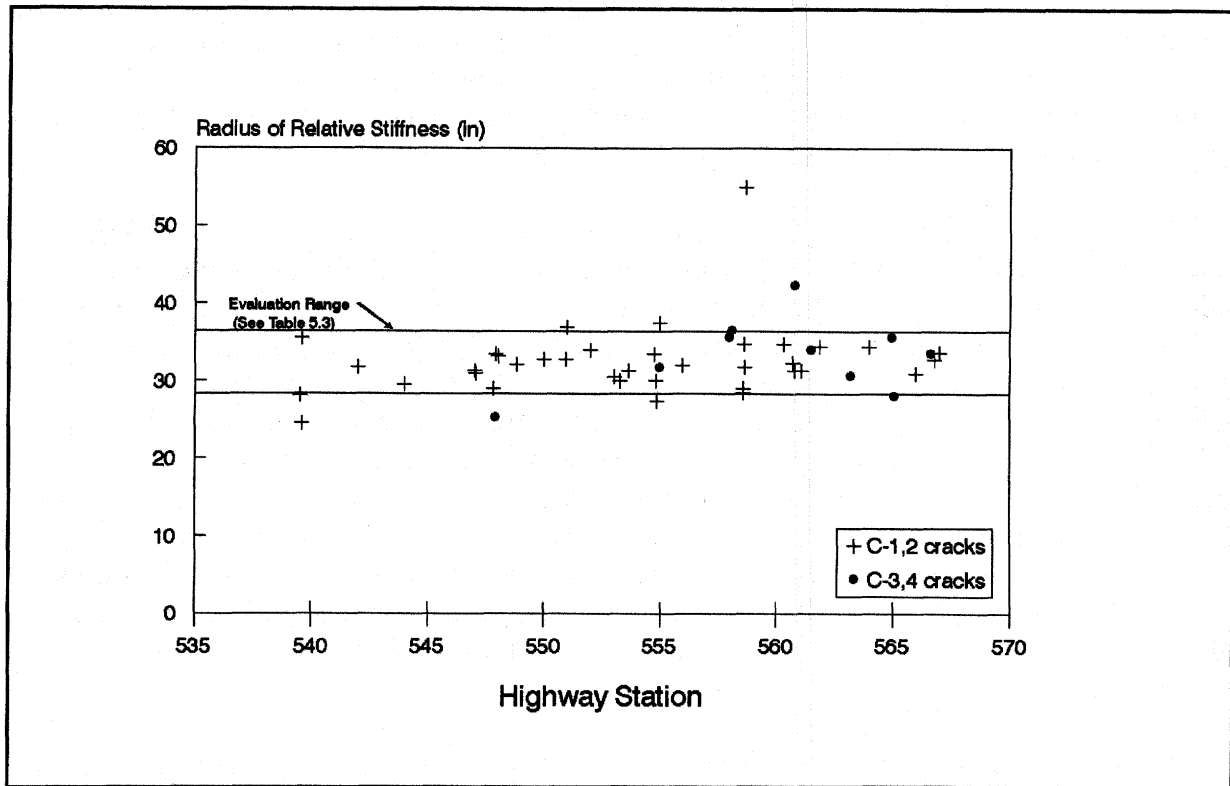


Figure 46b. Radius of relative stiffness, afternoon results (after 1300 h), I-72WB.<sup>(2)</sup>

load positions. The theoretical interior loading solution is applied to the wheel path load position in the actual pavement since the load behavior between the two positions was shown to be similar. Simplified forms of the Westergaard solutions rearranged to solve for  $k$  value (assuming  $\mu = 0.15$  for concrete) are given in equation 17 for the interior load position and for the edge load position.

Using the above procedure,  $l_k$  values are determined and shown for the test results for the I-72WB section (same as in figure 43) in figure 46a and b (203 mm (8 in) thickness). The response in terms of the radius of relative stiffness is similar to the parameters LTE,  $D_0$ , and Area. This suggests that  $l_k$  may also be useful in determining potential punchout areas in CRC pavement. Table 7 draws a comparison between deteriorated the transverse cracks (in the form of voids forming around the reinforcement), LTE, and  $l_k$ . Generally speaking, if transverse cracks have deteriorated, the LTE and the  $l_k$  values are low (below 80 percent and 25.0, respectively) and if they are not, the  $l_k$  are high. The data in table 7 indicate generally the ranges of  $l_k$  where problems may and may not be developing. This approach to CRC pavement evaluation can have some usefulness as an indicator of potential punchout since subbase erosion and transverse crack deterioration tend to lead to lower  $l_k$  values. Comparisons between the  $l_k$  values from the NDT data and calculated  $l_k$  values can provide a basis for evaluation of punchout potential. Calculated  $l_k$  values for E values of 20684 to 27579 mPa (3 to 4 million psi) are given in table 8, which, when compared with the data listed in table 7 (for the given thickness),

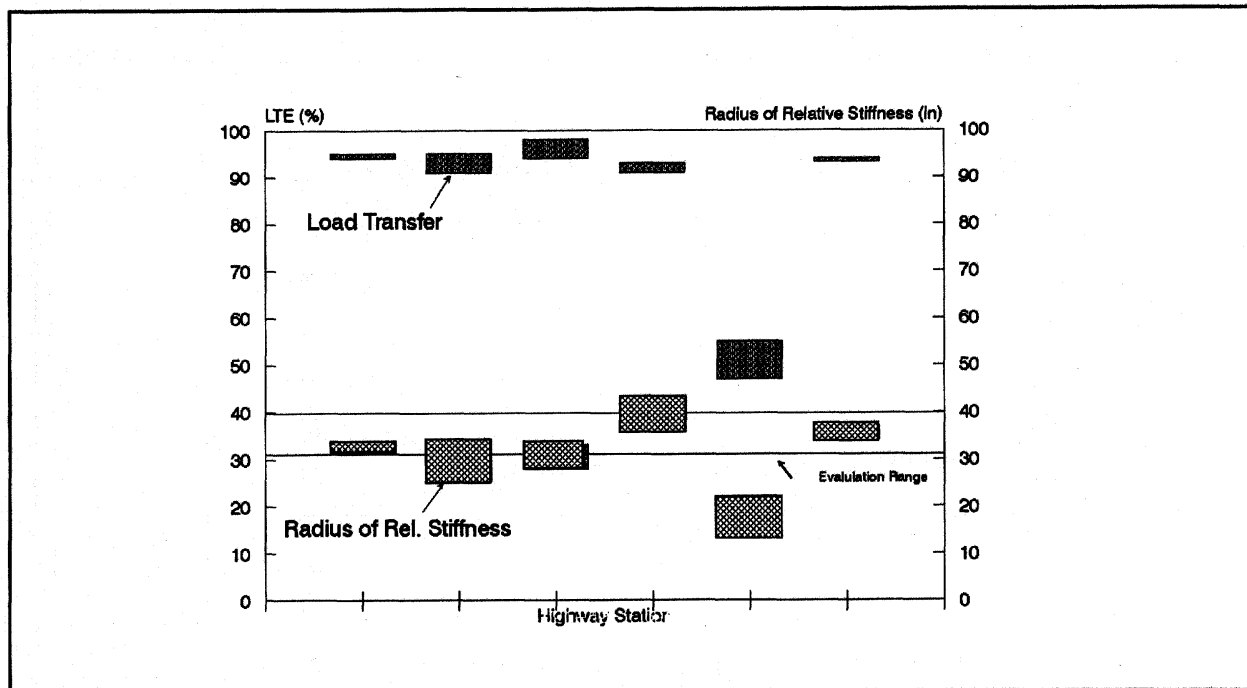


Figure 47a. Comparison of LTE and  $l_k$  for I-55WB.<sup>(2)</sup>

establish a minimum  $l_k$  value since these represent fully supported conditions. It may also be possible to use  $l$ -values backcalculated for the center of slab positions for this purpose as well. In this regard, the results given in tables 7 and 8 may be helpful in determining limits between adequate and low  $l_k$  values as illustrated in figure 47a and b.

Figure 47a shows a comparison of LTE's and  $l_k$  values determined for another Illinois pavement section on I-55SB (approach and leave data are illustrated). At two locations, low  $l_k$  values were determined which had corresponding LTE's over 90 percent, suggesting that the radius of relative stiffness may be more effective in terms of CRC pavement evaluation than LTE. The shaded area is the limit range below which potential problems may exist. Similar information is shown in figure 47b from a section of CRC pavement on I-77 in South Carolina.<sup>(2)</sup> The shaded limits in figures 46a and b (203 mm (8 in) thickness) are also listed in table 8. These limits allow the determination of the cracks, which may be suspect of faulting and punching out. It appears that this evaluation should be made with the morning test data. Evidently, potential punchout-related distress in CRC pavement may be evaluated from a combination of transverse crack observation, LTE, and pavement radius of relative stiffness values. It should also be pointed out, that based on findings provided in FHWA-RD-94-180 "Volume III - Analysis and Evaluation of Field Test Data," the slab rigidity (D) can also be included in the above list of evaluation parameters.

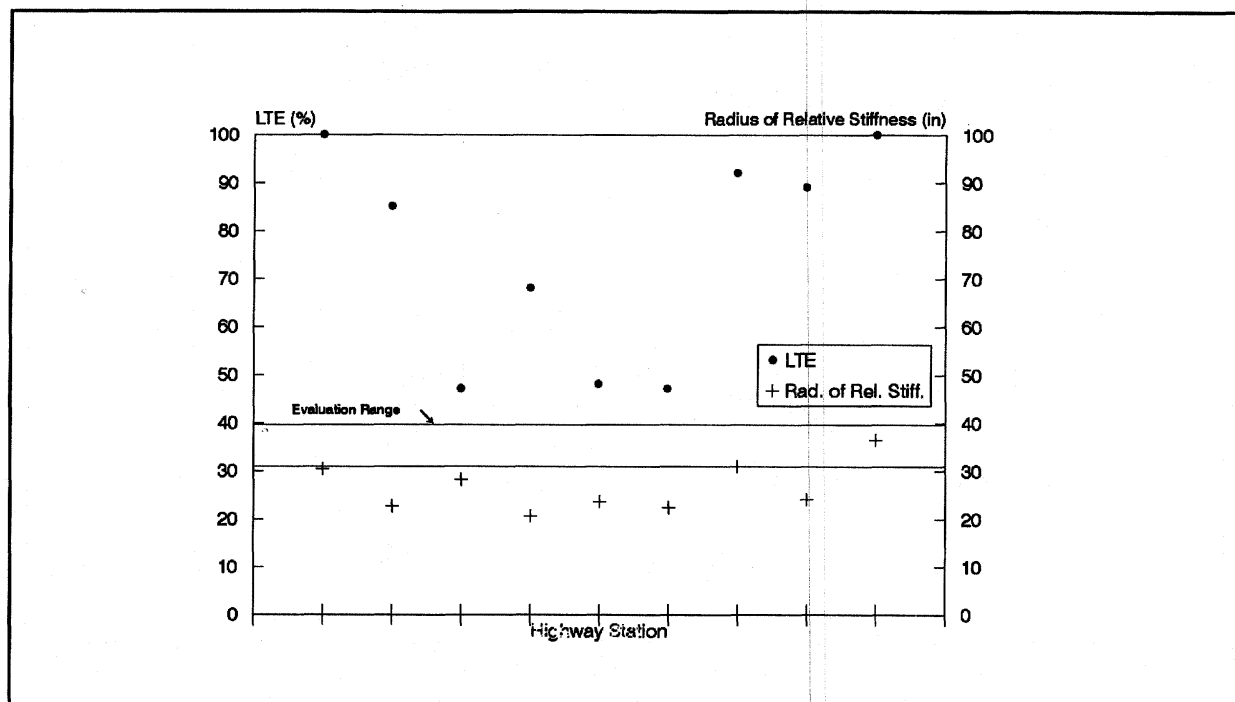


Figure 47b Comparison of LTE and  $l_k$  for I-77WB, South Carolina.<sup>(2)</sup>

### Evaluation Process

In light of the previous discussion, which has highlighted the important parameters relevant to the evaluation of CRC pavements, the evaluation process can now be elaborated. The evaluation approach subsequently discussed is intentionally configured to conform to the design process explained in chapter 3 in order to enhance the utility of the evaluation process by providing a direct comparison between the design life and the performance life of the pavement system. It should be pointed out that compatibility of this nature is most conveniently achieved by incorporating mechanistic principles and concepts, which is the case in both the design and evaluation processes. In this framework, the design process for CRC pavements will be referred to in this discussion with respect to the structural characteristics of CRC pavement behavior as contained within the design expressions given in chapter 3.

Using NDT data obtained from the use of an FWD, the radius of relative stiffness (RRS) is determined from basin area calculation using equation 23. The RRS and  $D_0$  values are also used to determine back-calculated k-values using equation 17. The RRS, k values, and the measured LTE's are then used to find the crack stiffness (AGG), for each tested transverse crack using equation 10. The present level of shear capacity ( $\tau h^2/P$ ) is next found from equation 11 (from known values of k,  $l$ , and AGG), which allows for the determination of the effective crack width of each tested transverse crack (equation 12). At this point, all of the necessary inputs are

Table 7. Transverse crack data.<sup>(2)</sup>

Route	Station	Classification	Rebar (Voids)	LTE (Morning)	$l_k$ (mm) (Morning)
I-72WB (203 mm thickness)	565+02	C-2	yes	73%	490.2
	563+13	C-4	yes	39%	523.4
I-39WB (254 mm thickness)	561+05	(0.1" Faulting) C-2	no	90%	810.3
	1563+70	C-2	yes	64%	414.0
	1610+08*	C-1, 2	forming	90%	736.6
	1610+97	C-1, 2	no	92%	825.5

+ Lowest LTE and  $l_k$  between approach of leave data

\* Afternoon results

Table 8. Radius of relative stiffness for a fully supported system.<sup>(2)</sup>

Thickness (mm)	k-Value (kPa/mm)	$l_k$	
		$E_c=20684$ (mPa)	$E_c=27579$ (mPa)
203	27.1	858.5 mm	924.6 mm
	54.3	721.4 mm	777.2 mm
229	27.1	939.8 mm	1008.4 mm
	54.3	787.4 mm	863.6 mm
254	27.1	1016.0 mm	1092.2 mm
	54.3	853.4 mm	916.9 mm

available to assess the remaining life of the CRC pavement system by using equations 12 and 13. For any level of expected future traffic, the loss in shear capacity can be assessed, allowing for the determination of a new crack stiffness value ( $AGG/Kl$  - at a lower level) which corresponds to a reduced LTE as predicted by equation 10. This approach should be useful in assessing structural integrity of widened transverse cracks and C-1 and C-2 cracks that may be associated with unsupported conditions.

Once the LTE is found, the corresponding bending stresses and cracking levels can be determined from equation 9 and equation 10, respectively. The variance of the predicted cracking levels can be evaluated in the same manner as described in chapter 3 with the exception of how the variance of the bending stress is evaluated. Since direct measurements are made of the LTE, cracking intervals, and the RRS, each of these are used in the estimate of stress variance which directly affects the variance of cracking. Therefore, it is evident that a reduction in the randomness of the cracking interval will lead to an improved performance level of the CRC pavement system since a higher level of performance can be achieved by improving the characteristics of the crack pattern.

### Application to Overlay Design

The utility of the above evaluation process is in the determination of overlay thickness as a function of the pavement condition from a structural stiffness perspective. For the purpose of structural analysis, it is important to consider whether the overlay is to be bonded or unbonded to the original pavement surface in the design process and whether or not the existing pavement layer is CRC or jointed concrete. The approach previously elaborated is used to represent a typical overlay condition as illustrated in figure 48 and representing it as an "effective" single-layer pavement system.

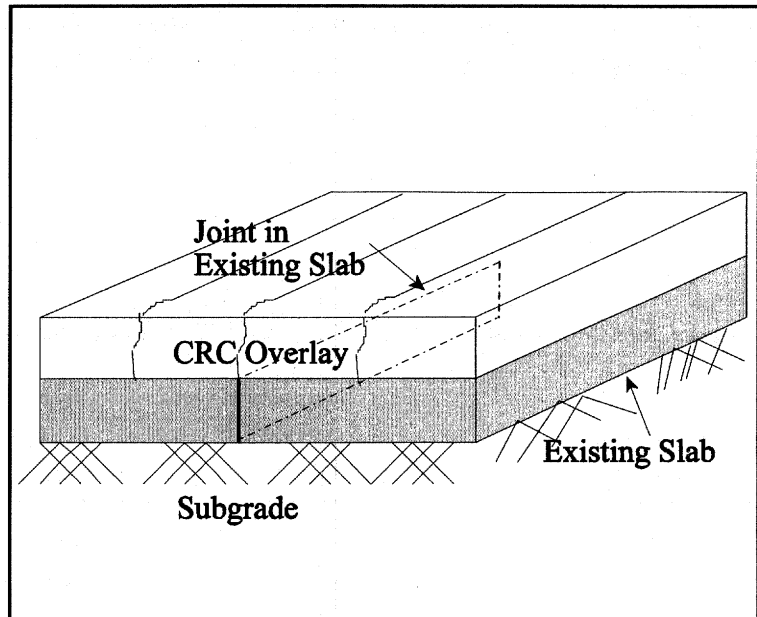


Figure 48. Section overlay and existing jointed pavement.

A bonded overlay may be modeled by treating the overlay and the existing slab as one layer in terms of an effective thickness by the use of the parallel axes theorem. Ioannides, et al.<sup>(28)</sup> used this theorem, which involved determining the neutral axis of a composite system in the calculation of an effective thickness ( $h_e$ ). This composite layer can be modeled atop the base or the subgrade using a back-calculated k-value for the slab support.<sup>(53)</sup> In the case of an

unbonded overlay, a back-calculated "effective" elastic modulus (for the existing pavement) and k-value at the top of the base are used in the modeling process.

### Design Criteria

CRC overlay thickness design criteria may be formulated relative to fully supported pavement behavior. Lack or loss of pavement support may occur in several forms, such as poor load transfer across an underlying joint or crack or other conditions at the joint location in the existing layer where the end result is usually a loss of deflection continuity (i.e., there are unequal deflection characteristics between adjacent slabs or segments of the supporting pavement that will cause the overlay and the original pavement to separate while under load causing, in effect, a temporary void).<sup>(2, 25, 26)</sup> Thus, the CRC overlay is forced to "bridge over" this void which causes highly localized stresses. This is a significant behavior defect and the minimization of such is the basis for the design approach discussed below. It is important to note that several CRC overlay projects have failed in the last 10 years due to this effect.<sup>(25, 26)</sup> The latest one was on I-30 near Texarkana in Arkansas.<sup>(44)</sup> Other rehabilitation alternatives may also be more appropriate, such as crack and seating coupled with an AC interlayer prior to overlay placement.

In terms of rehabilitation with an overlay, the level of stiffness of the existing concrete pavement system can be improved by placing an overlay on it. The benefit of an overlay can be assessed in terms of the increase in the overall stiffness of the pavement system. The effectiveness of an overlay can also be enhanced by improving the load transfer of the joints and cracks in the existing pavement layer prior to placement of the overlay. Whatever the case may be, the load transfer must be increased or the overlay thickness placed great enough to cause the composite pavement system to behave as though it is fully supported and maintain deflection continuity within the pavement system under load. The effect or contribution of these improvements is quantified relative to the increased overall pavement stiffness. This is accomplished using the equations described above for either unbonded or bonded conditions.

In order to establish design criteria to maintain deflection continuity between different layers of the pavement system, a limiting pavement stiffness for design purposes (Design  $Eh^3$ ) must be defined for fully supported conditions. This can be done using equation 22 and the  $l$ -value for a fully supported slab:

$$\text{Design } Eh^3 = l^4 12 (1-\nu^2) k$$

and the required overlay thickness:

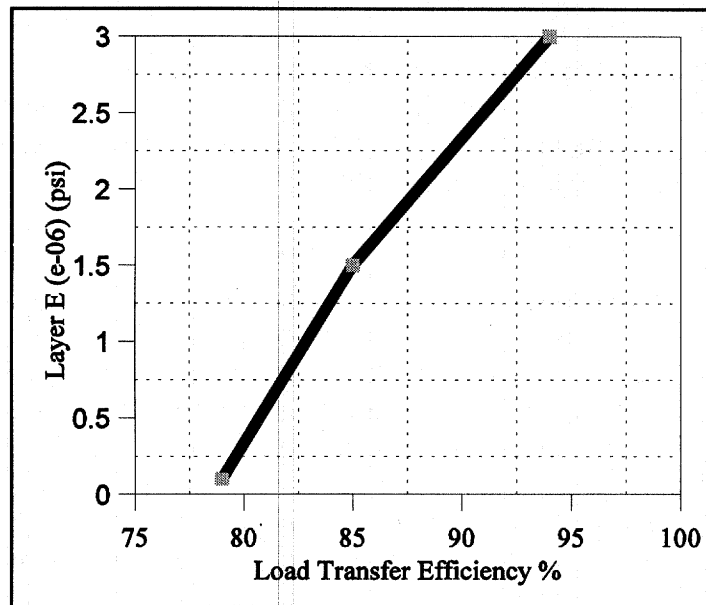
$$h_{OL} = \left[ \frac{\text{Design } Eh^3 - E_e h_e^3}{E_{OL}} \right]^{1/3} \quad (24)$$

where  $E_{OL}$  is the elastic modulus of the overlay concrete. The difference between fully supported pavement stiffness and the stiffness of the existing pavement system determines what the required overlay thickness should be. Design criteria can also be expressed in terms of basin area based on fully supported conditions for the corresponding  $\ell$  value (corresponding to the design  $Eh^3$ ):

$$\text{Design basin area} = \sqrt{(b_1 + b_2\ell + b_3\ell^2 + b_4\ell^3)}$$

where  $b_1 = -298.99$ ,  $b_2 = 67.722$ ,  $b_3 = -1.23$ , and  $b_4 = 0.01$  are regression constants with a  $r^2 = 0.999$  and a SEE of 0.098.

Design charts can be developed in terms of the basin area and the pavement stiffness. However, as previously pointed out, the effective stiffness of the existing pavement system can be improved by improving the load transfer conditions of cracks and joints in the existing slab. The quality of the load transfer in the existing pavement system is reflected in the measured basin areas. The basin area in turn affects the pavement "effective" stiffness where the effective stiffness may be found for different levels of load transfer across the joints/cracks in the original pavement layer. Improvement of the existing load transfer is represented in the design process by increasing the basin area and improving the "effective" pavement stiffness (equations 19 and



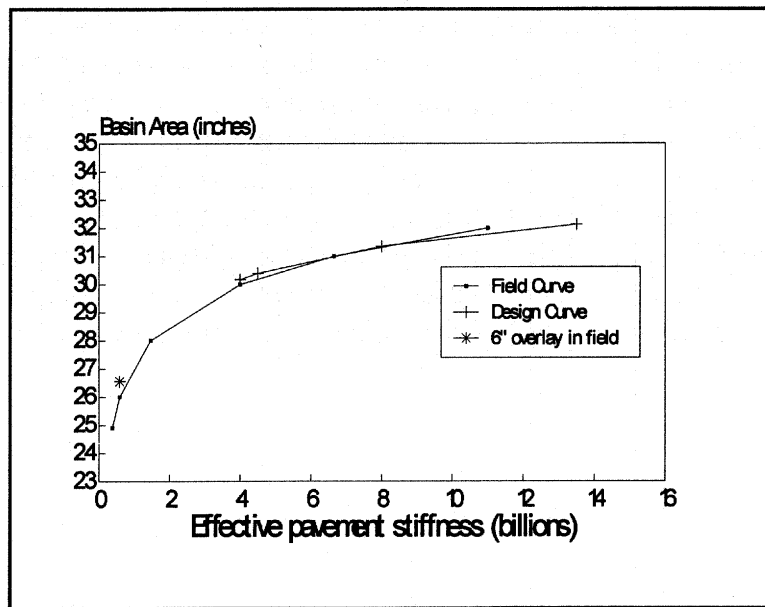
1 psi = 6.89 kPa

Figure 49. Improvement of layer modulus with load transfer efficiency.

20) of the pavement system and is illustrated by a relation (shown in figure 49 as based on ILLI SLAB results) between layer stiffness and load transfer. It is possible to consider various alternatives with this approach and their effect relative to the design criteria for pavement stiffness and basin area. The  $\ell$ -value used for a given alternate load transfer and overlay thickness is determined as a composite value using the composite stiffness:

$$\ell_c = \left( \frac{E_c h_c^3}{12 (1 - \nu^2)k} \right)^{\frac{1}{4}}$$

The thickness of the overlay at which the computed  $E_c h_c^3$  and the design  $Eh^3$  are equal may be considered to be the design thickness of the overlay to be placed upon an existing pavement to ensure adequate pavement behavior and performance as illustrated in figure 50. As pointed out previously, the phase of design analysis related to punchout development due to fatigue cracking caused by repetitive loading can be considered at this point in the design process as described in chapter 3.



1 in = 2.54 mm, 1 psi = 6.89 kPa

Figure 50. Overlay design: composite stiffness versus design criteria.

### Case Study

Data were obtained from I-30 in Arkansas for an existing 25.4 cm (10 in) JRC pavement that was hinge-jointed at 4.6 m (15 ft) intervals (and dowelled at 13.7 m (45 ft) intervals) that was later overlaid with an unbonded 15.2 cm (6 in) CRC pavement. From FWD measurements, the average basin area was found to be 63.3 cm (24.9 in) and the LTE was about 80 percent.

Using ILLI SLAB, the basin area and the deflection profile was matched for a 6,804 kg (15,000 lb) load positioned at mid-slab. Based on the information available regarding the R-value of the soil (approximately 5), the subgrade modulus or the k-value was approximated at 203.6 kPa/cm (75 psi/in). The modulus (E value) of the existing JRC pavement was found to be about 27,560 mPa (4,000,000 psi) from the testing of the cores. The E value for the 15.2 cm (6 in) cement treated base (CTB) that lay below the JRCP was taken as 275.6 mPa (40,000 psi). A back-calculated composite k-value of 670.4 kPa/cm (247 psi/in) was determined to account for a 15.2 cm (6 in) CTB that existed under the JRC in order to facilitate two-layer analysis since the overlay is to be unbonded. The two layers of the original 25.4 cm (10 in) JRCP was represented as an equivalent layer with different composite layer modulus in terms of different levels of load transfer as previously referred to. The basin area as measured in the field was matched to determine a composite k-value or an effective layer modulus.

After the field measured deflection basin was matched and the effective modulus of the existing pavement found, the pavement overlay was determined using equation 24. However, the effective layer stiffness was calculated at various levels of improved load transfer and increased overlay thickness that improved the overall or composite pavement stiffness. An increase in the pavement stiffness resulted in a different basin area for each thickness.

The relationship between the calculated basin area and the composite overlay stiffness was compared against the design criteria (basin area versus  $Eh^3$ ) as illustrated in figure 50. The curve developed by incrementally improving the existing pavement stiffness (field curve) was found to meet the design curve at a thickness of about 24.1 cm (9.5 in) (which was taken as the design thickness at 50 percent reliability). It should be pointed out that a certain length of I-30 that was overlaid in 1992 with the 15.2 cm (6 in) layer of CRC was tested with the FWD shortly after construction. The resulting basin area/effective stiffness is also noted in figure 50. From this figure, it is apparent that the 15.2 cm (6 in) overlay was underdesigned and, consequently, was in need of reconstruction within 4 years of construction.<sup>(44)</sup>

## CHAPTER 6 - SUMMARY, CONCLUSION, AND NEEDED RESEARCH

This volume has presented a systematic and comprehensive approach to the design, construction, and condition assessment of CRC pavement. This presentation represents a significant step forward in the development of rational and relational forms associating measurable characteristics of materials to those of performance and design. This is a key to the advancement and development of mechanistic design procedures for CRC pavement systems.

CRC pavement arguably stands above all other concrete pavement types as the premier pavement type for heavy traffic applications from a performance and maintenance standpoint. However punchout distress is the primary distress type that occurs in this pavement system and the minimization of it should be one of the focuses of its design. The causes and factors relating to punchout distress in CRC pavements have been a topic of discussion among investigators for many years. These discussions generally centered on the performance of the subbase, development of the crack spacing and associated crack widths, and the effect of the percentage of reinforcement on the pavement and punchout performance. However, it is clear that a failure mechanism for CRC pavement needed to be established in order for design advancements to take place. Little evidence has been available in the literature substantiating the process of punchout, which has manifested itself in the form of controversy and confusion regarding the primary causes and mechanisms of punchout distress and the role reinforcement steel plays in the punchout process. This study has reconfirmed that the primary cause of punchout distress is support related and consequently is frequently premature in nature. The occurrence of steel rupture is purely a consequence of this process. Steel fracture does not occur until a significant amount of faulting has formed. The loss of support relative to punchout development can occur in many different forms, and it is evident that stabilized bases do not constitute the optimal form of support for a CRC pavement system. Although several agencies have standardized the use of stabilized bases under CRC pavements, a need exists to incorporate subbase systems that manifest greater balance of flexibility, drainability, and erosion resistance. Curling and warping stresses should be included in CRC pavement stress calculations. The effect of curling and warping is not the same effect as attributed to nonuniform support on punchout development. The effect of curling and warping on punchout development must be judged according to its effect on the loss of shear capacity across the transverse crack. Broken steel at widened cracks has frequently been associated with significant levels of corrosion.

Field experience tends to suggest that the effect of crack spacing upon CRC pavement performance tends to be indirectly related. Theoretically, the relationship can be shown directly and it strongly suggests the minimization of short cracking intervals under 1 m (3 ft) although field experience<sup>(40-43)</sup> has indicated good performance has been attained with short crack intervals under this limit, but, invariably this performance has always been accompanied with good support. Unless the requisite degree of support can be provided, the only practical measure that can be implemented to guarantee against premature failure is to exercise control over the crack pattern to optimal crack spacing and widths to maintain stresses with acceptable limits. Experience has also indicated that the variability associated with a randomly developing crack

pattern can be quite high and that climatic conditions at the time of construction can significantly outweigh the effects of reinforcing steel. Crack induction using surface notching has proved to be an effective methodology to control the crack pattern (and significantly reduce the variability) particularly for coarse aggregate types that exhibit low bond strength.

Other measures to improve punchout resistance or increase pavement life need to be evaluated in terms of the mechanism of punchout distress. No information in this study was available to verify the benefits of extra steel placed on the outer edges of CRC pavement but certainly the possible merits of this measure are worth considering. The benefits, however, should be compared with those provided by a tied or extended concrete shoulders. Use of high performance concrete should also be assessed in a similar manner with the realization that higher strength concretes typically results in longer crack spacings and wider crack widths. The effect of high strength concrete will consequently require greater amount of reinforcing steel or improved bond patterns in order to control the crack widths to acceptable limits or require a greater amount of understanding of how climatic factors affect crack development since these factors are often equal or greater than those due to the reinforcement. This may suggest the use of minimum and maximum limits on concrete strength, as has been suggested in Australian specifications for CRC pavement construction. The benefits of higher strength concretes should also be considered in terms of increased shear capacity at the transverse cracks.

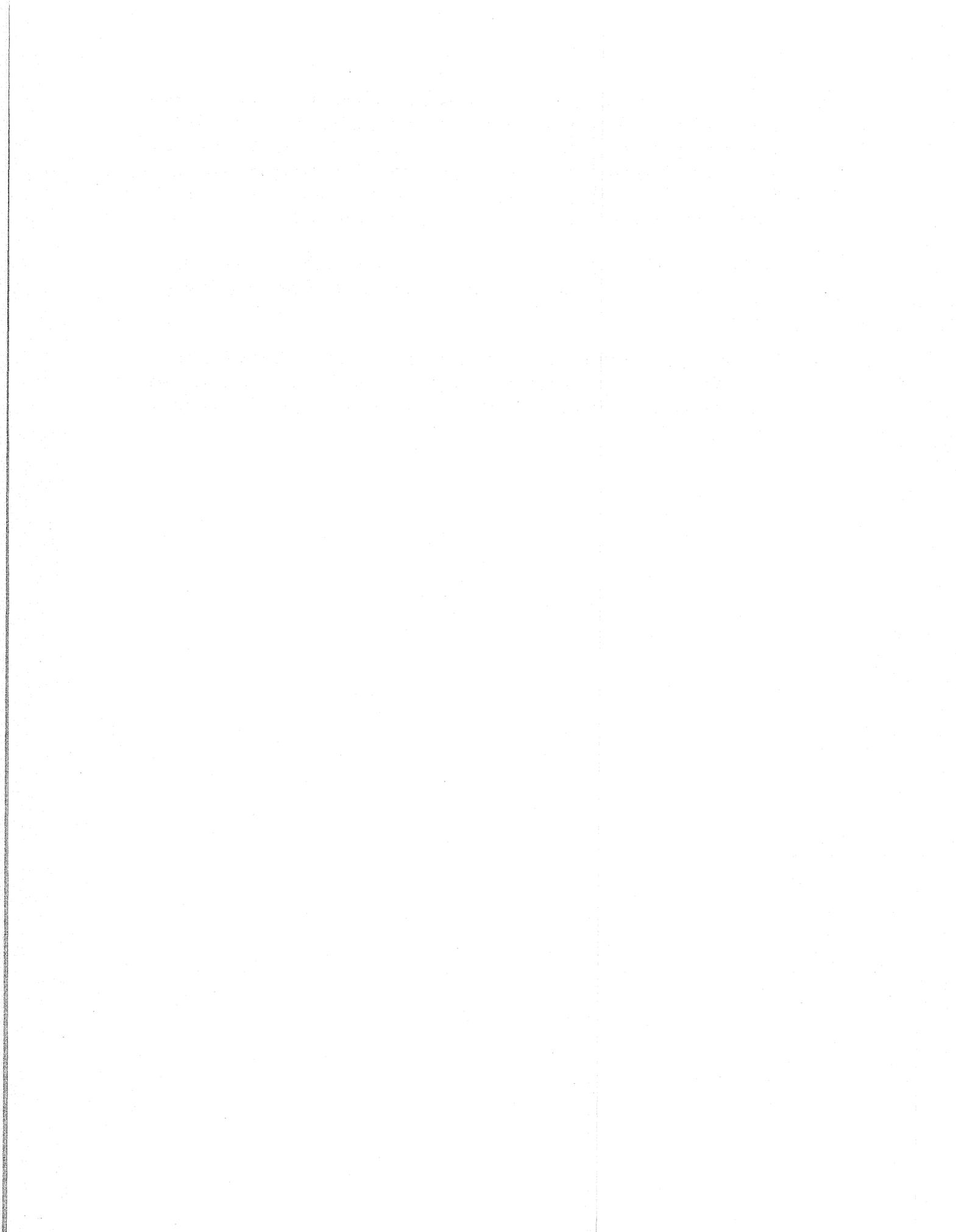
Current thickness design procedures do not adequately address punchout distress and mechanisms related to it. In fact, current CRC design procedures base thickness design more on jointed concrete behavior than on CRC pavement behavior which consequently results in overly conservative slab thicknesses. CRC pavement behavior is very different from jointed concrete behavior, and thickness design should not be based on jointed thickness design methods. Even though the current AASHTO Guide considers loss of support during the performance period, there is little connection between its development and punchout development. The variability associated with the cracking pattern should also be reflected in the design process and methods to control or reduce the variability should be accounted accordingly. The resistance to punchout development and the effect of crack pattern variability should be reflected in the shear capacity of the pavement system.

### **Suggestions for Further Research**

The following areas have been identified for further research to improve the design and performance of CRC pavement:

- (1) Development of subbase designs that are erosion-resistant, flexible, and provide long-term uniform support and drainage for CRC pavement. Consideration should also be given to the use of longer bar diameters near free, longitudinal edges.

- (2) Improvement of current models for the prediction of concrete and steel stresses in CRC pavement systems. Improvement of this nature will entail gaining a better understanding of bonding mechanisms and the effect of rebar bonding patterns. Nonlinear shrinkage and temperature gradients should be investigated in terms of their effect on crack initiation and the formation of the crack pattern. Suggested methods in this regard should be tested and verified in the field.
- (3) Development or improvement of design approaches to establish an optimized balance between concrete strength, steel content, climatic effects, and pavement thickness.
- (4) Improvement in materials and their properties relevant to the construction and construction practice in terms of long-term performance. Improvement of the level of understanding of the relationship between material properties and performance in the field.



## REFERENCES

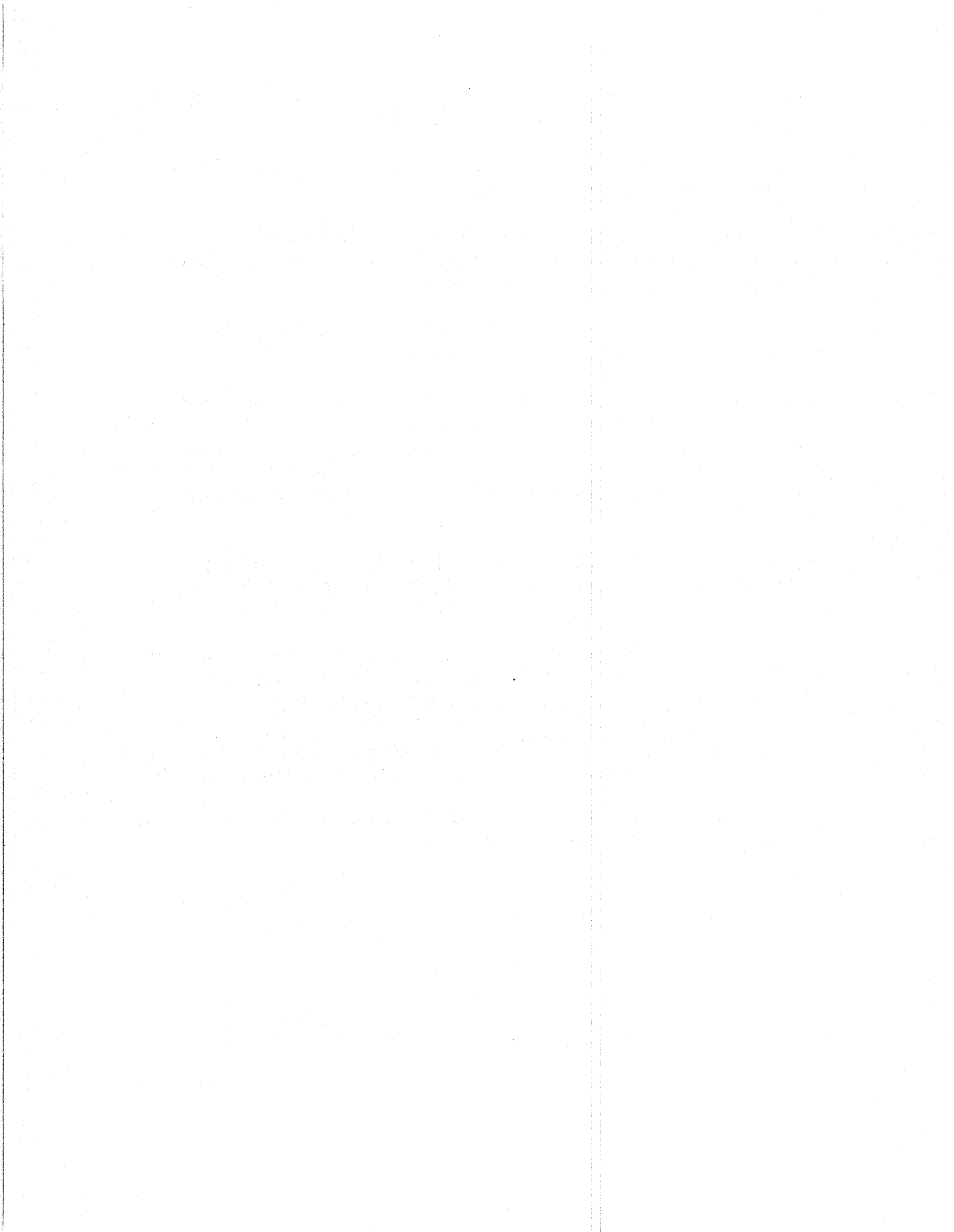
1. Won, M., K. Hankins, and B.F. McCullough, "Mechanistic Analysis of Continuously Reinforced Concrete Pavements Considering Material Characteristics, Variability, and Fatigue," Report No. 1169-2, Center for Transportation Research, University of Texas at Austin, April 1990.
2. Zollinger, D.G. and E.J. Barenberg, "Continuously Reinforced Pavements: Punchouts and Other Distresses and Implications for Design," Project IHR - 518, Illinois Cooperative Highway Research Program, University of Illinois, Urbana, Illinois, March 1990.
3. Van Breemen, W., "Ten-Year Report on Experimental Continuously Reinforced Concrete Pavements in New Jersey," HRB, Bulletin 214, 1959.
4. Kadiyala, S.M. and D.G. Zollinger, "Analysis of CRC Pavement Under Moisture, Temperature, and Creep Effects," Proceedings, Fifth International Conference on Concrete Pavement Design and Rehabilitation, April 20-22, 1993, Vol. 2, pp. 211-236, Purdue University.
5. Vetter, C.P. "Stresses in Reinforced Concrete Due to Volume Changes," ASCE, Proceedings, Paper No. 1848, February 1932.
6. McCullough, B.F., A.A. Ayyash, W.R. Hudson, and J.P. Randall, "Design of Continuously Reinforced Concrete Pavements for Highways," NCHRP 1-15, Center for Highway Research, The University of Texas at Austin, August 1975.
7. Burke, J.S. and J.S. Dhamrait, "A Twenty-Year Report on the Illinois Continuously Reinforced Pavement," Highway Research Record, No. 239, Highway Research Board, 1968.
8. Dhamrait, J.S., F.K. Jacobsen, and D.R. Schwartz, "Condition of Longitudinal Steel in Illinois Continuously Reinforced Concrete Pavements," Physical Research Report No. 43 (IHR-36), Illinois DOT.
9. McCullough, B.F. and W.B. Ledbetter, "LTS Design of Continuously Reinforced Concrete Pavement," Proceedings, ASCE, Vol. 86, HW4, December 1960, pp. 1-24.
10. Jiang, D.H., S.P. Shah, and A.T. Andonian, "Study of the Transfer of Tensile Forces by Bond," *ACI Journal*, Proceedings, Vol. 81, No. 3, May-June 1984, pp. 251-259.
11. Goto, Y., "Cracks Formed in Concrete Around Deformed Tension Bars," *ACI Journal*, Proceedings, Vol. 68, No. 4, April 1971, pp. 244-251.

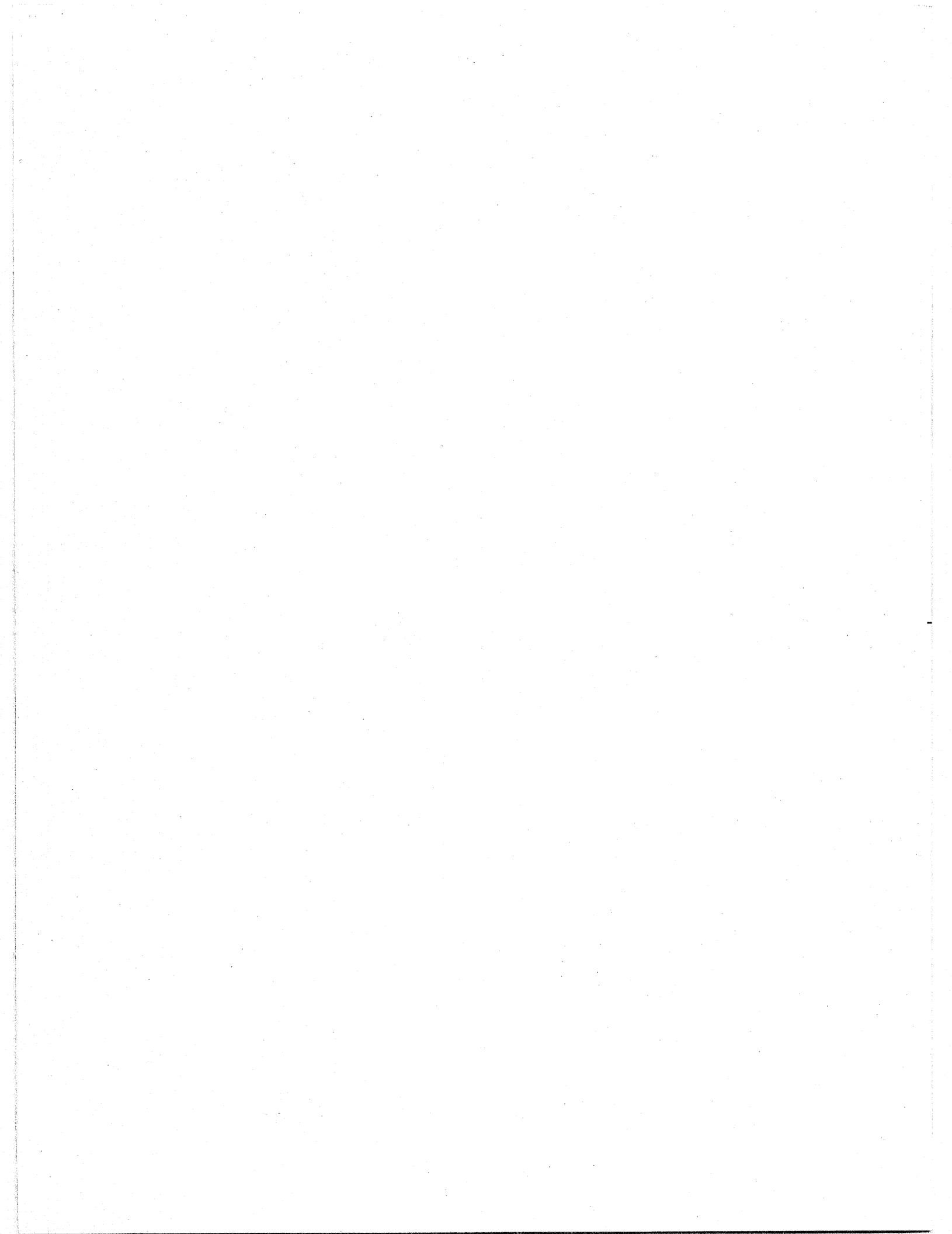
12. Mains, R.M., "Measurements of the Distribution of Tensile Stresses Along Reinforcing Bars," *ACI Journal*, Proceedings, Vol. 48, November 1951, pp. 225-252.
13. Krauthammer, T. and K.L. Western, "Joint Shear Transfer Effects on Pavement Behavior," *Journal of Transportation Engineering*, ASCE, Vol. 114, No. 5, September 1988.
14. Zuk, W., "Analysis of Special Problems in Continuously Reinforced Concrete Pavements," Highway Research Board, Bulletin 214, 1959.
15. Buch, N.J., "Development of Empirical-Mechanical Based Faulting Models in the Design of Plain Jointed Concrete Pavements," Ph.D. Dissertation, Texas A&M University, August 1995.
16. Colley, B.E. and H.A. Humphrey, "Aggregate Interlock at Joints in Concrete Pavements," Highway Research Record, No. 189, Highway Research Board, Washington, D.C., 1967.
17. Ioannides, A.M. and G.T. Korovesis, "Aggregate Interlock: A Pure Shear Load Transfer Mechanism," Transportation Research Record 1286, TRB, National Research Council, Washington, D.C., 1990.
18. Miner, M.A., "Cumulative Damage in Fatigue," Transactions, American Society of Mechanical Engineering, Vol. 67, 1945, pp. A159-A164.
19. Westergaard, H.M., "Analysis of Stresses in Concrete Pavements Due to Variations of Temperature," Proceedings of the Sixth Annual Meeting, Highway Research Board, 1927.
20. Bradbury, R.D., "Reinforced Concrete Pavements," Wire Reinforcement Institute, Washington, D.C., 1938.
21. Grzbowski, M. and S.P. Shah, "Model to Predict Cracking in Fiber Reinforced Concrete Due to Restrained Shrinkage," *Magazine of Concrete Research*, 41, No. 148, September 1989, pp. 125-135.
22. Zollinger, D.G. and E.J. Barenberg, "Development of Mechanistic-Based Design Procedure for Jointed Concrete Pavements," Research Report 518-3, Illinois Cooperative Highway Research Program, Transportation Research Laboratory, University of Illinois, Urbana, Illinois, 1986.

23. La Coursiere, S.A., M.I. Darter, and S.A. Smiley, "Performance of Continuously Reinforced Concrete Pavement in Illinois," *Civil Engineering Studies*, Transportation Engineering, Series No. 10, University of Illinois, Urbana, Illinois, 1978.
24. McCullough, B.F., J.C.M. Ma, and C.S. Noble, "Limiting Criteria for the Design of CRCP," Research Report 177-17, Center for Transportation Research, University of Texas, August 1979.
25. Turgeon, R. and K.D. Ishman, "Evaluation of Continuously Reinforced Concrete Overlay and Repairs on the Interstate Route 90, Erie County, Pennsylvania," Research Project 79-01, Commonwealth of Pennsylvania, Department of Transportation, November 1985.
26. Parry, J.M., "Investigation of Punchouts in Continuously Reinforced Concrete Overlay on I-94 in Jackson and Moore Counties," Research Project 0624-42-41, Study No. 85-5, Division of Highways and Transportation Services, Wisconsin Department of Transportation.
27. Foxworthy, P.T., "Concepts for the Development of a Nondestructive Testing and Evaluation System for Rigid Airfield Pavements," Ph.D. Dissertation, University of Illinois, Champaign-Urbana, Illinois, 1985.
28. Ioannides, A.M., L. Khazanovich, and L.J. Becque, "Structural Evaluation of Base Layers in Concrete Pavement Systems," Transportation Research Record 1370, TRB, National Research Council, Washington, D.C., 1992.
29. Young-Chan, S., B.F. McCullough, K.D. Hankins, "Development and Application of Randomness Index for Continuously Reinforced Concrete Pavement," Transportation Research Record 1307, TRB, National Research Council, Washington, D.C., 1991.
30. Ioannides, A.M., "Dimensional Analysis in NDT Rigid Pavement Evaluation," *ASCE Journal of Transportation Engineering*, Vol. 116, No.1, July 1990, pp. 23-36.
31. Ioannides, A.M., M.E. Thompson, and E.J. Barenberg, "The Westergaard Solutions Reconsidered," Transportation Research Record 1843, TRB, National Research Council, Washington, D.C., 1985, pp. 13-23.
32. Tang, T., Z.P. Bazant, S. Yang, and D.G. Zollinger, "Variable-Notch One-Sized Method for Fracture Energy and Process Zone Length," *Engineering Fracture Mechanics*, Vol. 55, No. 3, October 1996.

33. "New Rebars Ready for Use," *Transportation Research Board Research Digest*, Fall, 1994.
34. "Design of Continuously Reinforced Concrete for Highways," ARBP-CRSI, Chicago, Illinois, 1981.
35. Iwana, S., "Experimental Studies on the Structural Design of Concrete Pavement," Public Works Research Institute, Ministry of Construction, Japan, May 1964 (English Translation).
36. Appendix 6, "Structural Design Method for Rigid Pavement," *Manual for Asphalt Pavement*, Japan Road Association, 1989, pp. 219-233.
37. Iwana, S. and Y. Anzaki, "Concrete Pavement Technology in Japan Today," *Transportation Research Record 1182*, TRB, National Research Council, Washington, D.C., 1988.
38. Nakamura, T. and T. Iijama, "Evaluation of Performance and Structural Design Methods of Cement Concrete Pavements in Japan," Session 1 papers, 7<sup>th</sup> International Symposium on Concrete Roads, Vienna, Austria, October 3-5, 1994, pp. 109-114.
39. Tang, T., D.G. Zollinger, and B.F. McCullough, "Field Tests and Analyses of Concrete Pavement in Texarkana and La Porte, Texas," *Research Report 1244-7*, Texas Transportation Institute, Texas A&M University, College Station, Texas, October 1996.
40. Verhoeven, K., "Cracking and Corrosion in CRCP," *Belgium Cement Industry Collective Research Centre, Proceedings, Vol. 1, 5<sup>th</sup> International Conference on Concrete Pavement Design and Rehabilitation*, Purdue University, April 20-22, 1993, pp. 201-209.
41. Verhoeven, K., "Behavior of Continuously Reinforced Concrete," *RR CRIC 53-f-1992*, ISSN 0770-0725, 1992, 65 pp.
42. Verhoeven, K. and P. Van Audenjoive, "Cracking and Corrosion in CRCP," Session 5, 7<sup>th</sup> International Symposium on Concrete Roads, Vienna, Austria, October 1994, pp. 155-161.
43. Joffre, C., "Spanish Practice and Experience with Concrete Pavements," *Report on the 1992 U.S. Tour of European Concrete Highways*, Publication No. FHWA-SA-93-012, FHWA, U.S. DOT, Washington, D.C.
44. McDermott, L.B., "Parts of Local I-30 Being Repaved, Rebuilt," *Texarkana Gazette*, Vol. 122, No. 111, Texarkana, Texas/Arkansas.

45. Xin, D., "Crack Induction in CRC Pavement Based on Fracture Mechanics Analysis," Ph.D. Dissertation, Texas A&M University, August 1995.
46. Tabatabaie, A.M. and E.J. Barenberg, "Finite-Element Analysis of Cracked Concrete Pavements," Highway Research Record 671, 1978.
47. McCullough, B.F. and M.L. Cawley, "CRCP Based on Theoretical and Field Performance," Proceedings, Second International Conference on Concrete Pavement Design, Purdue University, April 1981, pp. 239-251.
48. Abou-Ayyash, A., "Mechanistic Behavior of Continuously Reinforced Concrete Pavement," Ph.D. Dissertation, University of Texas at Austin, May 1974.
49. PIARC, "Continuously Reinforced Concrete Pavements," Technical Committee in Concrete Roads, Permanent International Association of Roads Congresses, Paris, France, 1994.
50. Ayton, G.P., "Curing and Interlayer Debonding," Sixth International Purdue Conference on Concrete Pavements, Vol. 2, November 18-21, 1997, pp. 63-86.
51. Zwerneman, F.J., R.C. Donahey, H.S. Syed, and Srinivas R. Gunna, "Cracking of Concrete Pavement Continuously Reinforced with Epoxy-Coated Steel," *ACI Structural Journal*, Vol. 92, No. 6, November-December 1975, pp. 678-668.
52. Mohamed, A.R. and W. Hansen, "Effect of Nonlinear Temperature Gradient on Curling Stress in Concrete Pavements," *TRR No. 1568, Pavement Design, Management and Performance*, Pavement Rehabilitation and Design, Washington, D.C., pp. 65-71.
53. Darter, M.I., K.T. Hall, and C. Kuo, "Support Under Portland Cement Concrete Pavements," NCHRP Report 372, Transportation Research Board, Washington, 1995.
54. AASHTO Guide for Design of Pavement Structures 1993, American Association of State Highway and Transportation Officials, Washington, D.C.







HNR-30/2-99(791)E